University of Catania

Department of Biomedical and Biotechnological Sciences

PhD Program in Biotechnology

Biomedical and Preclinical Biotechnologies

XXIV Cycle

PhD thesis

Silvia Maria Ravalli

"Study Of Regenerative Engineering in Osteoarthritis and Prevention of Articular Cartilage Degeneration"

Coordinator: *Prof. Vito De Pinto*

Tutor: *Prof. Giuseppe Musumeci*

Academic years 2018/2022

INDEX

SINTESI

L'osteoartrite (OA) è una malattia degenerativa che colpisce l'intera articolazione, portando ad alterazioni del tessuto cartilagineo, dei legamenti, dell'osso subcondrale e della membrana sinoviale. Quarta causa di disabilità nel mondo, l'OA, il cui carico finanziario e sociale è destinato ad aumentare nel prossimo futuro, è la principale ragione alla base degli interventi di sostituzione articolare nelle società sviluppate. Sebbene precedentemente considerata esclusivamente come una malattia “da usura”, dovuta al fisiologico declino nella capacità della citoarchitettura cartilaginea di sostenere i carichi, l'OA è ormai evoluta nella definizione di una malattia multifattoriale e complessa. Si presume che uno squilibrio tra i processi anabolici e catabolici agisca di concerto con diversi fattori di rischio, rappresentati da età, sesso, genetica, obesità, metabolismo osseo, stress fisici, forza muscolare, traumi e lesioni sportive.

Il trattamento dei difetti condrali nella pratica clinica è ostacolato dalla scarsa capacità di auto-rigenerazione della cartilagine. L'ingegneria dei tessuti, che combina scaffold innovativi e cellule staminali, emerge quindi come una strategia promettente per la rigenerazione articolare. Uno degli obiettivi di questo lavoro è stato quello di sfruttare le attuali conoscenze in questo campo di ricerca per valutare la capacità di un cell-free scaffold a base di collagene di tipo I nel promuovere la riparazione cartilaginea dopo l'impianto ortotopico in vivo e, inoltre, analizzare l'effetto della presenza di una molecola naturale esogena, il Cicloastragenolo, durante la differenziazione condrogenica a partire da cellule staminali mesenchimali in vitro.

Infine, l’attuale letteratura scientifica sottolinea l'importanza della prevenzione e dell'intervento terapeutico precoce al fine di evitare la degenerazione della cartilagine e rallentare la progressione della patologia. Per questo motivo, un altro obiettivo di questo lavoro è stato quello di contribuire alla ricerca nel campo della prevenzione con nuove evidenze scientifiche sul ruolo della vitamina D nello sviluppo della cartilagine, sull'effetto dell'esercizio fisico nei sinoviociti durante la progressione della patologia, e sulle conseguenze dell'atrofia muscolare dovuta all'inattività, in una popolazione di cellule staminali.

ABSTRACT

Osteoarthritis (OA) is a degenerative disease that affects the entire joint, leading to alterations in articular cartilage, ligaments, subchondral bone, and synovium. Rated as the 4th leading cause of chronic disability worldwide, OA is the most common reason behind joint replacement in developed societies, and its financial and social burden is likely to increase in the next future. Once merely considered as a wear and tear disease, due to the physiological decline of cartilage architecture in weight-bearing tolerance, OA is by now evolved into the definition of a multifactorial and complex disease. An imbalance between anabolic and catabolic processes is assumed to act in concert with several risk factors, e.g., age, gender, genetics, obesity, bone metabolism, physical stresses, muscle strength, trauma, and sports injuries.

The treatment of chondral defects in clinical practice is hindered by the poor self-healing ability of cartilage. Tissue engineering, combining innovative scaffolds and stem cells, therefore emerges as a promising strategy for articular regeneration. One of the aims of this research was to exploit tissue engineering principles by evaluating the capability of a cell-free collagen I-based scaffold to promote cartilaginous repair after orthotopic implantation in vivo and observe the effect of an exogenous natural molecule, Cycloastragenol, in the chondrogenic differentiation of mesenchymal stem cells in vitro.

Furthermore, current literature underlines the importance of prevention and early intervention in order to avoid cartilage disruption and slow down the disease progression. For this reason, another aim of this work focused on contributing to the field of prevention of OA disease with new insights about the role of Vitamin D in cartilage development, the effect of physical exercise in OA synoviocyes and the consequence of muscle atrophy due to inactivity in a population of stem cells.

KEYWORDS AND ABBREVIATIONS

Keywords:

Articular cartilage; Chondrocytes; Synovium; Skeletal Muscle; Osteoarthritis; Tissue engineering; Human adipose-derived mesenchymal stem cells; Cycloastragenol; Scaffold; Functional food; Vitamin D; Lubricin; Physical Activity; Telocytes; Morphology; Immunohistochemistry.

Abbreviations:

ECM	Extracellular matrix	GAGs	Glycosaminoglycans
IL-1	Interleukin-1	TNF	Tumor Necrosis Factor
OA	Osteoarthritis	MMPs	Matrix Metalloproteases
MSCs	Mesenchymal Stem Cells	HA	Hyaluronic Acid
BMPS	Bone Morphogenic Proteins	TGF-B	Transforming Growth Factor B
IGF-1	Insulin-Like Growth Factor 1	BFGF	Basic Fibroblast Growth Factor
BDS	Biomolecule Delivery Systems	CAG	Cycloastragenol
hAMSCS	Adipose-Derived Mesenchymal Stem Cells	CM	Chondrogenic Medium
ACL	Articular Cartilage Lesions	S	Cell Free Collagen I-Based Scaffolds
ColI and ColII	Collagen Type I And II	Vit D	Vitamin D
VDR	Vitamin D Receptor	MPA	Moderate Physical Activity
H&E	Hematoxylin & Eosin Staining		

AFFILIATIONS

2018-2022 – PhD Student;

Department of Biomedical and Biotechnological Sciences, Human, Histology and Movement Science Section, University of Catania, Via S. Sofia 87, 95123 Catania, Italy

Nov 2021-Mar 2022 – Trainee Biostatistician - Erasmus+ Mobility Program for Traineeship Unipharma-Graduates;

ICRC-Weyer GmbH, Boelschestraße 35, 12587 Berlin, Germany

1. PROJECT SUMMARY

1.1 General Introduction

1.1.1 Structure and Function of Articular Cartilage

Articular cartilage is a complex connective tissue covering the ends of the bones constituting a diarthrodial joint and that can also be found in the growth plate of the metaphysis[1]. Its role is essential in providing a low friction surface and withstand weight bearing during the range of motion that allows to perform daily living activities. Articular cartilage is 2 to 4 mm thick hyaline cartilage and is populated by highly specialized cells called chondrocytes. The latter originate by chondrogenesis from mesenchymal stem cells and represent only about 2% of the total volume of tissue since they synthesize and produce a large volume of extracellular matrix (ECM)[2]. This material is so abundant that the resident cells result widely separated but it otherwise become responsible for the intrinsic characteristics and properties of the tissue itself[3].

The ECM has an amorphous and a fibrillar components. The first, called ground substance or hydrophilic gel, is composed of hydratable high-molecular-weight complexes able to withstand compressive forces, and therefore can be considered as a colloidal system formed by an aqueous phase in which a mixture of proteoglycans (e.g., Aggrecan, Lubricin), formed by chains of glycosaminoglycans (GAGs, e.g., hyaluronic acid, chondroitin-4 and 6-sulfate) linked to a protein core, structural and non-structural glycoproteins, enzymes, and mineral salts, are dispersed[1-3]. The GAGs, because of their acidic nature, dissociate, exposing numerous free anionic groups which, being hydrophilic, can bind water molecules. In this way, the water is distributed throughout the amorphous component, thus regulating osmotic exchanges within cell population, and maintaining cartilage unique viscoelastic and mechanical properties. Due to the molecular characteristics of the proteoglycans, the resulting network works as a molecular filter, which selectively prevents the passage of certain molecules and facilitates the diffusion of others. This creates an excellent barrier system capable of block the transit of molecules with a molecular weight between 40 and 180 kDa[4].

The fibrillar component, intertwined with proteoglycan aggregates, is instead organized in filamentous supramolecular structures, capable of resist traction and responsible for the final tissue architecture, providing articular cartilage with important shear and tensile properties, which help to stabilize the matrix. The most abundant macromolecule is collagen which represent about 60% of the dry weight of cartilage[5]. The 90% to 95% of the total collagen is represented by Type II collagen, while collagen types I, IV, V, VI, IX, and XI are also present but in a minor proportion. All members of the collagen family consist of 3 polypeptide chains (α-chains) wound into a triple helix structure. The amino acid composition of polypeptide chains is primarily glycine and proline, with hydroxyproline providing stability via hydrogen bonds along the length of the molecule [1].

Cartilage originates during the first weeks of intrauterine life from mesenchymal cells which subsequently acquire the characteristics of secreting cells (extended rough endoplasmic reticulum and Golgi apparatus) differentiating into chondroblasts[6]. When these cells begin the production of cartilage matrix, they are trapped and encapsulated in matrix niches by the proteoglycans, due to their gelatinous consistency and slow diffusion, therefore forming the basophilic capsule of the now mature chondrocytes. Since the cartilage matrix is not very fluid, chondroblasts, and in some cases chondrocytes, when increasing in number by mitosis, form the so-called isogenic groups or cell clones of three to five cells within the same capsule. The different distribution of cells in the cartilage tissue significantly affects the distribution of secreted proteoglycans, and thus basophilia. Alcian blue staining can evidence maximal basophilia in the immediate neighboring area to the cells, the so-called capsule; it decreases while remaining high in the matrix areas close to cells, especially in internal territorial areas; and noticeably decreases in the areas distant from the cells, the so-called external territorial areas (o inter-territorial)[7].

Articular cartilage presents a heterogeneous distribution of cell and matrix components through its width, identified in four zones: superficial, intermediate/medial, radial/deep and calcified zones[8]. The superficial zone protects the underlying layers from the shear and traction stresses imposed by the movement of the joint, due to the presence of type II and IX collagen fibers parallel to the surface of the tissue. It contains a large number of flattened chondrocytes, and it is in direct contact with the synovial fluid that provides the nourishment.

The middle zone is identified by obliquely oriented collagen fibers and by a low density of spherical chondrocytes. In addition, it contains most of the proteoglycans, thus providing compression resistance ability. However, the greatest resistance to compressive forces is guarantee by the deep zone, located at the cartilage-bone interface, where the collagen fibers are perpendicularly aligned to the surface. Here, the chondrocytes are typically arranged in columns. The tide mark separates the deep zone from the calcified zone. The latter connects the cartilage to the bone, by deeping the collagen fibrils to the subchondral bone. This part of the cartilage is populated by a scarce number of chondrocytes, which become hypertrophic[9].

Finally, cartilage is avascular, aneural, and alymphatic with a limited capacity of regeneration caused by low mitotic activity of chondrocytes, nourished by two potential pathways: diffusion from subchondral bone vessels and diffusion from the synovial fluid [10]. Another important role of synovial fluid is to reduce friction between the ends of the bones during the movement. Indeed, synovial joint is surrounded by a fibrous, highly vascular capsule called synovium, whose internal layer is lined with a synovial membrane, containing type B synoviocytes (fibroblast-like cell lines)[11]. Their primary function is to produce high molar mass hyaluronic acid (HA) within the fluid, in order to provide viscosity.

The structural integrity of articular cartilage depends on a delicate homeostatic balance of its cellular and molecular constituents and their interactions; the reasons and the consequences of the loss of this physiological equilibrium are discussed below.

1.1.2 Osteoarthritis

Cartilage continuously remodels itself solicited by external stimuli. In particular, daily mechanical forces induce deformations of the ECM which are captured by the mechanoreceptors and voltage-dependent channels present in the cell surface of the chondrocytes[12]. The activation of the chondrocytes triggers environmental modification of the pericellular milieu through the increase in concentration of proteoglycans, changes in ionic concentration and pH. The increase of proteoglycans in the matrix results in an increase in free anion groups which, being hydrophilic, can bind further water molecules allowing a growth in the volume of the amorphous component and therefore inducing a remodeling of the ECM. However, in the most stressed areas, inappropriate or persistent mechanical stimuli could eventually lead to cartilage injuries[13]. The absence of blood supply, lymphatic drainage and innervation makes cartilage repair more difficult. Chondrocytes synthesize the matrix and secrete digestive enzymes that degrade the various components during the physiological process of turnover. Pathological imbalance takes place when chondrocytes activate the catabolic enzymes, reduce the production of inhibitors and therefore leading to the accelerate degradation of the matrix. Cytokines such as Interleukin-1 (IL-1) and Tumor Necrosis Factor (TNF), which come from chondrocytes, synoviocytes, fibroblasts and inflammatory cells, trigger the process of degradation[14]. The destruction of the articular cartilage, carried out by cells of that district, is an important mechanism in many joint pathologies.

Osteoarthritis (OA) is a disease in the which chondrocytes respond to biochemical and mechanical stresses that lead to degeneration of the cartilage that causes the structural and functional failure of the synovial joint[15]. In the vast majority of cases, OA appears insidiously, without apparent initial cause, as a phenomenon linked to aging (idiopathic or primary osteoarthritis)[16,17]. In about 5% of cases, OA appears in younger subjects who present predisposing and genetic conditions, for example joint deformity, previous joint damage or an underlying systemic disease that puts the joints at risk, such as diabetes or marked obesity. In this context, the disease is called secondary OA[18]. Although historically OA was considered an inevitable process of “wear and tear”, this definition is reductive since the bases of this escalating damage rely on a compromised balance between anabolic and catabolic mechanisms, which can be consequent to several risk factors like ageing, muscle

atrophy, metabolic disorders, inflammatory conditions, injuries and overload, or wrong biomechanics of the joint.

Changes in chondrocytes can be divided into three stages: (1) damage to the chondrocytes, linked to genetic and biochemical factors; (2) Early OA, in which chondrocytes proliferate, forming aggregates, and secrete inflammatory mediators, collagens, proteoglycans and proteases that interact to remodel the cartilage matrix and initiate inflammatory changes secondary in the synovial membrane and subchondral bone. The water content of the matrix increases, while the concentration of proteoglycans decreases. In the surface layer, the normal horizontal arrangement of the Type II collagen fibers is disrupted and cracks; (3) Late OA, in which the repeated damage and chronic inflammation lead to disappearance of the chondrocytes, marked loss of cartilage, full-thickness cartilage fragments detach, and extensive changes in the subchondral bone which becomes exposed. There is therefore hardening and sclerosis (irreversible bone thickening) of the cancellous bone below. Small fractures of the joint bone and the empty spaces created by the fractures allow synovial fluid to penetrate subchondral regions. Osteophytes are formed on edges of the joint surface, and these are covered with fibrocartilage and hyaline cartilage, which gradually ossify. Matrix metalloproteases (MMPs) are the main responsible enzymes for Type II collagen breakdown, and the degradation of proteoglycans eventually outweighs their synthesis. The involvement of synovial membrane and the recruitment of inflammatory cells and mediators as TGFβ, TNF, prostaglandins, and nitric oxide, accelerates the process of tissue degeneration[19-22].

Symptoms of OA include deep pain that worsens with joint movement, morning stiffness, joint creaking, and limitations of range of motion. The knee joint is one of the most frequently affected articulation. Joint deformities may occur over time, but unlike rheumatoid arthritis joint fusion will not occur. The degree of severity of the disease detected radiographically does not often correlate well with pain and disability[23]. Due to the complexity of this multifactorial disease, currently we do not dispose of adequate means of prevention for primary OA, and since there is no effective way to stop its progression, only a number of treatments to help relieve the symptoms are available.

1.2. Aims, design and results of the presented studies

1.2.1. Mesenchymal Stem Cells and Tissue Engineering in Cartilage Regeneration

Sources:

Szychlinska M. A.; D'Amora U.; Ravalli S.; Ambrosio L.; Di Rosa M.; Musumeci G. (2019). Functional Biomolecule Delivery Systems and Bioengineering in Cartilage Regeneration. Curr. Pharm. Biotechnol. 2019, 20, 32–46.

Ravalli, S.; Szychlinska, M.A.; Lauretta, G.; Musumeci, G. New Insights on Mechanical Stimulation of Mesenchymal Stem Cells for Cartilage Regeneration. Appl. Sci. 2020, 10, 2927.

Scientific minds have always expressed a stubborn yearn to master the creation of artificial biological elements in order to emulate the delicate machinery of the human body. The idea of being able to control cell destiny and replace malfunctioning parts of the body with brand new tissues and organs has led to remarkable progress in biological fields such as tissue engineering and regenerative medicine. A promising application of this concept relies on the use of stem cells to originate functional and specialized tissues [24]. Mesenchymal stem cells (MSCs) constitute a specific subtype of multipotent stem cells, which can differentiate into a variety of cell types and offer the advantage of obtaining pure stem cell populations [25]. One of the most challenging ambitions in regenerative biomedicine is to restore damaged articular cartilage, as it is one of the most challenging tissue types to heal by virtue of its anatomical and structural complexity. Chondrogenic differentiation from MSCs requires the involvement of transcription factors including Runx2, Sox9, PPARγ, MyoD, GATA4 and GATA6 [26-29], and growth factors, e.g. transforming growth factor β family (TGF- β-1,-2,-3), as well as bone morphogenic proteins (BMPs) [30]. In vitro, chondrogenic differentiation of MSCs is demonstrated to be induced by a culture medium supplemented with ascorbic acid phosphate, dexamethasone, bovine serum albumin, linoleic acid, sodium pyruvate, transferrin, selenous acid, proline, L-glutamine along with TGF-β1 [31]. In addition, insulin-like growth factor 1 (IGF-1) and basic fibroblast growth factor (bFGF), are crucial for the cartilage homeostasis maintenance [32-34]. It has been shown that MSC chondrogenesis is particularly enhanced by hypoxic conditions [35]. Beside these last ones, also anti-angiogenic factors such as endostatin [36], suramin [37], vascular endothelial

growth factor receptor 1 (VEGFR1), [38] and bevacizumab [39], have been considered to inhibit blood vessel growth and restore cartilage tissue to its native avascular state. Moreover, several others anti-inflammatory therapies such as cytokines, chemokines, hormones and other drugs have also been explored in the cartilage regeneration approach. Stromal cell-derived factor- 1 (SDF-1) is a key chemokine with the potential to enhance cartilage repair through increased MSC migration to the cartilage defect site [40]. In the parathyroid hormone (PTH) family, peptide segments of PTH have been shown to inhibit the OA progression of and promote the chondral defects repair [41]; PTH-related proteins (PTHrP), synthesized by chondrocytes, can suppress induction of hypertrophy [42]. Inhibitory factors on necrosis, apoptosis, metalloproteases (MMPs) and aggrecanases, have also shown potential in the treatment of cartilage lesions [43-46].

Conventional treatments for OA, ranging from injections to surgical procedures, still suffer, in many cases, from wide variation in clinical outcomes, complications, effectiveness and long-term reliability [47]. MSCs injection as anti-inflammatory and immune-modulating remedy is a minimally invasive procedure which has been reported to induce pain relief and improvement in articular function [48–51]. However, the efficacy of this procedure is controversial, since after injection, cells might not survive or remain in situ [52,53], due to failure in cells attachment to ECM [54,55]. For this reason, tissue engineering is based on the use of a three-dimensional (3D) scaffold [56, 57]. The latter is a biomaterial matrix used as a template, which plays a pivotal role in the support and organization of the newly formed tissue, which should resemble mature cartilage and have the capacity to be integrated into the surrounding tissues, promoting cell adhesion. It is widely recognized that employed technologies and materials are strictly linked between them. Mechanical and morphological features such as roughness, micro and nanotopography, porosity, interconnectivity of the pores, surface energy as well as scaffold stiffness, strongly depend on material chemistry but also on technology and together have a critical influence on cell behaviour. With regard to cartilage tissue engineering, from a biomechanical point of view, it should be taken into consideration that articular cartilage supports and distributes applied loads acting as a multiphasic fiber-reinforced material with viscoelastic properties. Along with structural and biomechanical properties, the viability of cells first depends on the chemistry of scaffold (natural or synthetic) on which they are seeded. A variety of synthetic polymers (such as,

aliphatic poly- esters: polyglycolic acid (PGA), polylactic acid (PLLA), their copolymers (PLGA), polyethylenglicol (PEG) and polycaprolactone (PCL)), with chondrogenic properties, have been considered and commonly employed for the design of cartilage tissue engineered scaffolds. However, only some of them are now commercially available for clinical use. Even if they still present a limit of missing 3D structure for cartilage with appropriate mechanical properties, common natural biodegradable polymers such as, polysaccharides (alginate, chitosan), glycosaminoglycans (GAGs, hyaluronic acid derivative) and proteins (collagen, alginate, fibrin, silk fibroin (SF) have been widely investigated for culturing cells.

However, still today, the stem cell-based tissue engineering fails to fully reproduce the structural and biomechanical features of native tissue. Cartilage tissue engineering still needs to be optimized to allow its advance into a clinical practice. The use of exogenous biomolecules such as growth factors, drugs, molecular activators/inhibitors, as well as other influencers such as mechanical stimulation and epigenetic modifications, could contribute to enhance cartilage regeneration and represent a promising approach aiming to overcome the mentioned limits [56,57]. For example, natural anti-inflammatory molecules, like Resveratrol, Sulforaphane and Curcumin, have been explored for cartilage repair therapy, to contrast the inflammatory milieu of the affected joint after implantation. Beyond any doubt, the design of functional biomolecule delivery systems (BDS) based on innovative biomaterials, with suitable mechanical and mass transport properties, able to release bioactive molecules stimulating the extracellular matrix (ECM) deposition, cell aggregation, mesenchymal stem cells (MSCs) "healthy" phenotype and chondrgenesis, MSCs endogenous recall to the injury site and immunomodulatory and anti-inflammatory effects, should continue to be a major research focus for cartilage regeneration.

Having regard of what said above, the aims of the following two research articles were to contribute to the field of tissue engineering with new insights about the possible role of a natural compound in chondrogenic differentiation of MSCs in vitro and the efficacy of a cell-free Type I collagen in repairing cartilage tissue in vivo:

Cycloastragenol As An Exogenous Enhancer Of Chondrogenic Differentiation Of Human Adipose-Derived Mesenchymal Stem Cells. A Morphological Study

Stem cell therapy and tissue engineering represent a promising approach for cartilage regeneration. However, they present limits in terms of mechanical properties and premature de-differentiation of engineered cartilage. Cycloastragenol (CAG), a triterpenoid saponin compound and a hydrolysis product of the main ingredient in Astragalus membranaceous, has been explored for cartilage regeneration. The aim of this study was to investigate CAG's ability to promote cell proliferation, maintain cells in their stable active phenotype, and support the production of cartilaginous extracellular matrix (ECM) in human adipose-derived mesenchymal stem cells (hAMSCs) in up to 28 days of three-dimensional (3D) chondrogenic culture. The hAMSC pellets were cultured in chondrogenic medium (CM) and in CM supplemented with CAG (CAG–CM) for 7, 14, 21, and 28 days. At each time-point, the pellets were harvested for histological (hematoxylin and eosin (H&E)), histochemical (Alcian-Blue) and immunohistochemical analysis (Type I, II, and X collagen, aggrecan, SOX9, lubricin). After excluding CAG's cytotoxicity (MTT Assay), improved cell condensation, higher glycosaminoglycans (sGAG) content, and increased cell proliferation have been detected in CAG–CM pellets until 28 days of culture. Overall, CAG improved the chondrogenic differentiation of hAMSCs, maintaining stable the active chondrocyte phenotype in up to 28 days of 3D in vitro chondrogenic culture. It is proposed that CAG might have a beneficial impact on cartilage regeneration approaches.

Evaluation of a Cell-Free Collagen Type I-Based Scaffold for Articular Cartilage Regeneration in an Orthotopic Rat Model

The management of chondral defects represents a big challenge because of the limited self-healing capacity of cartilage. Many approaches in this field obtained partial satisfactory results. Cartilage tissue engineering, combining innovative scaffolds and stem cells from different sources, emerges as a promising strategy for cartilage regeneration. The aim of this study was to evaluate the capability of a cell-free collagen I-based scaffold to promote cartilaginous repair after orthotopic implantation in vivo. Articular cartilage lesions (ACL) were created at the femoropatellar groove in rat knees and cell free collagen I-based scaffolds

(S) were then implanted into right knee defect for the ACL-S group. No scaffold was implanted for the ACL group. At 4-, 8- and 16-weeks post-transplantation, degrees of cartilage repair were evaluated by morphological, histochemical and gene expression analyses. Histological analysis shows the formation of fibrous tissue, at 4-weeks replaced by a tissue resembling the calcified one at 16-weeks in the ACL group. In the ACL-S group, progressive replacement of the scaffold with the newly formed cartilage-like tissue is shown, as confirmed by Alcian Blue staining. Immunohistochemical and quantitative real-time PCR (qRT-PCR) analyses display the expression of typical cartilage markers, such as collagen type I and II (ColI and ColII), Aggrecan and Sox9. The results of this study display that the collagen I-based scaffold is highly biocompatible and able to recruit host cells from the surrounding joint tissues to promote cartilaginous repair of articular defects, suggesting its use as a potential approach for cartilage tissue regeneration.

1.2.2. Prevention: Nutrition and Physical Activity

Sources:

Ravalli, S.; Szychlinska, M.A.; Leonardi, R.M.; Musumeci, G. Recently highlighted nutraceuticals for preventive management of osteoarthritis. World J Orthop. 2018, 9, 255-261.

Ravalli, S.; Castrogiovanni, P.; Musumeci, G. Exercise as medicine to be prescribed in osteoarthritis. World J Orthop. 2019, 10, 262-267.

The management of OA focuses on alleviating its secondary effects since there is currently no resolutive cure. Nonsteroidal anti-inflammatory drugs and analgesics are generally prescribed to patients to reduce pain and improve joint function, but they fail in modifying disease progression in terms of prevention and chondroprotection[58]. The chronic nature of OA forces the use of pharmacological approaches that can be considered safe for long term use and, at the same time, might be able to slow its progression. The basis of articular damage relies on impaired balance between anabolic and catabolic mechanisms, which can be influenced by dietary compounds like nutraceuticals[59]. Due to their minimal side effects, especially in the long term, their easy extraction and low costs of production, they may represent a valid preventive management of OA. Forty-seven percent of people who suffer from OA use complementary medications including nutraceuticals due to their anti-inflammatory and antioxidant activities[60].

Herbal and natural products have been used since ancient times. A 5000-year-old Sumerian clay tablet is the first proof of plants use as medicament, especially to treat pain and inflammation[61]. During the 19th century, improvement in chemical technologies allowed for the extraction of active substances from medicinal plants such as alkaloids, tannins, saponosides, etheric oils, vitamins and glycosides, isolated in pure form[62]. The term “nutraceutical”, resulting from the combination of the words “nutrition” and “pharmaceutical”, is used to define any natural or food-derived molecule able to exert a potential therapeutic effect that could be integrated into a daily diet[63]. Statutory law of these type of medicaments differs by country. For example, in the United States, they are considered dietary supplements by the Dietary Supplement Health and Education Act of 1994[64]. The Food and Drug Administration is in charge of reviewing and approving any

health claims about these products. In some countries of the European Union, nutraceuticals may require registration whereas in others, they could be easily sold as food preparations[65].

Nutraceuticals offer a wide range of molecules able to exert anti-inflammatory and antioxidant properties that ameliorate cartilage conditions, suggesting that they should be integrated into a framework of prevention. A robust literature supports, for example, the efficacy of olive oil at reducing IL-6 and increasing lubricin and hyaluronan synthesis in synovial cells; the efficacy of curcumin, at decreasing TNF-α, IL-1β, IL-6 and MMP3 and MMP13 expression; the role of sanguinarin as down-regulator of catabolic proteases through interaction with IL-1β; and vitamin D, as anti-oxidant and anti-inflammatory molecule.

As previous mentioned, pharmacological treatment of OA involves the use of non-steroidal anti-inflammatory drugs, opioid and non-opioid analgesics, and intra-articular injections of steroids and hyaluronic acid, which may have significant negative gastrointestinal side effects[66]. This has led physicians to consider non-pharmacological, regenerative and behavioural treatments[67,68]. Among these, exercise is a good and useful tool to alleviate symptoms of OA and slow its progression[69-71]. The literature has demonstrated that physical exercise has short-term benefits in reducing pain, improving physical function, balance, muscle strength and flexibility[72,73]. Training tailored to improve OA includes anaerobic, aerobic, flexibility workouts and aquatic exercise[74,75]. It is essential to plan a protocol of movement whose type, duration and intensity represents the best approach to induce positive changes within the joint and for the chondrogenesis[76], but does not worsen the pathological condition by excessive load bearing or exhausting exercise[77]. It seems that a combination of aerobic fitness training and strengthening exercises should be optimal to address the spectrum of impairments associated with OA, taking into account the preferences and tolerance of patients in order to maintain a high level of adherence to the exercise program[78,79].

The most important effect of exercise on articular cartilage is that it keeps the joints lubricated and facilitates cycles of catabolism and anabolism within the tissue. Mechanical stresses facilitate diffusion of nutrients and stimulates the synthesis of the molecular components of ECM. Sedentary and immobilization eventually compromise the lubricant properties of joint, although this can be reversed with activity. Otherwise, after long periods of immobility, the

joints become stiff and lose some of their range of movement, also not supported by the muscle who can incur in atrophy. Efficacy of exercise is also extended to other components of the joints such as the synovium, muscle, ligaments, tendons, and bone[80]. Synovial fluid produced by the synovial membrane within the joints has a short-term response to exercise, thus requiring regular exercise to stay lubricated, nourished, and healthy. In response to physical activity, osteoblasts are engaged in remodeling and building new bone tissue and in improving density, being more able to withstand mechanical loads. In addition, muscles respond rapidly to exercise by synthesizing proteins and increasing in size. The integrity of tendons and ligaments is critical for joint function, which become stronger and more resistant to injury when exercised[80].

Having regard of what said above, the aims of the following three research articles were to contribute to the field of prevention of OA with new insights about the role of Vitamin D in cartilage development, the effect of exercising in OA synoviocyes and the consequence of atrophy in a population of stem cells in healthy muscle:

Assessment of Vitamin D Supplementation on Articular Cartilage Morphology in a Young Healthy Sedentary Rat Model

Deficiency in vitamin D (Vit D) has been widely associated with several musculoskeletal diseases. However, the effects of the exogenous Vit D supplementation are still unclear in the prevention of the latter, especially in the cartilage developmental period. The aim of this study was to compare the effects of Vit D supplementation and restriction on the articular cartilage development in healthy young sedentary rats. To this aim, twelve nine-week-old healthy Sprague-Dawley male rats were subjected to Vit D-based experimental diets: R, with a content in Vit D of 1400 IU/kg; R-DS, with a Vit D supplementation (4000 IU/kg); R-DR, with a Vit D restriction (0 IU/kg) for 10 weeks. The morphology, thickness and expression of cartilage-associated molecules such as collagen type II/X, lubricin and Vit D receptor (VDR), were assessed. Histological, histomorphometric and immunohistochemical evaluations were made on rat tibial cartilage samples. In the present experimental model, restriction of Vit D intake induced: The lower thickness of cartilage compared both to R ($p = < 0.0001$) and R-DS ($p = < 0.0001$); reduction of proteoglycans in the extracellular matrix (ECM) compared both to R ($p = 0.0359$) and R-DS ($p = < 0.0001$); decreased collagen II

(Col II) with respect both to R ($p = 0.0076$) and R-DS ($p = 0.0016$); increased collagen X (Col X) immunoexpression when compared both to R ($p = < 0.0001$) and R-DS ($p = < 0.0001$), confirming data from the literature. Instead, supplementation of Vit D intake induced: Higher cartilage thickness with respect both to R ($p = 0.0071$) and R-DR ($p = < 0.0001$); increase of ECM proteoglycan deposition compared both to R ($p = 0.0175$) and R-DR ($p = < 0.0001$); higher immunoexpression of lubricin with respect both to R ($p = 0.001$) and R-DR ($p = 0.0008$). These results suggest that Vit D supplementation with diet, already after 10 weeks, has a favorable impact on the articular cartilage thickness development, joint lubrication and ECM fibers deposition in a young healthy rat model.

Moderate Physical Activity as a Prevention Method for Knee Osteoarthritis and the Role of Synoviocytes as Biological Key

The purpose of this study was to investigate the influence of moderate physical activity (MPA) on the expression of osteoarthritis (OA)-related (IL-1β, IL-6, TNF-α, MMP-13) and anti-inflammatory and chondroprotective (IL-4, IL-10, lubricin) biomarkers in the synovium of an OA-induced rat model. A total of 32 rats were divided into four groups: Control rats (Group 1); rats performing MPA (Group 2); anterior cruciate ligament transection (ACLT)-rats with OA (Group 3); and, ACLT-rats performing MPA (Group 4). Analyses were performed using Hematoxylin & Eosin (H&E) staining, histomorphometry and immunohistochemistry. In Group 3, OA biomarkers were significantly increased, whereas, IL-4, IL-10, and lubricin were significantly lower than in the other experimental groups. We hypothesize that MPA might partake in rescuing type B synoviocyte dysfunction at the early stages of OA, delaying the progression of the disease.

Morphological Evidence of Telocytes in Skeletal Muscle Interstitium of Exercised and Sedentary Rodents

Skeletal muscle atrophy, resulting from states of hypokinesis or immobilization, leads to morphological, metabolic, and functional changes within the muscle tissue, a large variety of which are supported by the stromal cells populating the interstitium. Telocytes represent a recently discovered population of stromal cells, which has been increasingly identified in several human organs and appears to participate in sustaining cross-talk, promoting regenerative mechanisms and supporting differentiation of local stem cell niche. The aim of

this morphologic study was to investigate the presence of Telocytes in the tibialis anterior muscle of healthy rats undergoing an endurance training protocol for either 4 weeks or 16 weeks compared to sedentary rats. Histomorphometric analysis of muscle fibers diameter revealed muscle atrophy in sedentary rats. Telocytes were identified by double-positive immunofluorescence staining for CD34/CD117 and CD34/vimentin. The results showed that Telocytes were significantly reduced in sedentary rats at 16 weeks, while rats subjected to regular exercise maintained a stable Telocytes population after 16 weeks. Understanding of the relationship between Telocytes and exercise offers new chances in the field of regenerative medicine, suggesting possible triggers for Telocytes in sarcopenia and other musculoskeletal disorders, promoting adapted physical activity and rehabilitation programmes in clinical practice.

1.3. General conclusions

Traditional treatments for OA involving the use of non-steroidal anti-inflammatory drugs (NSAID) and opioids are effective as pain reliefers but fail in restoring tissue degeneration and commonly present several adverse events. Current efforts in scientific research of OA are devolved to understanding the morpho-molecular mechanisms and pathophysiological changes occurring in the tissue, in order to plan future preventive measure and treatments for this complex and spreading disease. Regenerative engineering for cartilage, in the means of use of MSCs, scaffolds and functional biomolecules, is emerging as a promising alternative and solution to tissue defects for the support of neocartilage formation. Nevertheless, application of engineered structures deals with phenotypic instability of the cells in long-term cultures and, consequently, poor neo-tissue morphological properties. For this reason, in the first presented study, our work was addressed to improve chondrogenic properties of the cells differentiated from MSCs. The results demonstrated that CAG was able to maintain a stable phenotype of the chondrocyte, enhanced metabolic activity and cartilaginous ECM deposition and increased lubricin expression, up to 28 days of 3D in vitro culture of hMSCs. Therefore, it is here proposed that CAG might have a beneficial impact on future approaches for cartilage regeneration. Similarly, other molecules investigated in literature have demonstrated to improve in vitro culture, therefore their presence should be considered when designing tissue engineering constructs. In the second study the collagen I-based scaffolds were confirmed to be biocompatible by histological, histochemical, immunohistochemical and gene expression analysis, as suggested by total biodegradation and replacement of the biomaterial with the newly formed cartilage-like tissue at 16-weeks post-implantation, and absence of scar-like tissue formation and inflammatory cell infiltration at the interface between the scaffold and peri-native cartilage tissue. Therefore, it is proposed that this scaffold could offer a promising tool for cartilage tissue engineering and repair approaches, also in absence of external source of progenitor cells. As already stated, tissue damage depends on impaired balance between anabolic and catabolic processes, which can be influenced by dietary compounds like nutraceuticals with anti-inflammatory and antioxidant activities. Due to their minimal side effects, low costs, and easy availability in nature, they may represent a valid preventive measure against OA. The third study investigated the influence of introducing Vit D supplementation in the daily diet in standard health conditions,

supporting the use of functional foods beneficial for articular cartilage, especially during the developmental period in young age. Diet supplemented with Vit D leads to thicker tibial cartilage and to higher expression of the glycoprotein lubricin, supporting its beneficial effect on morphology/physiology of the articular cartilage. The clinical relevance of study could be recognized considering this supplementation as a non-pharmacological treatment in early osteoarthritic patients with a non-established diagnosis. Also regarding to prevention, the benefits of MPA in OA patients have demonstrated to exert protective effect on joints as a non-surgical and non-pharmacological treatment, re-establishing the physiological function of cell populations, preventing the onset of OA, and/or postponing the need for joint replacement. The purpose of fourth study was to investigate the influence of MPA on the expression of OA-related biomarkers as well as anti-inflammatory and chondroprotective markers by synoviocytes type B in OA rat model, which are involved in the production of hyaluronic acid. The MPA-based approach stimulates joint tribology and synovial lubrication, aiming at improving joint function and providing pain relief. Based on fact that OA animals that were not performing exercise showed significantly increased OA biomarkers, whereas significantly lower IL-4, IL-10, and lubricin, our resulting hypothesis is that the adapted MPA may counteract synoviocyte Type B dysfunction at the early stages of OA, impeding progression of OA. Finally, last morphological study was intended to observe the presence of telocytes in tibialis anterior muscle of healthy rats who underwent a protocol of endurance training. The understanding of the mechanisms between the cells involved in the muscle tissue remodeling offers new chances in regenerative tissue strategies and insights about finding triggers in sarcopenia and other musculoskeletal disorders like OA that are affected by muscle integrity. Exercise training has been shown to sustaining muscle maintenance of telocytes, therefore promoting adapted physical activity and rehabilitation programmes for healthy subjects and OA patients. The therapeutic and preventive approaches for OA still represent a difficult challenge for the clinical and scientific research fields. In conclusion, the present research project highlights some potential useful aspects concerning tissue engineering strategies and preventive methods aimed, respectively, to resolve and avoid osteoarthritic disease and cartilage degeneration.

1.4. References

1. Sophia Fox, A. J.; Bedi, A.; Rodeo, S. A. The basic science of articular cartilage: structure, composition, and function. *Sports health*, **2009**, 1(6), 461–468.
2. Bhosale, A.M.; Richardson, J.B. Articular cartilage: structure, injuries and review of management, *British Medical Bulletin*, **2008**, 87(1), 77–95.
3. Carballo, C. B.; Nakagawa, Y.; Sekiya, I.; Rodeo, S. A. Basic Science of Articular Cartilage. *Clinics in sports medicine*, **2017**, 36(3), 413–425.
4. Knudson, C. B.; Knudson, W. Cartilage proteoglycans. *Seminars in cell developmental biology*, **2001**, 12(2), 69–78.
5. Eyre, D. Collagen of articular cartilage. *Arthritis research*, **2002**, 4(1), 30–35.
6. Somoza, R. A.; Welter, J. F.; Correa, D.; Caplan, A. I. Chondrogenic differentiation of mesenchymal stem cells: challenges and unfulfilled expectations. *Tissue engineering. Part B, Reviews*, **2014**, 20(6), 596–608.
7. Terry, D. E.; Chopra, R. K.; Ovenden, J.; Anastassiades, T. P. Differential use of Alcian blue and toluidine blue dyes for the quantification and isolation of anionic glycoconjugates from cell cultures: application to proteoglycans and a high-molecular-weight glycoprotein synthesized by articular chondrocytes. *Analytical biochemistry*, **2000**, 285(2), 211–219.
8. Rolauffs, B.; Williams, J. M.; Grodzinsky, A. J.; Kuettner, K. E.; Cole, A. A. Distinct horizontal patterns in the spatial organization of superficial zone chondrocytes of human joints. *Journal of structural biology*, **2008**, 162(2), 335–344.
9. Poole, A. R.; Kojima, T.; Yasuda, T.; Mwale, F.; Kobayashi, M.; Laverty, S. Composition and structure of articular cartilage: a template for tissue repair. *Clinical orthopaedics and related research*, **2001**, (391 Suppl), S26–S33.
10. Wang, Y.; Wei, L.; Zeng, L.; He, D.; Wei, X. Nutrition and degeneration of articular cartilage. *Knee surgery, sports traumatology, arthroscopy: official journal of the ESSKA*, **2013**, 21(8), 1751–1762.
11. Pap, T.; Dankbar, B.; Wehmeyer, C.; Korb-Pap, A.; Sherwood, J. Synovial fibroblasts and articular tissue remodelling: Role and mechanisms. *Seminars in cell developmental biology*, **2020**, 101, 140–145.
12. Mobasheri, A.; Lewis, R.; Maxwell, J. E.; Hill, C.; Womack, M.; Barrett-Jolley, R. Characterization of a stretch-activated potassium channel in chondrocytes. *Journal of cellular physiology*, **2010**, 223(2), 511–518.
13. Heijink, A.; Gomoll, A. H.; Madry, H.; Drobnič, M.; Filardo, G.; Espregueira-Mendes, J.; Van Dijk, C. N. Biomechanical considerations in the pathogenesis of osteoarthritis of the knee. *Knee surgery, sports traumatology, arthroscopy: official journal of the ESSKA*, **2012**, 20(3), 423–435.
14. Wojdasiewicz, P.; Poniatowski, Ł. A.; Szukiewicz, D. The role of inflammatory and anti-inflammatory cytokines in the pathogenesis of osteoarthritis. *Mediators of inflammation*, **2014**, 561459.
15. Xia, B.; Di Chen, Zhang, J.; Hu, S.; Jin, H.; Tong, P. Osteoarthritis pathogenesis: a review of molecular mechanisms. *Calcified tissue international*, **2014**, 95(6), 495–505.
16. Sacitharan P. K. Ageing and Osteoarthritis. *Sub-cellular biochemistry*, **2019**, 91, 123–159.
17. Shane Anderson, A.; Loeser, R. F. Why is osteoarthritis an age-related disease? Best practice research. *Clinical rheumatology*, **2010**, 24(1), 15–26.
18. Van Spil, W. E.; Kubassova, O.; Boesen, M.; Bay-Jensen, A. C.; Mobasheri, A. Osteoarthritis phenotypes and novel therapeutic targets. *Biochemical pharmacology*, **2019**, 165, 41–48.
19. Geyer, M.; Schönfeld, C. Novel Insights into the Pathogenesis of Osteoarthritis. *Current rheumatology reviews*, **2018**, 14(2), 98–107.
20. Mobasheri, A.; Rayman, M. P.; Gualillo, O.; Sellam, J.; van der Kraan, P.; Fearon, U. (2017). The role of metabolism in the pathogenesis of osteoarthritis. *Nature reviews. Rheumatology*, **2017**, 13(5), 302–311.
21. Dieppe, P. A.; Lohmander, L. S. Pathogenesis and management of pain in osteoarthritis. *Lancet (London, England)*, **2005**, 365(9463), 965–973.
22. Lambova, S. N.; Müller-Ladner, U. Osteoarthritis - Current Insights in Pathogenesis, Diagnosis and Treatment. *Current rheumatology reviews*, **2018**, 14(2), 91–97.
23. Abramoff, B.; Caldera, F. E. Osteoarthritis: Pathology, Diagnosis, and Treatment Options. *The Medical clinics of North America*, **2020**, 104(2), 293–311.

24. Szychlinska, M.A.; Castrogiovanni, P.; Nsir, H.; Di Rosa, M.; Guglielmino, C.; Parenti, R.; Calabrese, G.; Pricoco, E.; Salvatorelli, L.; Magro, G.; et al. Engineered cartilage regeneration from adipose tissue derived-mesenchymal stem cells: A morphomolecular study on osteoblast, chondrocyte and apoptosis evaluation. *Exp. Cell. Res*. **2017**, 357, 222–235.
25. Rosenbaum, A.J.; Grande, D.A.; Dines, J.S. The use of mesenchymal stem cells in tissue engineering: A global assessment. *Organogenesis* **2008**, 4, 23–27.
26. Grassel, S. Influence of cellular microenvironment and paracrine signals on chondrogenic differentiation. *Front. Biosci.,* **2007**, 12(12), 4946.
27. Bonyadi Rad, E.; Musumeci, G.; Pichler, K.; Heidary, M.; Szychli-_nska, M.A.; Castrogiovanni, P.; Marth, E.; Böhm, C.; Srinivasaiah, S.; Krönke, G.; Weinberg, A.; Schäfer, U. Runx2 mediated Induction of novel targets ST2 and Runx3 leads to cooperative regulation of hypertrophic differentiation in ATDC5 chondrocytes. *Sci. Rep.,* **2017**, 7(1), 17947.
28. Jiang, X.; Huang, X.; Jiang, T.; Zheng, L.; Zhao, J.; Zhang, X. The role of Sox9 in collagen hydrogel-mediated chondrogenic differentiation of adult mesenchymal stem cells (MSCs). *Biomater. Sci.,* **2018**, 6(6), 1556-1568.
29. Almalki, S.G.; Agrawal, D.K. Key transcription factors in the differentiation of mesenchymal stem cells. *Differentiation*, **2016**, 92(1-2), 41-51.
30. López-Ruiz, E.; Jiménez, G.; Kwiatkowski, W.; Montañez, E.; Arrebola, F.; Carrillo, E.; Choe, S.; Marchal, J.A.; Perán, M. Im-_pact of TGF-β family-related growth factors on chondrogenic differentiation of adipose-derived stem cells isolated from lipoaspirates and infrapatellar fat pads of osteoarthritic patients. *Eur. Cells Mater.,* **2018**, 35, 209-224.
31. Vater, C.; Kasten, P.; Stiehler, M. Culture media for the differentia-_tion of mesenchymal stromal cells. *Acta Biomater*., **2011**, 7(2), 463-477.
32. Schmidt, M.B.; Chen, E.H.; Lynch, S.E. A review of the effects of insulin-like growth factor and platelet derived growth factor on in vivo cartilage healing and repair. Osteoarthritis cartilage. *Os-_teoarthritis Cartilage*, **2006**, 14(5), 403-412.
33. Gugjoo, M.B.; Amarpal; Abdelbaset-Ismail, A.; Aithal, H.P.; Kin-_javdekar, P.; Pawde, A.M.; Kumar, G.S.; Sharma, G.T. Mesenchymal stem cells with IGF-1 and TGF- β1 in laminin gel for oste-_ochondral defects in rabbits. *Biomed. Pharmacother.,* **2017**, 93, 1165-1174.
34. Ellman, M.B.; An, H.S.; Muddasani, P.; Im, H.J. Biological impact of the fibroblast growth factor family on articular cartilage and intervertebral disc homeostasis. *Gene*, **2008**, 420(1), 82-89.
35. Bae, H.C; Park, H.J.; Wang, S.Y.; Yang, H.R.; Lee, M.C.; Han, H.S. Hypoxic condition enhances chondrogenesis in synovium-derived mesenchymal stem cells. *Biomater Res*., **2018**, 26, 22-28.
36. Jeng, L.; Olsen, B.R.; Spector, M. Engineering endostatin-_producing cartilaginous constructs for cartilage repair using nonviral transfection of chondrocyte-seeded and mesenchymal-_stem-cell-seeded collagen scaffolds. *Tissue Eng. Part A.,* **2010**, 16(10), 3011-3021.
37. Emans, P.J.; van Rhijn, L.W.; Welting, T.J.M.; Cremers, A.; Wijnands, N.; Spaapen, F.; Voncken, J.W.; Shastri, V.P. Autolo-_gous engineering of cartilage. *Proc. Natl. Acad. Sci.,* **2010**, 107(8), 3418-3423.
38. Matsumoto, T.; Cooper, G.M.; Gharaibeh, B.; Meszaros, L.B.; Li, G.; Usas, A.; Fu, F.H.; Huard, J. Cartilage repair in a rat model of osteoarthritis through intraarticular transplantation of muscle-_derived stem cells expressing bone morphogenetic protein 4 and soluble Flt-1. *Arthritis Rheum.,* **2009**, 60(5), 1390-1405.
39. Nagai, T.; Sato, M.; Kutsuna, T.; Kokubo, M.; Ebihara, G.; Ohta, N.; Mochida, J. Intravenous administration of anti-vascular endothelial growth factor humanized monoclonal antibody bevacizumab improves articular cartilage repair. *Arthritis Res. Ther*., **2010**, 12(5), R178.
40. Chen, P.; Tao, J.; Zhu, S.; Cai, Y.; Mao, Q.; Yu, D.; Dai, J.; Ouyang, H.W. Radially oriented collagen scaffold with SDF-1 promotes osteochondral repair by facilitating cell homing. *Biomaterials*, **2015**, 39, 114-123.
41. Orth, P.; Cucchiarini, M.; Zurakowski, D.; Menger, M.D.; Kohn, D.M.; Madry, H. Parathyroid hormone improves articular cartilage surface architecture and integration and subchondral bone reconsti-_tution in osteochondral defects in vivo. *Osteoarthr. Cartil.,* **2013**, 21(4), 614-624.
42. Zhang, W.; Chen, J.; Tao, J.; Hu, C.; Chen, L.; Zhao, H.; Xu, G.; Heng, B.C.; Ouyang, H.W. The promotion of osteochondral repair by combined intra-articular injection of parathyroid hormone-_related protein and implantation of a bi-layer collagen-silk scaffold. *Scaffold Biomat.,* **2013**, 34(25), 6046-6057.
43. Dang, A.C.; Warren, A.P.; Kim, H.T. Beneficial effects of intra-_articular caspase inhibition therapy following osteochondral injury. *Osteoarthr. Cartil.,* **2006**, 14(6), 526-532.

44. Gilbert, S.J.; Singhrao, S.K.; Khan, I.M.; Gonzalez, L.G.; Thom- son, B.M.; Burdon, D.; Duance, V.C.; Archer, C.W. Enhanced tissue integration during cartilage repair in vitro can be achieved by inhibiting chondrocyte death at the wound edge. *Tissue Eng. Part A*, **2009**, 15(7), 1739-1749.
45. Yamamoto, A.; Warren, A.P.; Kim, H.T. Minocycline reduces articular cartilage damage following osteochondral injury. *Knee*, **2012**, 19(5), 680-683.
46. Chen, P.; Zhu, S.; Wang, Y.; Mu, Q.; Wu, Y.; Xia, Q.; Zhang, X.; Sun, H.; Tao, J.; Hu, H.; Lu, P.; Ouyang, H. The amelioration of cartilage degeneration by ADAMTS-5 inhibitor delivered in a hyaluronic acid hydrogel. *Biomaterials*, **2014**, 35(9), 2827-2836.
47. Ashammakhi, N.; Ahadian, S.; Darabi, M.A.; El Tahchi, M.; Lee, J.; Suthiwanich, K.; Sheikhi, A.; Dokmeci, M.R.; Oklu, R.; Khademhosseini, A. Minimally Invasive and Regenerative Therapeutics. *Adv. Mater*. **2018**, 31, 1804041.
48. Wang, Y.; Yuan, M.; Guo, Q.-Y.; Lu, S.-B.; Peng, J. Mesenchymal Stem Cells for Treating Articular Cartilage Defects and Osteoarthritis. *Cell. Transplant.* **2015**, 24, 1661–1678.
49. Li, L.; Duan, X.; Fan, Z.; Chen, L.; Xing, F.; Xu, Z.; Chen, Q.; Xiang, Z. Mesenchymal Stem Cells in Combination with Hyaluronic Acid for Articular Cartilage Defects. *Sci. Rep.* **2018**, 8, 9900.
50. ter Huurne, M.; Schelbergen, R.; Blattes, R.; Blom, A.; de Munter, W.; Grevers, L.C.; Jeanson, J.; Noël, D.; Casteilla, L.; Jorgensen, C.; et al. Antiinflammatory and chondroprotective effects of intraarticular injection of adipose-derived stem cells in experimental osteoarthritis. *Arthritis Rheum.* **2012**, 64, 3604–3613.
51. Vega, A.; Martín-Ferrero, M.A.; Del Canto, F.; Alberca, M.; García, V.; Munar, A.; Orozco, L.; Soler, R.; Fuertes, J.J.; Huguet, M.; et al. Treatment of Knee Osteoarthritis With Allogeneic Bone Marrow Mesenchymal Stem Cells: A Randomized Controlled Trial. *Transplantation* **2015**, 99, 1681–1690.
52. Pas, H.I.; Winters, M.; Haisma, H.J.; Koenis, M.J.; Tol, J.L.; Moen, M.H. Stem cell injections in knee osteoarthritis: A systematic review of the literature. *Br. J. Sports Med*. **2017**, 51, 1125–1133.
53. Zwolanek, D.; Satué, M.; Proell, V.; Godoy, J.R.; Odörfer, K.I.; Flicker, M.; Hoffmann, S.C.; Rülicke, T.; Erben, R.G. Tracking mesenchymal stem cell contributions to regeneration in an immunocompetent cartilage regeneration model. *JCI Insight* **2017**, 2, 87322.
54. Satué, M.; Schüler, C.; Ginner, N.; Erben, R.G. Intra-articularly injected mesenchymal stem cells promote cartilage regeneration, but do not permanently engraft in distant organs. *Sci. Rep.* **2019**, 9, 10153.
55. Enomoto, T.; Akagi, R.; Ogawa, Y.; Yamaguchi, S.; Hoshi, H.; Sasaki, T.; Sato, Y.; Nakagawa, R.; Kimura, S.; Ohtori, S.; et al. Timing of Intra-Articular Injection of Synovial Mesenchymal Stem Cells Affects Cartilage Restoration in a Partial Thickness Cartilage Defect Model in Rats. *Cartilage* **2020**, 11, 122–129.
56. Musumeci, G.; Loreto, C.; Castorina, S.; Imbesi, R.; Leonardi, R.; Castrogiovanni, P. New perspectives in the treatment of cartilage damage. Poly(ethylene glycol) diacrylate (PEGDA) scaffold. *A review. Ital. J. Anat. Embryol.*, **2013**, 118(2), 204-210.
57. Szychlinska, M.A.; Stoddart, M.J.; D'Amora, U.; Ambrosio, L.; Alini, M.; Musumeci, G. Mesenchymal stem cell-based cartilage regeneration approach and cell senescence: Can we manipulate cell aging and function? *Tissue Eng. Part B Rev*., **2017**, 23(6), 29-539.
58. Cheng, D.S.; Visco, C.J. Pharmaceutical therapy for osteoarthritis. *PM R* **2012**; 4: S82-S88
59. Musumeci, G.; Mobasheri, A.; Trovato, F.M.; Szychlinska, M.A.; Imbesi, R.; Castrogiovanni, P. Post-operative rehabilitation and nutrition in osteoarthritis. *F1000Res* **2014**; 3: 116
60. Akhtar, N.; Haqqi, T.M. Current nutraceuticals in the management of osteoarthritis: a review. *Ther Adv Musculoskelet Dis* **2012**; 4: 181-207
61. Petrovska, B.B. Historical review of medicinal plants' usage. *Pharmacogn Rev* **2012**; 6: 1-5
62. Dervendzi, V. Contemporary treatment with medicinal plants. *Skopje: Tabernakul* **1992**; 5-43.
63. Castrogiovanni, P.; Trovato, F.M.; Loreto, C.; Nsir, H.; Szychlinska, M.A.; Musumeci, G. Nutraceutical Supplements in the Management and Prevention of Osteoarthritis. *Int J Mol Sci* **2016**; 17
64. Finley, J.W.; Finley, J.W.; Ellwood, K.; Hoadley, J. Launching a new food product or dietary supplement in the United States: industrial.; regulatory.; and nutritional considerations. *Annu Rev Nutr* **2014**; 34: 421-447
65. Gulati, O.P.; Berry Ottaway, P. Legislation relating to nutraceuticals in the European Union with a particular focus on botanical-sourced products. *Toxicology* **2006**; 221: 75-87
66. Zhang, W.; Moskowitz, R.W.; Nuki, G.; Abramson, S.; Altman, R.D.; Arden, N.; Bierma-Zeinstra, S.; Brandt, K.D.; Croft, P.; Doherty, M.; Dougados, M.; Hochberg, M.; Hunter, D.J.; Kwoh, K.;

Lohmander, L.S.; Tugwell, P. OARSI recommendations for the management of hip and knee osteoarthritis.; part I: critical appraisal of existing treatment guidelines and systematic review of current research evidence. *Osteoarthritis Cartilage* **2007**; 15: 981-1000
67. Musumeci, G.; Carnazza, M.L.; Loreto, C.; Leonardi, R.; Loreto, C. β-Defensin-4 (HBD-4) is expressed in chondrocytes derived from normal and osteoarthritic cartilage encapsulated in PEGDA scaffold. *Acta Histochem* **2012**; 114: 805-812
68. Musumeci, G.; Loreto, C.; Imbesi, R.; Trovato, F.M.; Di Giunta, A.; Lombardo, C.; Castorina, S.; Castrogiovanni, P. Advantages of exercise in rehabilitation.; treatment and prevention of altered morphological features in knee osteoarthritis. A narrative review. *Histol Histopathol* **2014**; 29: 707-719
69. Castrogiovanni, P.; Di Rosa, M.; Ravalli, S.; Castorina, A.; Guglielmino, C.; Imbesi, R.; Vecchio, M.; Drago, F.; Szychlinska, M.A.; Musumeci, G. Moderate Physical Activity as a Prevention Method for Knee Osteoarthritis and the Role of Synoviocytes as Biological Key. *Int J Mol Sci* **2019**; 20: pii: E511
70. Di Rosa, M.; Castrogiovanni, P.; Musumeci, G. The Synovium Theory: Can Exercise Prevent Knee Osteoarthritis? The Role of "Mechanokines".; A Possible Biological Key. *J Funct Morphol Kinesiol* **2019**;4: 11
71. Musumeci, G.; Castrogiovanni, P.; Trovato, F.M.; Imbesi, R.; Giunta, S.; Szychlinska, M.A.; Loreto, C.; Castorina, S.; Mobasheri, A. Physical activity ameliorates cartilage degeneration in a rat model of aging: a study on lubricin expression. *Scand J Med Sci Sports* **2015**; 25: e222-e230
72. Szychlinska, M.A.; Castrogiovanni, P.; Trovato, F.M.; Nsir, H.; Zarrouk, M.; Lo Furno, D.; Di Rosa, M.; Imbesi, R.; Musumeci, G. Physical activity and Mediterranean diet based on olive tree phenolic compounds from two different geographical areas have protective effects on early osteoarthritis.; muscle atrophy and hepatic steatosis. *Eur J Nutr* **2019**; 58: 565-581
73. Musumeci, G. Effects of exercise on physical limitations and fatigue in rheumatic diseases. *World J Orthop* **2015**; 6: 762-769
74. Uthman, O.A.; van der Windt, D.A.; Jordan, J.L.; Dziedzic, K.S.; Healey, E.L.; Peat, G.M.; Foster, N.E. Exercise for lower limb osteoarthritis: systematic review incorporating trial sequential analysis and network meta-analysis. *BMJ* **2013**; 347: f5555
75. Castrogiovanni, P.; Musumeci, G. Which is the Best Physical Treatment for Osteoarthritis? *J Funct Morphol Kinesiol* **2016**; 1: 54-68
76. Gardner, O.F.W.; Musumeci, G.; Neumann, A.J.; Eglin, D.; Archer, C.W.; Alini, M.; Stoddart, M.J. Asymmetrical seeding of MSCs into fibrin-poly(ester-urethane) scaffolds and its effect on mechanically induced chondrogenesis. *J Tissue Eng Regen Med* **2017**; 11: 2912-2921
77. Musumeci, G.; Trovato, F.M.; Imbesi, R.; Castrogiovanni, P. Effects of dietary extra-virgin olive oil on oxidative stress resulting from exhaustive exercise in rat skeletal muscle: a morphological study. *Acta Histochem* **2014**; 116: 61-69
78. Bennell, K.L.; Hinman, R.S. A review of the clinical evidence for exercise in osteoarthritis of the hip and knee. *J Sci Med Sport* **2011**; 14: 4-9
79. Roddy, E.; Zhang, W.; Doherty, M.; Arden, N.K.; Barlow, J.; Birrell, F.; Carr, A.; Chakravarty, K.; Dickson, J.; Hay, E.; Hosie, G.; Hurley, M.; Jordan, K.M.; McCarthy, C.; McMurdo, M.; Mockett, S.; O'Reilly, S.; Peat, G.; Pendleton, A.; Richards, S. Evidence-based recommendations for the role of exercise in the management of osteoarthritis of the hip or knee--the MOVE consensus. *Rheumatology (Oxford)* **2005**; 44: 67-73
80. Gahunia H. K.; Pritzker, K. P. Effect of exercise on articular cartilage. *The Orthopedic clinics of North America*, **2012**; 43(2).; 187–v

2. CYCLOASTRAGENOL AS AN EXOGENOUS ENHANCER OF CHONDROGENIC DIFFERENTIATION OF HUMAN ADIPOSE-DERIVED MESENCHYMAL STEM CELLS. A MORPHOLOGICAL STUDY

Marta Anna Szychlinska[1], Giovanna Calabrese[2], Silvia Ravalli[1], Nunziatina Laura Parrinello[3], Stefano Forte[4], Paola Castrogiovanni[1], Elisabetta Pricoco[5], Rosa Imbesi[1], Sergio Castorina[6], Rosalia Leonardi[7], Michelino Di Rosa[1] and Giuseppe Musumeci[1,8,9,]*

[1]Department of Biomedical and Biotechnological Sciences, Anatomy, Histology and Movement Sciences Section, School of Medicine, University of Catania, 95123 Catania, Italy

[2]Department of Biomedical and Biotechnological Sciences, University of Catania, 95123 Catania, Italy

[3]Division of Hematology, AOU "Policlinico-Vittorio Emanuele", 95125 Catania, Italy

[4]IOM Ricerca, 95029 Viagrande, Italy

[5]Department of Medical and Surgical Sciences and Advanced Technologies, Anatomic Pathology Section, School of Medicine, University of Catania, 95124 Catania, Italy

[6]Department of Medical, Surgical and Advanced Technological Sciences "G.F. Ingrassia", University of Catania, 95124 Catania, Italy

[7]Department of General Surgery and Medical-Surgical Specialties, University of Catania, 95124 Catania, Italy

[8]Research Center on Motor Activities (CRAM), University of Catania, 95123 Catania, Italy

[9]Department of Biology, Sbarro Institute for Cancer Research and Molecular Medicine, College of Science and Technology, Temple University, Philadelphia, PA 19122, USA

[*]Author to whom correspondence should be addressed.

Cells 2020, 9(2), 347; DOI: 10.3390/cells9020347

2.1. Introduction

Articular cartilage shows poor regenerative properties, due to its alymphatic, avascular, aneural nature and the limited cellularity of the tissue, composed of chondrocytes sparsely embedded within the collagen and proteoglycan-based extracellular matrix (ECM) [1]. Changes in biomechanical and metabolic features of articular cartilage, related to aging or injury, lead to matrix degradation, resulting in progressive tissue degeneration and causing severe pain and disability of the joint. An inadequate tissue repair, followed by a progressive loss of cartilage and remodeling of the underlying subchondral bone, leads to osteoarthritis (OA), a very common form of severe degenerative articular cartilage disease [2]. OA is a multifactorial disease, but aging represents the most prominent risk factor contributing to its development. It has been shown that one of the most important age-related epigenetic factors associated with OA is accelerated telomere shortening [3]. The latter implies that OA chondrocytes lose their ability to synthesize matrix components and begin to synthesize proteins, which contribute to ECM degradation [4]. Current cartilage repair treatment approaches help to repair the articular cartilage lesions and reduce pain in affected joints, but only to some degree and are considered ineffective [5,6]. The limitations of cartilage repair itself, coupled with inadequate clinical strategies and rising incidence rates of OA, have compelled cell-based therapies for sustained recovery of the functional properties of native tissue [7]. Mesenchymal stem cells (MSCs) have emerged as a promising cell source for cartilage repair. Major advantages of using MSCs for cartilage regeneration are due to their easy availability, proliferative capacity, and multilineage potency [7,8]. However, the current cartilage engineering techniques still present limitations for clinical application. The major challenges are represented by phenotypic instability after implantation, poor integration into cartilage defects and the surrounding tissues, and the insufficient mechanical properties of the engineered cartilage that do not replicate the properties of the native tissue. Accumulating data from literature demonstrated that during long-term culture, MSCs undergo spontaneous transformation, showing typical features of senescence, including the premature and progressive telomere shortening, which results in cell loss and impaired regenerative potential [9]. These features resemble a similar pattern activated in chondrocytes, leading to OA development, as stated above. Moreover, inflammation in the osteoarthritic joints is another barrier to overcome for successful cartilage repair. MSC behavior can be influenced

by multiple exogenous microenvironmental stimuli that act as chondrogenic inducers [10,11]. As an external signal, the mechanical forces represent an important modulator of the native articular cartilage metabolic activities and serve to maintain the cartilage homeostasis [12]. Bioactive molecules are other chondrogenesis-enhancing factors. Among these, transforming growth factor-βs (TGF-βs), insulin-like growth factor-I (IGF-I), fibroblast growth factor (FGF) and bone morphogenetic proteins (BMPs) are reported to stimulate the proteoglycan synthesis, improve the repair of osteochondral defects, and enhance the MSC-based chondrogenesis. In addition, cell–cell and cell–ECM interactions and adhesion properties are crucial for maintaining cell phenotype and for inducing effective MSC-chondrogenesis [1]. 3D cell culture methods facilitate these interactions, allowing cells to create an "in vivo-like" microenvironment and better preserve the stem cell phenotype and to reproduce the native tissue morphology [13,14]. Native hyaline cartilage development starts with the migration and condensation of mesenchymal progenitor cells differentiating into active chondrocytes [15]. Cartilage formation from self-assembling MSCs in vitro recapitulates important cellular events during mesenchymal condensation that precedes native cartilage development. In pellet culture, cells form spherical aggregates that deposit matrix and grow over time [16–19]. Cycloastragenol (CAG) is a triterpenoid saponin compound and a hydrolysis product of astragaloside IV, the main active ingredient of Astragalus membranaceus Bunge (Leguminosae). It has been used for centuries as an important medicine to reinforce vital energy, strengthen superficial resistance and promote the growth of new tissues. An increasing body of evidence indicates that CAG has a wide spectrum of pharmacological functions such as wound healing, and anti-apoptotic and anti-tumor activities, which are attracting attention in the research community [20–22]. Among the most interesting pharmacological effects of CAG, that catch attention as a potential chondrogenic enhancer and anti-osteoarthritic molecule, are represented by telomerase activation, telomere elongation, and anti-inflammatory and anti-oxidative properties [23]. In addition, CAG has been proven to possess anti-arthritic properties and to suppress joint inflammation via the inhibition of IL 1β, TNF α, and iNOS production in the arthritis rat model [24–27]. For these reasons, the present study aimed to investigate, for the first time in literature, the effects of CAG on chondrogenic differentiation of human adipose-derived MSCs (hAMSCs) cultured as self-assembling 3D spherical aggregates, in terms of

maintenance of stable chondrocyte phenotype, anti-hypertrophic property, and ECM component deposition.

2.2. Materials and Methods

2.2.1. Cycloastragenol

Cycloastragenol (CAG) (purity ≥ 98%) was purchased from Sigma-Aldrich (St. Louis, MO, USA). The CAG powder has been dissolved in dimethyl sulfoxide (DMSO) to make stock solutions and then it has been stored at −20 °C.

2.2.2. Cell Culture and Phenotypic

Characterization Three human visceral adipose tissue biopsies of 10–15 g of weight, harvested from three different donors (two women aged 52 and 56, and one man aged 54), have been used in the present study to isolate hAMSCs, as previously reported [28]. The samples have been supplied by the Mediterranean Institute of Oncology (IOM) (Viagrande, Italy) under an approved Institutional Review Board protocol (project ID code: 829_1 of 8 February 2013, IOM Institutional Review Board). The hAMSCs were characterized by flow cytometry and immunofluorescence analyses using positive (CD105 and CD90), and negative (CD45 and CD34) mesenchymal stem cells surface markers. For flow cytometry, cells (80% of confluence) were detached with 0.05% trypsin/EDTA and washed in PBS 1X. 1×10^4 cells/tube were stained with the following antibodies: CD105 PE (clone1G2), CD90 FITC (clone F15.42.1.5), CD45 FITC (clone J.33), CD34 PE (clone 581), and respective isotopic controls according to manufacturer indications. All antibodies were purchased from Beckman Coulter (Milano, Italy). All tubes were incubated in the dark for 20 min at room temperature. Cells were then washed with PBS 1X and finally analyzed by flow cytometry using an FC-500 five-color flow cytometer (Beckman Coulter, Pasadena, CA, USA). For each tube, 1000 events were acquired. CXP Analysis software (Beckman Coulter, Inc.) was used for data analysis. Immunofluorescence analysis was assessed on hAMSCs seeded in eight-well BD Falcon culture slides at the density of 5×10^3 cells/cm^2. hAMSCs were fixed in 4% paraformaldehyde (PFA), permeabilized in 0.4% Triton and then blocked by incubation in 5% goat serum for 1 h. The primary incubation was assessed with the following anti-human antibodies: mouse CD105 (1:50, Novus Biologicals, Littleton, CO, USA), mouse CD90 (1:50, Santa Cruz Biotechnology, Dallas, TX, USA), rabbit CD45 (1:100, Epitomics, Burlingame, CA, USA), and rabbit CD34 (1:100, Epitomics) overnight at 4 °C. The following day slides were washed and incubated with the appropriate secondary AlexaFluor antibodies (1:2000, LifeTechnologies Italia, Monza, Italy) for 2 h at room temperature. Nuclei were counterstained with DAPI (1:5000) for 5 min. Finally, slides were mounted in fluorescent mounting medium Permafluor (Thermo Scientific, Waltham, MA, USA) and images were acquired using a Leica DMI4000B fluorescence microscope (Leica, Wetzlar, Germany).

2.2.3. CAG Cytotoxicity Assay

CAG cytotoxicity for hAMSCs was assessed by the MTT assay (Roche Life Science), which measures the conversion of 3-[4,5-dimethylthiazol-2-yl]-2,5 diphenyl tetrazolium bromide to formazan crystals by living cells, which process determines the mitochondrial activity that can be photometrically detected (492 nm). The hAMSCs were seeded at 1×10^4 cells/cm^2 in flat-bottomed 96-well plates, in 100 µL of basal culture medium (DMEM, low-glucose, Carlo Erba, Milan, Italy) with 2 mM L-glutamine, 1% pen/strep and 10% Fetal Bovine Serum. After 24 h, cells were cultured in different conditions: (1) basal medium and (2) basal medium supplemented with different concentrations of CAG (0.1/0.1/1/10/25 µM). To obtain CAG solutions at micromolar concentrations the CAG–DMSO stock solution has been highly diluted in basal medium (1:800–1:2000). The metabolic activity was then assessed by MTT conversion for 24 and 48 h. A blank control comprising the only medium was also included. For each measurement, three replicates per condition were included.

2.2.4. Three-Dimensional Pellet Cultures of hAMSCs

2.5×10^5 hAMSCs/tube/mL were seeded in 2.5 mL polypropylene tubes. Cell pellets were formed by centrifugation (390×g for 5 min) and cultured in basal medium (BM)—Dulbecco's Modified Eagle's Medium (DMEM, low-glucose, Carlo Erba, Milan, Italy) with 2 mM L-glutamine, 1% pen/strep and 10% Fetal Bovine Serum (BSA), in a CO2 incubator at 37°C. Tube lids were loosely maintained on top of each tube to allow gas exchange. After 24 h, the pellets were cultured in different conditions in triplicate: (1) chondrogenic medium (CM), MSC chondrogenic differentiation medium, (PromoCell, Heidelberg, Germany); (2) CM supplemented with CAG (0.1 µM), for 7, 14, 21, and 28 days. The media were changed twice per week during 28 days of culture.

2.2.5. Analysis of Pellet Size

The size of the pellets was analyzed at 7, 14, 21, and 28 days. The cellular pellets presented an ellipsoidal shape and their surface at different time points was calculated as follows: the histological sections (objective lens: 2.5×) of the middle part of pellets, stained by hematoxylin and eosin (H&E) have been used. The pellet surface has been calculated by using an image-analysis software (AxioVision Release 4.8.2-SP2 Software, Carl Zeiss Microscopy GmbH, Jena, Germany) and expressed in µm^2. Image analysis was performed on four pellets per condition.

2.2.6. Histological Analysis

At 7, 14, 21, and 28 days, cell pellets were harvested and histologically processed as previously described [29]. The pellets were rinsed in PBS, fixed in 10% buffered formalin (Bio-Optica, Milan, Italy). After an overnight wash, specimens were dehydrated in graded ethanol, cleared in xylene, and paraffin-embedded. After wax infiltration, pellets were orientated in the cassettes in the same direction. Sections (5 µm thick) were cut from

paraffin blocks using a rotary manual microtome (Leica RM2235, Milan, Italy), mounted on silane-coated slides (Menzel-Gläser, Braunschweig, Germany) and stored at room temperature. Afterwards, the sections were dewaxed in xylene, hydrated by graded ethanol, and stained by H&E to evaluate cell morphology and the presence or absence of morphological alterations. The slides were examined with a Zeiss Axioplan light microscope (Carl Zeiss, Oberkochen, Germany), and pictures were taken with a digital camera (AxioCam MRc5, Carl Zeiss, Oberkochen, Germany).

2.2.7. Analysis of sGAGs by Histochemistry

The sections were obtained as previously described. Alcian Blue (Bio-Optica, Milan, Italy) was used to assess synthesis of sulphated glycosaminoglycans (sGAGs) containing proteoglycans in cell pellets. The assessment was made by computerized densitometric measurements as reported below. The sections were examined with a Zeiss Axioplan light microscope (Carl Zeiss, Oberkochen, Germany) and photomicrographs were captured using a digital camera (AxioCam MRc5, Carl Zeiss, Oberkochen, Germany).

2.2.8. Immunohistochemistry

For immunohistochemical analysis, cell pellets were processed as previously described [30]. Briefly, the slides were dewaxed in xylene, hydrated using graded ethanols, and incubated for 30 min in 0.3% H2O2 /PBS to quench endogenous peroxidase activity before being rinsed for 20 min with PBS (Bio-Optica, Milan, Italy). The sections were heated (5 min × 3) in capped polypropylene slide-holders with citrate buffer—pH 6 (pH 6.0; Bio-Optica, Milan, Italy) or Tris-EDTA buffer (pH 8.0; Bio-Optica, Milan, Italy), using a microwave oven (750 W, LG Electronics Italia S.p.A., Milan, Italy) to unmask antigenic sites. Following antigenic retrieval, the sections were incubated overnight at 4°C with diluted rabbit polyclonal antibodies against type I collagen (ab34710; Abcam, Cambridge, UK), type II collagen (ab34712; Abcam, Cambridge, UK), and type X collagen (ab58632; Abcam, Cambridge, UK), rabbit monoclonal anti-SOX9 (ab185966; Abcam, Cambridge, UK), rabbit polyclonal anti-lubricin antibody (ab28484; Abcam, Cambridge, UK), and anti-aggrecan (ab3778; Abcam, Cambridge, UK) diluted 1:100 in PBS (Sigma-Aldrich, Milan, Italy). Immune complexes were then treated with biotinylated link antibodies (horseradish peroxidase polymer (HRP)-conjugated anti-rabbit and anti-mouse were used as secondary antibodies) and then detected with peroxidase-labelled streptavidin, both incubated for 10 min at room temperature (LSAB + System-HRP, K0690, Dako, Glostrup, Denmark). Immunoreactivity was visualized by incubating the sections for 2 min in 0.1% 3,3 0 -diaminobenzidine (DAB) (DAB substrate Chromogen System; Dako, Glostrup, Denmark). The sections were lightly counterstained with Mayer's hematoxylin (Histolab Products AB, Göteborg, Sweden), mounted in Glycerol Vinyl Alcohol (GVA) (Zymed Laboratories, San Francisco, CA, USA), observed with an Axioplan Zeiss light microscope (Carl Zeiss, Oberkochen, Germany), and photographed with a digital camera (AxioCam MRc5, Carl Zeiss, Oberkochen, Germany).

2.2.9. Computerised Densitometric Measurements and Image Analysis

Four pellets per group, the area of each of which was about 3,500,000 Pixel^2, were analyzed for histochemical evaluation of Alcian Blue staining, which detects mucosubstance content (GAGs) and to quantify the level of immunostaining of positive anti-Col I, anti-Col II, anti-Col X, anti-aggrecan, anti-SOX9, and anti-lubricin antibodies immunolabeling. It was used as an image-analysis software (AxioVision Release 4.8.2-SP2 Software, Carl Zeiss Microscopy GmbH, Jena, Germany), which quantifies the level of staining in the densitometric count (pixel^2) normalized to the area of each section expressed in pixel^2. Digital micrographs were taken using the Zeiss Axioplan light microscope (Carl Zeiss, Oberkochen, Germany), using a lens with a magnification of ×10, i.e., total magnification 100) fitted with a digital camera (AxioCam MRc5, Carl Zeiss, Oberkochen, Germany). Three blinded investigators (two anatomical morphologists and one histologist) made the evaluations that were assumed to be correct if the recorded values had no statistically significant difference. If disputes concerning interpretation occurred, a unanimous agreement was reached after sample re-evaluation.

2.2.10. Statistical Analysis

The statistical analysis was performed using GraphPad Instat ® Biostatistics version 3.0 software (GraphPad Software, Inc., La Jolla, CA, USA). Datasets were tested for normal distribution with the Kolmogorov–Smirnov test. All variables were normally distributed. Ordinary one-way-ANOVA (Tukey's multiple comparisons test) was used for comparisons between more than two groups. The p-values <0.05 were considered statistically significant; p-values >0.05 were considered not significant (ns). The data are presented as the mean ± SD.

2.3. Results

2.3.1. CAG Cytotoxicity in hAMSCs

The cytotoxicity of CAG in hAMSCs was addressed. The mitochondrial activity was evaluated through MTT assay during a 48 h period after CAG addition and compared with control cultures. The results show that CAG was not cytotoxic for hAMSCs at any of the selected concentrations (Figure 1B). CAG concentration was maintained at 0.1 µM to conduct the following study.

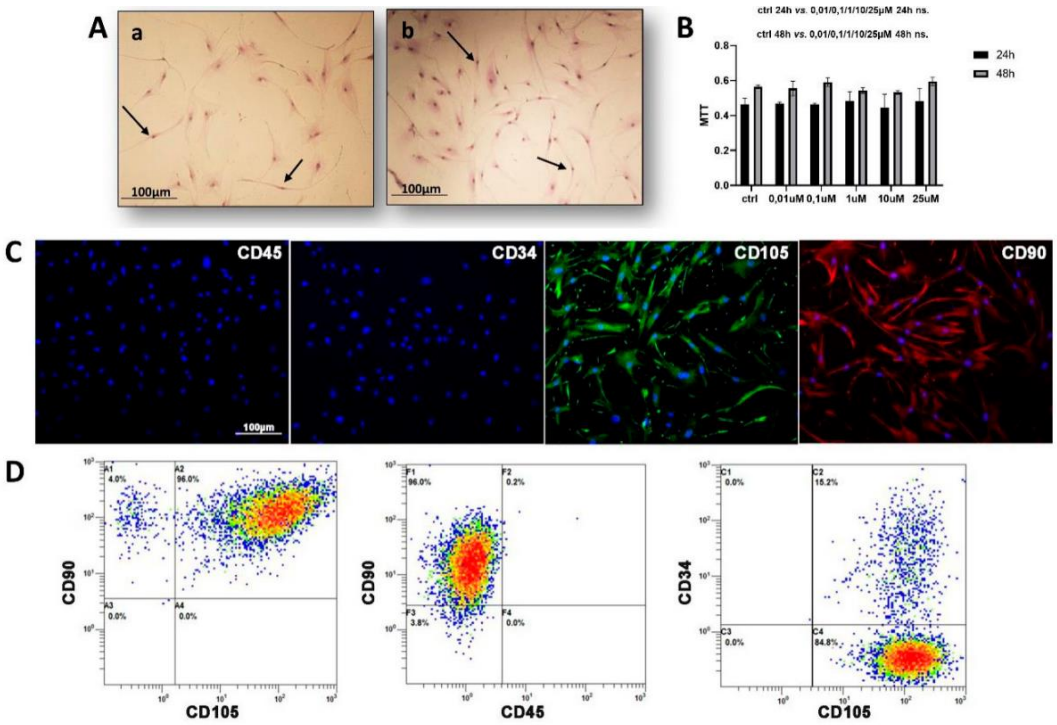

Figure 1. (A) The micrographs (a,b) of adipose tissue-derived mesenchymal stem cells (AMSCs) cultured in basal medium at different passages (Aa: p. 10; Ab: p. 12), evidenced by May–Grünwald Giemsa staining. The AMSCs show a characteristic fibroblast-like morphology (black arrows). Objective lens: 2.5×, scale bar: 100 µm. (B) Cycloastragenol (CAG) cytotoxicity for AMSCs cultured with basal medium (CTRL) and with different concentrations of CAG (0.01/0.1/1/10/25 µM), assessed by the MTT assay at 24 h and 48 h. See the Materials and Methods section for details. Results were presented as the mean ± SD. ANOVA was used to evaluate the significance of the results. (C) Phenotypic characterization of human AMSCs (hAMSCs) by immunofluorescence and (D) flow cytometry of negative hematopoietic markers (CD45 and CD34) and positive MSC surface markers (CD105 and CD90). In C) CD105 expression is stained in green and CD90 in red. The hAMSC nuclei are counterstained with DAPI (blue). Power magnification: 20×. Scale bar: 100 µm.

2.3.2. hAMSC Characterization

The images of hAMSCs at passages 10 (Figure 1Aa) and 12 (Figure 1Ab) cultured in BM and evidenced by May–Grünwald Giemsa staining, were analyzed. The cells showed a characteristic fibroblast-like morphology (Figure 1A), which represents their normal aspect in two-dimensional (2D) conditions. After isolation, immunofluorescence and flow cytometry analyses have been performed on hAMSCs using two negative (CD45 and CD34) and two positive (CD105 and CD90) MSC surface markers. The results of both analyses have

confirmed that hAMSCs were negative for CD34 and CD45, whereas they expressed high levels of CD105 and CD90 (Figure 1C,D).

2.3.3. Histological Analysis of hAMSC 3D Cell Pellets

To promote the production of cartilaginous ECM, the hAMSCs were cultured in three-dimensional (3D) conditions. After centrifugation, the hAMSCs were able to form cell aggregates (pellets) within 24 h. Subsequently, the pellets were switched and cultured in CM that served as a control and in CAG-supplemented CM (as described in the Materials and Methods section) during 28 days of culture. The H&E staining was used to observe the morphology of 3D hAMSCs after chondrogenic differentiation at different time points: 7, 14, 21, and 28 days, in the presence of CM (control, Figure 2A) and CAG-supplemented CM (Figure 2B). Our data show that the cells within the control pellets, after seven days of chondrogenic differentiation, are able to form aggregates and 3D structure, even if their internal organization is still disordered (Figure 2A). After 14 days, some cells within the pellets show the chondrocyte-like rounded morphology and the deposition of fibers parallel to the pellet surface (Figure 2A). At 21 days the cells are organized into columns that represent a continuum of chondrocyte differentiation and they are located into lacunae (Figure 2A). At 28 days of CM culture, the pellets show an involution activity represented by cell enlargement, indicative of hypertrophy and evident thickening of the external capsule (Figure 2A). In CAG-supplemented CM conditions (Figure 2B), the pellets at 7 and 14 days show a similar morphology relative to the seven-days control pellets (Figure 2B). At 21 days, the pellets show the cartilage-like morphology (Figure 2B). At 28 days of CAG–CM culture, the cells within the pellets seem to maintain their phenotypic stability, suggested by poor cellular hypertrophy phenomena (Figure 2B). Overall, CAG shows to increase cellular aggregation, exhibiting a cartilage tissue-like morphology up to 28 days of 3D culture. These results have been confirmed by the pellet size analysis (Figure 2C).

2.3.4. Analysis of sGAG Production by hAMSC 3D Pellet Cultures

To evaluate the effects of CAG on the production of cartilaginous matrix deposition and sGAG content, the pellet sections were analyzed through Alcian Blue staining after 7, 14, 21, and 28 days of CM culture with and without CAG supplementation. The sGAG deposition is represented as intense blue within pellet ECM. Experimental data obtained using image-

analysis software, which quantifies the level of Alcian Blue staining expressed as densitometric count (pixel^2)/area(pixel^2) report that the control pellets cultured in CM show a linear increase in sGAG deposition up to 21 days of culture (Figure 3A). At 28 days, a significant decrease ($p < 0.001$) in sGAG and ECM deposition is observed within the control pellets when compared to 21-day control pellets (Figure 3C), confirming the histological analysis (Figure 2A). On the contrary, the pellets cultured with the CAG-supplemented CM, show a linear increase in sGAG deposition up to 28 days of culture (Figure 3B) and a significant increase ($p < 0.0001$) in sGSG deposition when confronted with 28-day control pellets (Figure 3C), confirming the histological analysis (Figure 3B). Moreover, the statistical analysis, when compared to the controls, demonstrate that CAG significantly enhances ($p < 0.01$) the sGAG deposition within the ECM at 21 days of culture (Figure 3C).

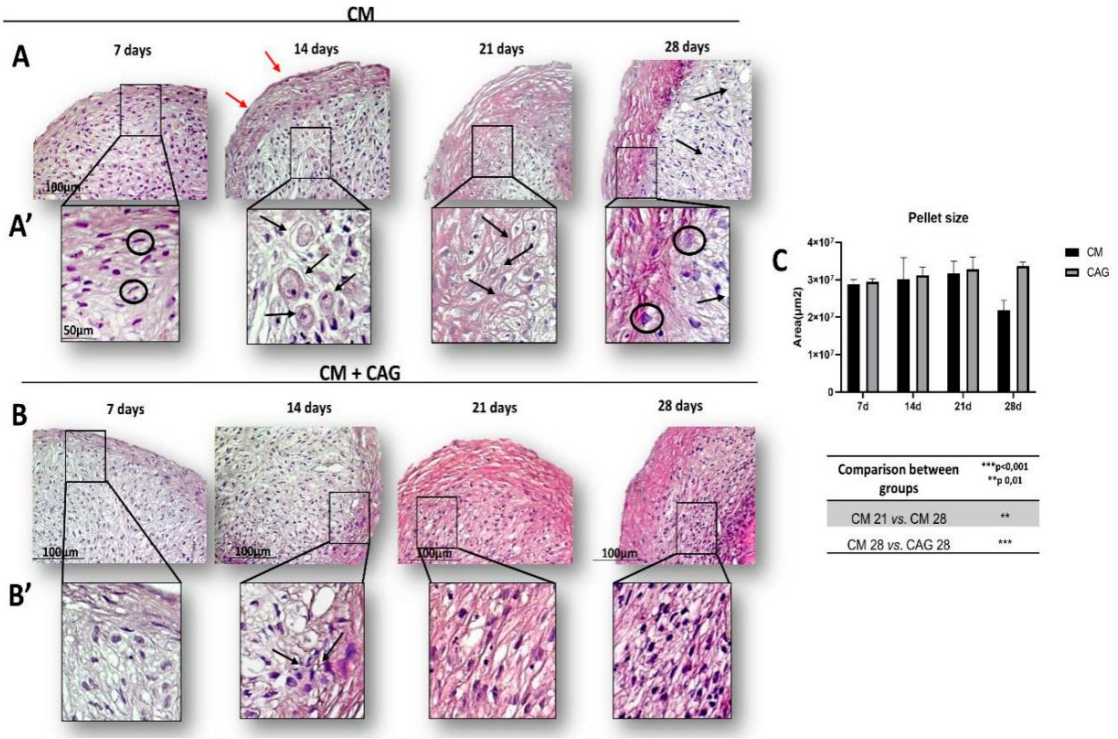

Figure 2. Time-based chondrogenic differentiation of hAMSC pellets, either without (A) or with (B) the supplementation of CAG (0.1 µM), evidenced by hematoxylin and eosin (H&E) staining at 7, 14, 21 and 28 days. (A) control group (chondrogenic medium: CM); (B) CAG-supplemented group (CM + CAG). (A',B') The inserts representing the image magnifications (objective lens, 20×; scale bar: 50 µm), to evidence the morphology changes observed in a time-dependent manner. In the control group (A') we observe: at 7 days, fibroblast-like cell shape (black circles), high cell ability to aggregate and form 3D pellets, not much evident extracellular matrix (ECM); at 14 days, some cells show the chondrocyte-like rounded morphology and presence of lacunae (black arrows), and external perichondral capsule formation (red arrows); at 21 days the pellets exhibit the cartilage-like morphology: the cells are organized into columns, lacunae are well-evidenced (black arrows) and ECM production increases; at 28 days the pellets show decreased ECM deposition, especially in the middle zone (black arrows), an evident thickening of the external capsule and cell enlargement (black circles), indicative of hypertrophy. In the CAG-supplemented group (B'), the pellets at 7 and 14 days show a similar morphology when compared to the seven-days control pellets (A'), seemingly with the increased cell proliferation activity (black arrows); at 21 days, the pellets show an increased cell proliferation and ECM deposition activity, evidenced by the intense H&E staining; at 28 days, the cells within the pellets seem to maintain their phenotypic stability, suggested by the enhanced ECM deposition, apparent increase of cell proliferation activity, and poor cellular hypertrophy phenomena. The increased cell proliferation, cellular aggregations, and ECM deposition activity, exhibiting a cartilage tissue-like morphology are observed in the CAG-supplemented group (B'). Objective lens, 10×; scale bar: 100 µm. (C) The pellet-size analysis was assessed by image-analysis software and expressed in μm^2. Results were presented as the mean ± SD. ANOVA was used to evaluate the significance of the results. ** $p < 0.01$; *** $p < 0.001$.

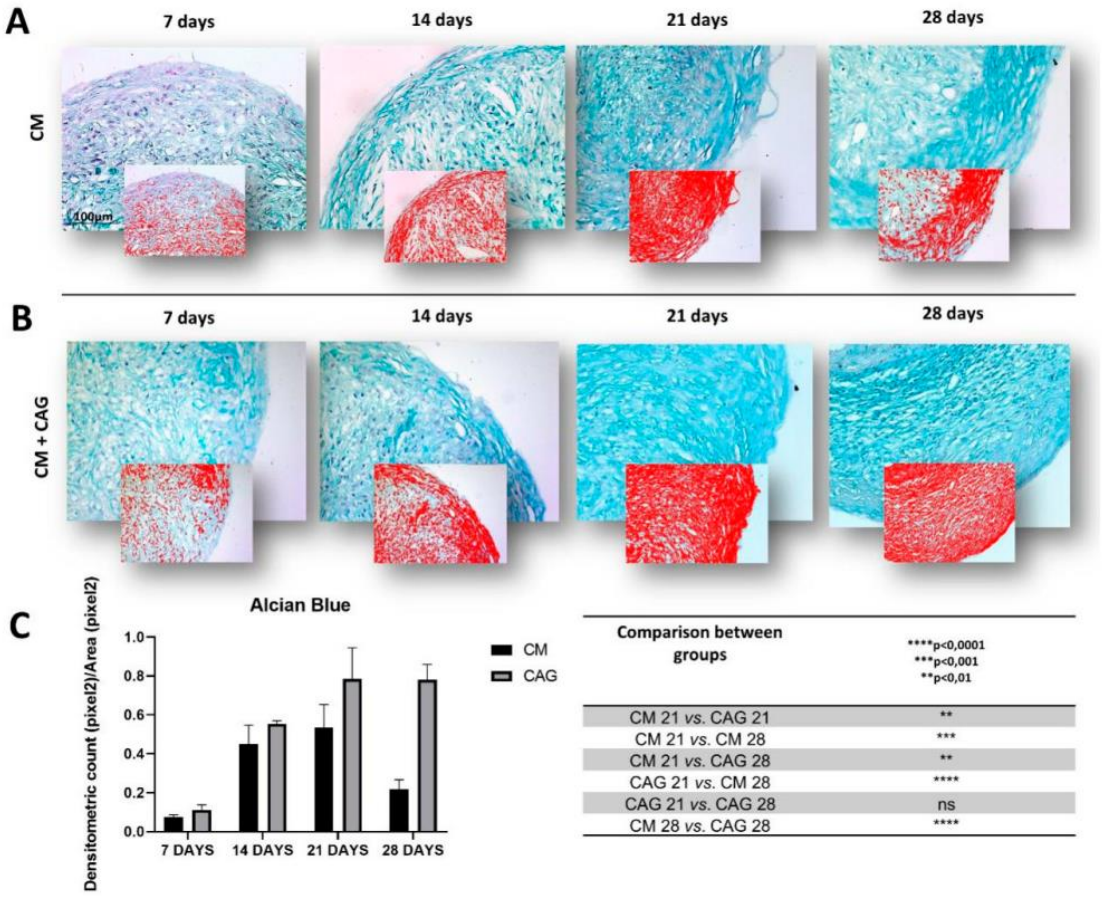

Figure 3. Histochemical evaluation of the mucosubstance content glycosaminoglycan (GAGs) in 3D AMSC-derived chondropellets at 7, 14, 21, and 28 days of culture by Alcian Blue staining through computerized densitometric measurements and image analysis. (A) control group (chondrogenic medium: CM); (B) CAG-supplemented group (CM + CAG). The smaller attached images represent the image analyses by the software: red color corresponds to high-intensity Alcian Blue staining confirming the sGAG synthesis. (C) Graph representing the level of staining expressed as densitometric count (pixel^2) normalized to the area of each section expressed in pixel^2. Results were presented as the mean ± SD. ANOVA was used to evaluate the significance of the results. ** $p < 0.01$; *** $p < 0.001$; **** $p < 0.0001$; ns, not significant. See the Materials and Methods section for details. (A,B) Objective lens, 10×; scale bar: 100 µm.

2.3.5. Analysis of SOX9, Col II, Col I, Col X, Aggrecan, and Lubricin Expression in Chondrogenic hAMSC 3D Pellet Cultures

In the present study, the expression of SOX9 is significantly higher in CAG-supplemented pellets, respectively at 21 ($p < 0.005$) and 28 ($p < 0.0001$) days of culture (Figure 4A–C), when compared to the controls. Col type I was expressed in early condensed mesenchymal

bodies mainly observed at 7 and 14 days and, subsequently, reduced and expressed especially at the perichondral margin (external capsule) at 21 days of 3D culture both in CM-cultured pellets and CAG-supplemented ones (Figure 5A). At 28 days of culture, there is a significant difference in the expression of Col I when compared to 21-day pellets, which appeared further reduced ($p < 0.05$) in CAG-supplemented pellets (Figure 5A,B) and highly increased ($p < 0.0001$) in the control ones (Figure 5A,B). This latter is also probably due to the thickening of the perichondral margin in the control pellets where we can see the accumulation of Col type I deposition in the superficial zone and some degenerative phenomena in the inner zone.

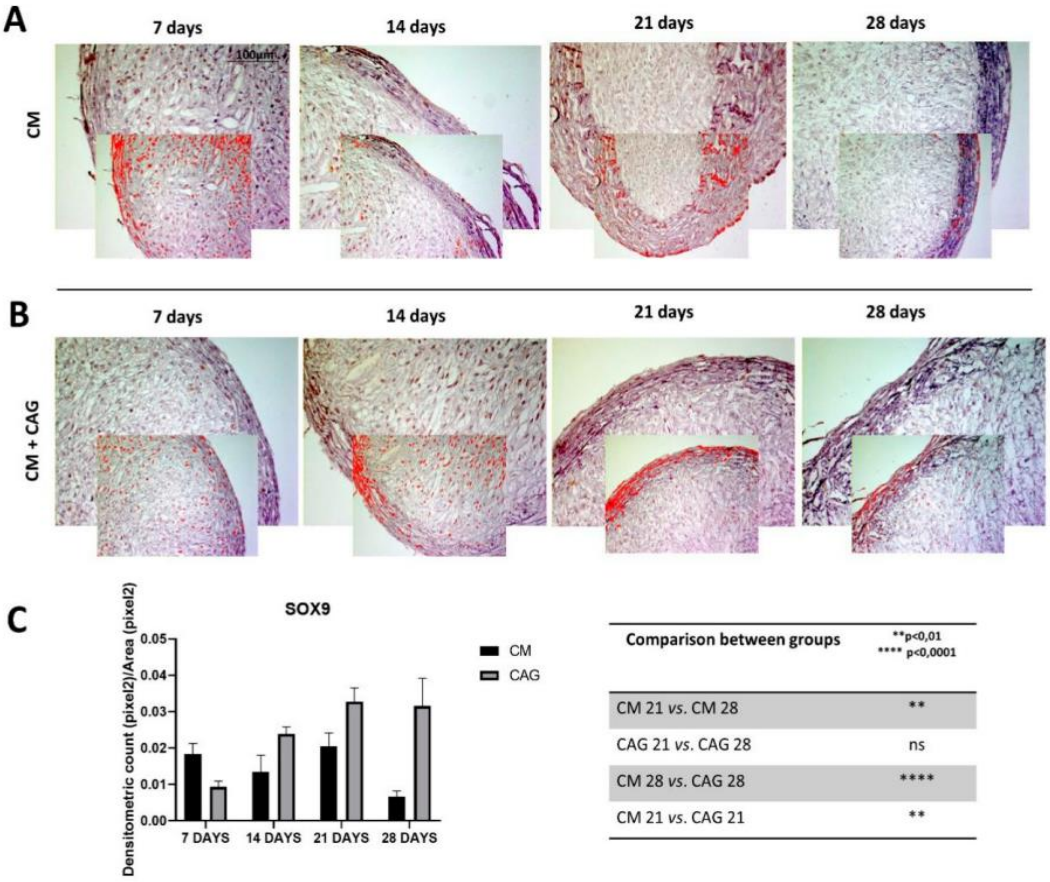

Figure 4. SOX9 immunohistochemical evaluation in 3D AMSC-derived chondropellets at 7, 14, 21, and 28 days of culture through computerized densitometric measurements and image analysis. (A) control group (chondrogenic medium: CM); (B) CAG-supplemented group (CM + CAG). The smaller attached images represent the image analyses by the software: red color corresponds to brown staining (immune complexes labelled with chromogen). (C) Graph representing the level of staining expressed as densitometric count (pixel 2) normalized to the area of each section expressed in pixel^2. Results were presented as the mean ± SD. ANOVA

was used to evaluate the significance of the results. ** $p < 0.01$; **** $p < 0.0001$; ns, not significant. See the Materials and Methods section for details. (A,B) Objective lens, 10×; scale bar: 100 µm.

Seemingly, Col type II is highly expressed in the hAMSC-derived pellets up to 21 days of culture both in CM (Figure 5C) and CAG-supplemented CM conditions (Figure 5C), suggesting the cartilage formation. Contrarily to the Col I expression, at 28 days of 3D culture the Col II expression decreases drastically ($p < 0.0001$) in CM conditions (Figure 5C,D), while in CAG-supplemented 28 day pellets it decreases less significantly ($p < 0.05$) and it remains comparable to the 21-day pellets of the same group (Figure 5C,D). The expression of aggrecan follows the similar expression profile of Col type II, even if in lesser amounts (Figure 5E,F).

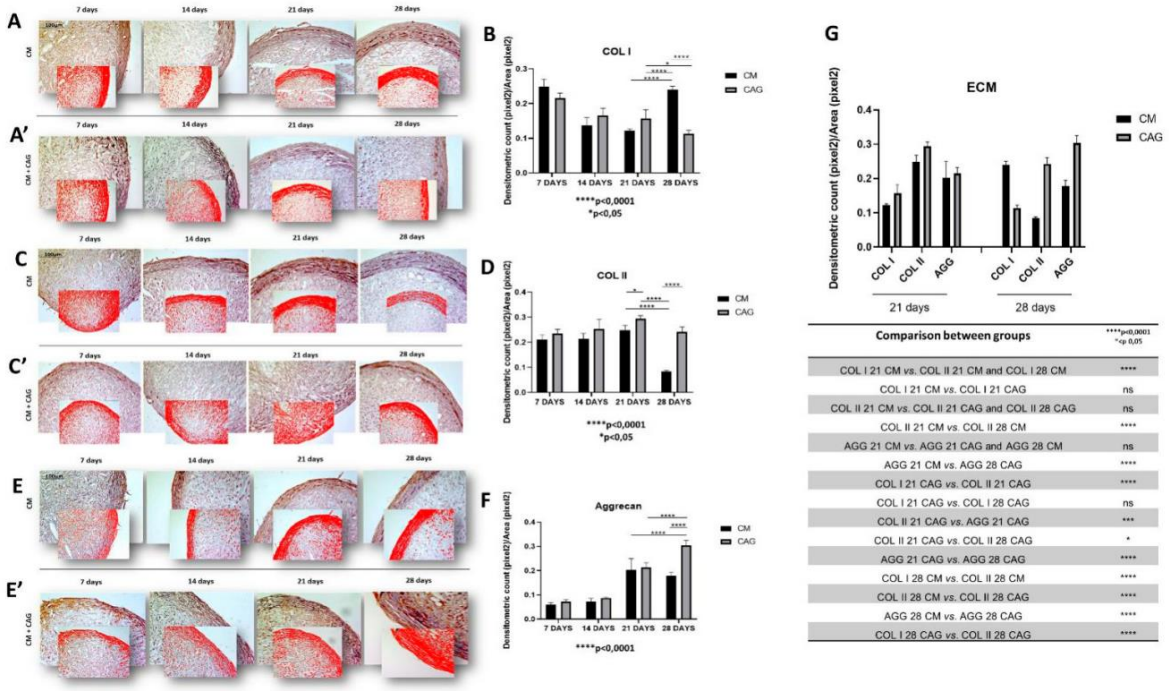

Figure 5. (A) Col type I, (C) Col type II, and (E) aggrecan immunohistochemical evaluation in 3D AMSC-derived chondropellets at 7, 14, 21, and 28 days of culture through computerized densitometric measurements and image analysis. (A,C,E) Control groups (chondrogenic medium: CM); (A',C',E') CAG-supplemented groups (CM + CAG). The smaller attached images represent the image analyses by the software: red color corresponds to brown staining (immune complexes labelled with chromogen). (B,D,F) Graphs representing the level of respective immunolabelings expressed as densitometric count (pixel^2) normalized to the area of each section expressed in pixel 2 . Objective lens, 10×; scale bar: 100 µm. (G) Graph representing the comparison

of densitometric count (pixel^2) of ECM components (Col I, Col II, AGG) immunolabeling identified among groups and compared between them at 21 and 28 days of 3D culture. All results were presented as the mean ± SD. ANOVA was used to evaluate the significance of the results. * $p < 0.05$; *** $p < 0.001$, **** $p < 0.0001$; ns, not significant.

The expression profiles of the ECM cartilage structural molecules, represented by Col type I, Col type II and aggrecan, are compared in Figure 5G, taking into account two most representative time-points (21 and 28 days), in which the most significant changes between the control and the experimental pellets are seen. Due to the 3D sphere culture, all the factors dissolved into the medium probably need to diffuse within the pellets to reach the inner zone, which might explain the differences in chondrogenic markers detection between the inner and external zones of the pellets. The ECM components expression follows the expression profile of SOX9 (Figure 4A–C). Furthermore, the expression of lubricin within the pellets has been evaluated. The results demonstrate the increase in lubricin expression in a time-dependent manner, especially in the superficial pellet zone, up to 28 days of 3D culture, both in CM and CAG-supplemented conditions (Figure 6A–C). At 28 days, lubricin expression profile is similar to that of SOX9, Col II and aggrecan. When compared to the 21-day control pellets, it increases in a not-significant manner in the CM pellets, while it increases significantly ($p < 0.05$) in the CAG-supplemented pellets, both in the superficial and inner pellet zone. Therefore, we can notice a very significant increase ($p < 0.001$) of its expression when compared to 28-day control pellets (Figure 6C), confirming the data reported above.

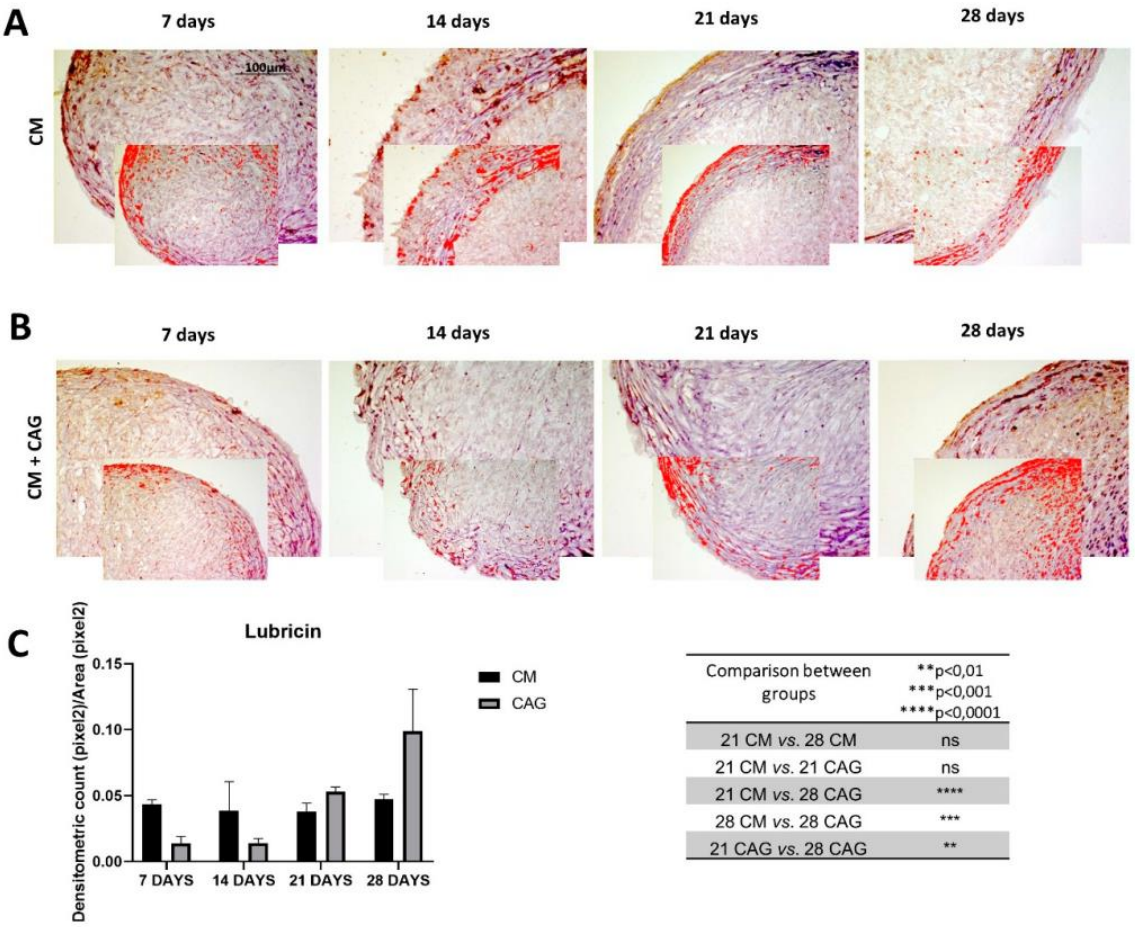

Figure 6. Lubricin immunohistochemical evaluation in 3D AMSC-derived chondropellets at 7, 14, 21, and 28 days of culture through computerized densitometric measurements and image analysis. (A) control group (chondrogenic medium: CM); (B) CAG-supplemented group (CM + CAG). The smaller attached images represent the image analyses by the software: red color corresponds to brown staining (immune complexes labelled with chromogen). (C) Graph representing the level of staining expressed as densitometric count (pixel^2) normalized to the area of each section expressed in pixel^2. Results were presented as the mean ± SD. ANOVA was used to evaluate the significance of the results. ** $p < 0.01$; *** $p < 0.001$; **** $p < 0.0001$; ns, not significant. See the Materials and Methods section for details. Objective lens, 10×; scale bar: 100 µm.

Finally, the expression of Col type X (Figure 7A–C) has been assessed to evaluate the premature cell entry into hypertrophy under the in vitro cell culture conditions. The results demonstrated that pellets cultured in CM undergo hypertrophic de-differentiation at 28 days of the in vitro culture (Figure 7A), highlighted by the increased Col X expression ($p < 0.0001$) when compared to the 21-day control (Figure 7A,C). On the contrary, the pellets supplemented with CAG at 28 days of culture (Figure 7B) demonstrate a significantly lower

($p < 0.0001$) expression profile of Col type X when compared to the 28-day control pellets (Figure 7C).

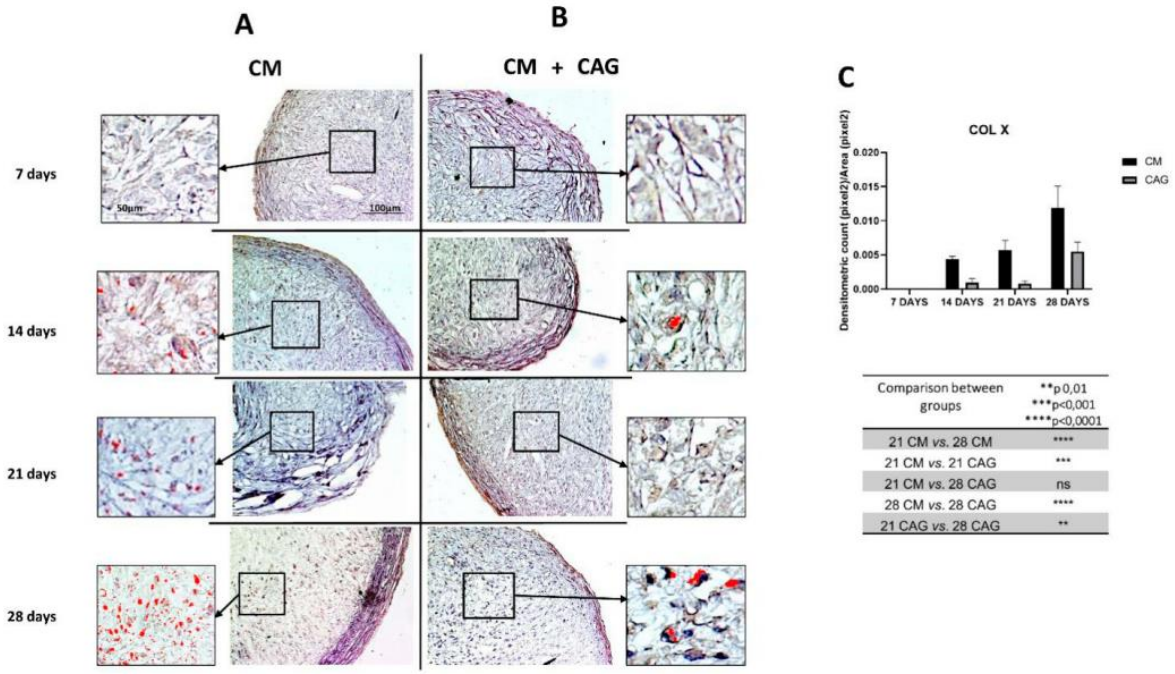

Figure 7. Col type X immunohistochemical evaluation in 3D AMSC-derived chondropellets at 7, 14, 21, and 28 days of culture through computerized densitometric measurements and image analysis. (A) control group (chondrogenic medium: CM); (B) CAG-supplemented group (CM + CAG). The inserts represent the image magnifications (objective lens, 20×; scale bar: 50 µm), to evidence the image analyses by the software in the pellet middle zone: red color corresponds to brown staining (immune complexes labelled with chromogen). (C) Graph representing the level of staining expressed as densitometric count (pixel^2) normalized to the area of each section expressed in pixel^2. Results were presented as the mean ± SD. ANOVA was used to evaluate the significance of the results. ** $p < 0.01$; *** $p < 0.001$; **** $p < 0.0001$; ns, not significant. See the Materials and Methods section for details. Objective lens, 10×; scale bar: 100 µm.

2.4. Discussion

It is well-known that, from the embryological point of view, the cartilage is the first skeletal tissue to be formed and it participates in endochondral ossification within skeletal development. It is characterized by chondrogenesis and subsequent bone formation, which is a multi-developmental process regulated by dynamic morphogenetic and phenotypic changes [31]. It has been well-established that, at certain point of chondrogenic differentiation in vitro,

the cells enter into hypertrophy, losing their active chondrocyte phenotype and becoming less suitable for cartilage regeneration approaches, representing the main challenge for their clinical application [32]. Tissue engineering offers possibilities for optimization of cartilage regeneration by combining MSCs, 3D cell culture conditions, mechanical stimuli, growth factors, and biomolecules for the support of neocartilage formation [11]. Although several procedures have been developed, no standardized protocol has yet been established and in vitro cartilage regeneration presents several limits. Therefore, the application of the existing knowledge regarding the multifactorial aspects of OA disease, complex articular cartilage structure, chondrogenesis enhancing factors, and exogenous stimuli, aimed at developing phenotypically stable engineered cartilage is a promising outcome of the future research. CAG is a bioactive Radix Astragali-derived triterpene aglycone, which has been demonstrated to have various pharmacological actions including regenerative and wound healing effects [20,33], anti-aging effects through telomerase activation [21], anti-fibrosis [34], anti-apoptosis [35], and anti-inflammation [22]. According to existing in vitro and in vivo studies, CAG is safe, and it did not induce any toxic or genotoxic effects, as confirmed by the result of bacterial reverse mutation assay, in vitro chromosome aberration assay, and in vivo erythrocyte micronucleus assay [36]. In the present study, the ability of CAG to enhance hAMSC chondrogenesis and maintain the phenotypic stability of the neocartilage up to 28 days of culture has been investigated. The results of the histological analysis show a good cell condensation and aggregation capacity in both CM and CAG-supplemented groups, which formed spherical pellets already at seven days of 3D culture and maintained this condition up to 28 days. In parallel, the same experiment on MSCs cultured in basal medium (DMEM without chondrogenic factors) in the same experimental conditions has been conducted, but several difficulties in the inclusion of the obtained micro-masses has been encountered, since the cells did not undergo aggregation process and no pellets have formed. For this reason, it was impossible to conduct parallel morphological analysis on these samples, which have been excluded from the study. In CM conditions, at seven days the pellets resemble the prechondrogenic mesenchyme tissue, evidenced by high expression of Col type I, confirming data from developmental studies reporting that it is highly expressed in early chondrogenesis [37–42]. The latter has then been further confirmed by the SOX9 expression [37], in both CM and CAG-supplemented pellets (Figure 4A–C). Data from

literature indicate that SOX9 expression starts in the prechondrogenic mesenchyme and is sustained at high levels in fully differentiated chondrocytes where it directs Col type II and aggrecan deposition [43]. At 14 days of CM culture, a differentiation into chondrocytes and fibril structure formation within pellets were more evident in the CM group, while the CAG-supplemented group showed the morphological features of prechondrogenic mesenchyme, suggesting that CAG might delay the chondrogenesis developmental stages in vitro. These last results were also confirmed by the SOX9 expression profile. At 21 days of chondrogenic culture, a deposition of cartilaginous ECM and cartilage formation were shown in both groups (Figure 5G). However, the ECM synthesis and cell proliferation were more evident in the CAG-supplemented group, underlined by the H&E and Alcian Blue strong stainings and high ECM component expression (Figure 2B,C, Figure 3B,C and Figure 5G). Col type I to Col type II transition can be seen at this time point, suggesting chondrogenic differentiation and confirming data from the literature [44]. The interesting results come from the SOX9 expression profiles, where the increased Col type II and aggrecan deposition is not accompanied by the sustained upregulation of SOX9. Similar results have been observed in a study by Murdoch et al., which stated that it appears probable that the expression of this gene in the prechondrogenic mesenchyme stage is already sufficient to support the ECM component deposition in later stages of differentiation [44]. Seemingly, it is conceivable that there are other mechanisms that complement or enhance the activity of SOX9 transcription during chondrogenic differentiation. This aspect should be certainly further studied. From the morphological point of view, at this time point, we can notice a reasonably uniform matrix deposition within the pellets in both groups. However, in some pellets, we observed the formation of the external fibrous capsule at the perichondral margin, with the main deposition of collagen fibers, especially in the CM control pellets, and the increased ECM deposition within the internal pellet zone. This might be due to the dissimilar culture medium-associated factor diffusion distances due to the spherical shape of the pellets. The latter may also determine the differences in the cell density and oxygen concentration within the pellets. At 28 days of culture, we can notice the most important and evident differences between the experimental and control groups. The hypertrophy and degradation of cartilage ECM are marked in the CM group, evidenced by the histological and immunohistochemical analysis. On the contrary, at the same time point, the CAG-supplemented group demonstrated the

morphologic features similar to the 21-day pellets, poor hypertrophic de-differentiation process, and absence of degenerative phenomena (Figure 2B). At this time point, we can also notice an overexpression of lubricin (Figure 6B), an important chondrocyte marker [39]. These results confirm the data from literature, which report that the overexpression of SOX9 in human MSCs leads to enhanced proliferative, biosynthetic, and chondrogenic activities, and a reduction or delay in the hypertrophic differentiation of the cells [42]. Overall, according to these results, we can state that the CAG-supplemented group, especially at 21 and 28 days of 3D chondrogenically induced culture, showed an enhanced metabolic activity, emphasized by the enhanced cartilaginous ECM deposition, increased lubricin expression, and delayed chondrogenic de-differentiation with the maintenance of the phenotypically stable chondrocyte up to 28 days of 3D culture. Certainly, these preliminary results suggest that there would be value in pursuing this study and investigating the CAG's effects on hMSCs for longer periods and from different sources.

2.5. Conclusions

Clinical application of engineered cartilage faces challenges, derived from phenotypic instability of the cells in long-term cultures, and poor neo-tissue morphological and regenerative properties. A comprehensive understanding of signaling molecules involved in chondrogenesis and their actions on MSC-derived neocartilage, as well as the studies of exogenous enhancers, able to overcome the stated challenges, became crucial. The results of the present study demonstrate that CAG improves a chondrogenic differentiation of hAMSCs, maintaining stable the active chondrocyte phenotype up to 28 days of 3D in vitro culture. Therefore, it is proposed that CAG might have a beneficial impact on future approaches for cartilage regeneration.

Author Contributions

Conceptualization, Methodology, Writing—Original Draft, Visualization, M.A.S.; Conceptualization, Methodology, Writing—Original Draft, G.C.; Investigation, Validation, S.R.; Validation, N.L.P.; Resources, S.F.; Formal analysis, Data Curation, P.C.; Investigation, E.P.; Formal analysis, Data Curation, R.I.; Resources, S.C.; Resources, R.L.; Validation, Formal analysis, M.D.R. Supervision, Project administration, Writing—Review & Editing, G.M. All authors have read and agreed to the published version of the manuscript.

Funding

This study was supported by the University Research Project Grant (Triennial Research Plan 2016–2018), Department of Biomedical and Biotechnological Sciences (BIOMETEC), University of Catania, Italy.

Conflicts of Interest

The authors declare no conflict of interest.

2.6. References

1. Demoor, M.; Ollitrault, D.; Gomez-Leduc, T.; Bouyoucef, M.; Hervieu, M.; Fabre, H.; Lafont, J.; Denoix, J.M.; Audigié, F.; Mallein-Gerin, F.; et al. Cartilage tissue engineering: Molecular control of chondrocyte differentiation for proper cartilage matrix reconstruction. *Biochim. Biophys. Acta* **2014**, *1840*, 2414–2440.
2. Glyn-Jones, S.; Palmer, A.J.; Agricola, R.; Price, A.J.; Vincent, T.L.; Weinans, H.; Carr, A.J. Osteoarthritis. *Lancet Oncol.* **2015**, *386*, 376–387.
3. Kuszel, L.; Trzeciak, T.; Richter, M.; Czarny-Ratajczak, M. Osteoarthritis and telomere shortening. *J. Appl. Genet.* **2015**, *56*, 169–176.
4. Loeser, R.F. Aging and osteoarthritis: The role of chondrocyte senescence and aging changes in the cartilage matrix. *Osteoarthr. Cartil.* **2009**, *17*, 971–979.
5. Smith, G.D.; Knutsen, G.; Richardson, J.B. A clinical review of cartilage repair techniques. *J. Bone Jt. Surg.* **2005**, *87*, 445–449.
6. Wieland, H.A.; Michaelis, M.; Kirschbaum, B.J.; Rudolphi, K.A. Osteoarthritis—An untreatable disease? *Nat. Rev.* **2005**, *4*, 331–344.
7. Goldring, M.B.; Berenbaum, F. Emerging targets in osteoarthritis therapy. *Curr. Opin. Pharm.* **2015**, *22*, 51–63.
8. Szychlinska, M.A.; Castrogiovanni, P.; Nsir, H.; Di Rosa, M.; Guglielmino, C.; Parenti, R.; Calabrese, G.; Pricoco, E.; Salvatorelli, L.; Magro, G.; et al. Engineered cartilage regeneration from adipose tissue-derived mesenchymal stem cells: A morphomolecular study on osteoblast, chondrocyte and apoptosis evaluation. *Exp. Cell Res.* **2017**, *357*, 222–235.
9. Castorina, A.; Szychlinska, M.A.; Marzagalli, R.; Musumeci, G. Mesenchymal stem cells-based therapy as a potential treatment in neurodegenerative disorders: Is the escape from senescence an answer? *Neural Regen. Res.* **2015**, *10*, 850–858.
10. Kwon, H.; Paschos, N.K.; Hu, J.C.; Athanasiou, K. Articular cartilage tissue engineering: The role of signalling molecules. *Cell. Mol. Life Sci.* **2016**, *73*, 1173–1194.
11. Szychlinska, M.A.; D'Amora, U.; Ravalli, S.; Ambrosio, L.; Di Rosa, M.; Musumeci, G. Functional Biomolecule Delivery Systems and Bioengineering in Cartilage Regeneration. *Curr. Pharm. Biotechnol.* **2019**, *20*, 32–46.
12. Pattappa, G.; Zellner, J.; Johnstone, B.; Docheva, D.; Angele, P. Cells under pressure—The relationship between hydrostatic pressure and mesenchymal stem cell chondrogenesis. *Eur. Cells Mater.* **2019**, *37*, 360–381.
13. Ng, J.; Wei, Y.; Zhou, B.; Burapachaisri, A.; Guo, E.; Vunjak-Novakovic, G. Extracellular matrix components and culture regimen selectively regulate cartilage formation by self-assembling human mesenchymal stem cells in vitro and in vivo. *Stem Cell Res.* **2016**, *7*, 183.
14. Musumeci, G.; Mobasheri, A.; Trovato, F.M.; Szychlinska, M.A.; Graziano, A.C.; Lo Furno, D.; Avola, R.; Mangano, S.; Giuffrida, R.; Cardile, V. Biosynthesis of collagen I, II, RUNX2 and lubricin at different time points of chondrogenic differentiation in a 3D in vitro model of human mesenchymal stem cells derived from adipose tissue. *Acta Histochem.* **2014**, *116*, 1407–1417.
15. Hall, B.K.; Miyake, T. Divide, accumulate, differentiate: Cell condensation in skeletal development revisited. *Int. J. Dev. Biol.* **1995**, *39*, 881–893.
16. Calabrese, G.; Forte, S.; Gulino, R.; Cefalì, F.; Figallo, E.; Salvatorelli, L.; Maniscalchi, E.T.; Angelico, G.; Parenti, R.; Gulisano, M.; et al. Combination of Collagen-Based Scaffold and Bioactive Factors Induces Adipose-Derived Mesenchymal Stem Cells Chondrogenic Differentiation In vitro. *Front. Physiol.* **2017**, *8*, 50.
17. Chan, B.P.; Hui, T.Y.; Yeung, C.W.; Li, J.; Mo, I.; Chan, G.C. Self-assembled collagen-human mesenchymal stem cell microspheres for regenerative medicine. *Biomaterials* **2007**, *28*, 4652–4666.
18. Elder, S.H.; Cooley, A.J., Jr.; Borazjani, A.; Sowell, B.L.; To, H.; Tran, S.C. Production of hyaline-like cartilage by bone marrow mesenchymal stem cells in a self-assembly model. *Tissue Eng. Part A* **2009**, *15*, 3025–3036.
19. Hu, J.C.; Athanasiou, K.A. A self-assembling process in articular cartilage tissue engineering. *Tissue Eng.* **2006**, *12*, 969–979.
20. Sevimli-Gür, C.; Onbaşılar, I.; Atilla, P.; Genç, R.; Cakar, N.; Deliloğlu-Gürhan, I.; Bedir, E. In vitro growth stimulatory and in vivo wound healing studies on cycloartane-type saponins of Astragalus genus. *J. Ethnopharmacol.* **2011**, *134*, 844–850.

21. Yu, Y.; Zhou, L.; Yang, Y.; Liu, Y. Cycloastragenol: An exciting novel candidate for age-associated diseases. *Exp. Ther. Med.* **2018**, *16*, 2175–2182.
22. Deng, G.; Chen, W.; Wang, P.; Zhan, T.; Zheng, W.; Gu, Z.; Wang, X.; Ji, X.; Sun, Y. Inhibition of NLRP3 inflammasome-mediated pyroptosis in macrophage by cycloastragenol contributes to the amelioration of imiquimod-induced psoriasis-like skin inflammation in mice. *Int. Immunopharmacol.* **2019**, *74*, 105682.
23. Ip, F.C.; Ng, Y.P.; An, H.J.; Dai, Y.; Pang, H.H.; Hu, Y.Q.; Chin, A.C.; Harley, C.B.; Wong, Y.H.; Ip, N.Y. Cycloastragenol is a potent telomerase activator in neuronal cells: Implications for depression management. *Neurosignals* **2014**, *22*, 52–63.
24. Choi, S.I.; Heo, T.R.; Min, B.H.; Cui, J.H.; Choi, B.H.; Park, S.R. Alleviation of osteoarthritis by calycosin-7-O-beta-D-glucopyranoside (CG) isolated from Astragali Radix (AR) in rabbit osteoarthritis (OA) model. *Osteoarthr. Cartil.* **2007**, *15*, 1086–1092.
25. Wang, B.; Chen, M.Z. Astragaloside IV possesses an antiarthritic effect by preventing interleukin 1β-induced joint inflammation and cartilage damage. *Arch. Pharm. Res.* **2014**, *37*, 793–802.
26. Liu, J.; Meng, Q.; Jing, H.; Zhou, S. Astragaloside IV protects against apoptosis in human degenerative chondrocytes through autophagy activation. *Mol. Med. Rep.* **2017**, *16*, 3269–3275.
27. Xu, H.; Wang, C.Y.; Zhang, H.N.; Lv, C.Y.; Wang, Y.Z. Astragaloside IV suppresses inflammatory mediator production in synoviocytes and collagen-induced arthritic rats. *Mol. Med. Rep.* **2016**, *13*, 3289–3296.
28. Vicari, L.; Calabrese, G.; Forte, S.; Giuffrida, R.; Colarossi, C.; Parrinello, N.L.; Memeo, L. Potential Role of Activating Transcription Factor 5 during Osteogenesis. *Stem Cells Int.* **2016**, *2016*, 5282185.
29. Musumeci, G.; Magro, G.; Cardile, V.; Coco, M.; Marzagalli, R.; Castrogiovanni, P.; Imbesi, R.; Graziano, A.C.; Barone, F.; Di Rosa, M.; et al. Characterization of matrix metalloproteinase-2 and -9, ADAM-10 and N-cadherin expression in human glioblastoma multiforme. *Cell Tissue Res.* **2015**, *362*, 45–60.
30. Szychlinska, M.A.; Imbesi, R.; Castrogiovanni, P.; Guglielmino, C.; Ravalli, S.; Di Rosa, M.; Musumeci, G. Assessment of Vitamin D Supplementation on Articular Cartilage Morphology in a Young Healthy Sedentary Rat Model. *Nutrients* **2019**, *11*, 1260.
31. Quintana, L.; zur Nieden, N.I.; Semino, C.E. Morphogenetic and regulatory mechanisms during developmental chondrogenesis: New paradigms for cartilage tissue engineering. *Tissue Eng. Part B Rev.* **2009**, *15*, 29–41.
32. Mueller, M.B.; Tuan, R.S. Functional characterization of hypertrophy in chondrogenesis of human mesenchymal stem cells. *Arthritis Rheum.* **2008**, *58*, 1377–1388.
33. Zhang, X.; Chen, J. The mechanism of astragaloside IV promoting sciatic nerve regeneration. *Neural Regen. Res.* **2013**, *8*, 2256–2265.
34. Le Saux, C.J.; Davy, P.; Brampton, C.; Ahuja, S.S.; Fauce, S.; Shivshankar, P.; Nguyen, H.; Ramaseshan, M.; Tressler, R.; Pirot, Z.; et al. A novel telomerase activator suppresses lung damage in a murine model of idiopathic pulmonary fibrosis. *PLoS ONE* **2013**, *8*, e58423.
35. Jia, Y.; Zuo, D.; Li, Z.; Liu, H.; Dai, Z.; Cai, J.; Pang, L.; Wu, Y. Astragaloside IV inhibits doxorubicin-induced cardiomyocyte apoptosis mediated by mitochondrial apoptotic pathway via activating the PI3K/Akt pathway. *Chem. Pharm. Bull.* **2014**, *62*, 45–53.
36. Szabo, N.J. Dietary safety of cycloastragenol from Astragalus spp: Subchronic toxicity and genotoxicity studies. *Food Chem. Toxicol.* **2014**, *64*, 322–334.
37. Lefebvre, V.; Dvir-Ginzberg, M. SOX9 and the many facets of its regulation in the chondrocyte lineage. *Connect. Tissue Res.* **2017**, *58*, 2–14.
38. Becerra, J.; Andrades, J.A.; Guerado, E.; Zamora-Navas, P.; López-Puertas, J.M.; Reddi, A.H. Articular cartilage: Structure and regeneration. *Tissue Eng. Part B Rev.* **2010**, *16*, 617–627.
39. Szychlinska, M.A.; Leonardi, R.; Al-Qahtani, M.; Mobasheri, A.; Musumeci, G. Altered joint tribology in osteoarthritis: Reduced lubricin synthesis due to the inflammatory process. New horizons for therapeutic approaches. *Ann. Phys. Rehabil. Med.* **2016**, *59*, 149–156.
40. Mwale, F.; Rampersad, S.; Richard, H.; Guoying, Y.; Al Rowas, S.; Madiraju, P.; Antoniou, J.; Laverty, S. The constitutive expression of type x collagen in mesenchymal stem cells from osteoarthritis patients is reproduced in a rabbit model of osteoarthritis. *J. Tissue Eng.* **2011**.
41. Von der Mark, K. Immunological studies on collagen type transition in chondrogenesis. *Curr. Top. Dev. Biol.* **1980**, *14*, 199–225.

42. Von der Mark, K.; Von der Mark, H. Immunological and biochemical studies of collagen type transition during in vitro chondrogenesis of chick limb mesodermal cells. *J. Cell. Biol.* **1977**, *73*, 736–747.
43. Green, J.D.; Tollemar, V.; Dougherty, M.; Yan, Z.; Yin, L.; Ye, J.; Collier, Z.; Mohammed, M.K.; Haydon, R.C.; Luu, H.H.; et al. Multifaceted signaling regulators of chondrogenesis: Implications in cartilage regeneration and tissue engineering. *Genes Dis.* **2015**, *2*, 307–327.
44. Murdoch, A.D.; Grady, L.M.; Ablett, M.P.; Katopodi, T.; Meadows, R.S.; Hardingham, T.E. Chondrogenic differentiation of human bone marrow stem cells in transwell cultures: Generation of scaffold-free cartilage. *Stem Cells* **2007**, *25*, 2786–2796.

3. EVALUATION OF A CELL-FREE COLLAGEN TYPE I-BASED SCAFFOLD FOR ARTICULAR CARTILAGE REGENERATION IN AN ORTHOTOPIC RAT MODEL

Marta Anna Szychlinska[1,†], Giovanna Calabrese[2,†], Silvia Ravalli[1], Anna Dolcimascolo[2], Paola Castrogiovanni[1], Claudia Fabbi[3], Caterina Puglisi[4], Giovanni Lauretta[1], Michelino Di Rosa[1], Alessandro Castorina[5,6], Rosalba Parenti[2] and Giuseppe Musumeci[1,7,8,]*

[1]Department of Biomedical and Biotechnological Sciences, Anatomy, Histology and Movement Sciences Section, School of Medicine, University of Catania, 95123 Catania, Italy;

[2]Department of Biomedical and Biotechnological Sciences, Physiology Section, School of Medicine, University of Catania, 95123 Catania, Italy;

[3]Fin-Ceramica Faenza, 48018 Faenza, Italy;

[4]Istituto Oncologico del Mediterraneo (IOM), 95029 Viagrande, 95123 Catania, Italy;

[5]School of Life Science, Faculty of Science, University of Technology Sydney, Sydney, NSW 123, Australia;

[6]Discipline of Anatomy & Histology, School of Medical Sciences, The University of Sydney, Sydney, NSW 123, Australia

[7]Research Center on Motor Activities (CRAM), University of Catania, 95123 Catania, Italy

[8]Department of Biology, Sbarro Institute for Cancer Research and Molecular Medicine, College of Science and Technology, Temple University, Philadelphia, PA 19122, USA

[*]Correspondence: g.musumeci@unict.it; Tel.: +095-378-2036

[†]These authors have contributed equally to this work.

Materials 2020, 13(10), 2369; DOI: 10.3390/ma13102369

3.1. Introduction

The repair and healing capacity of articular cartilage after injury is complicated due to its avascular, hypo-cellular and aneural nature [1]. For this reason, even a minor lesion may lead to progressive damage and cartilage degeneration, determining osteoarthritis (OA) development. OA is a common progressively degenerative disease involving primarily articular cartilage and further all joint tissues and leading to severe pain and joint disability [2,3]. Several therapeutic approaches have been developed for the treatment of articular cartilage defects, including autografts and osteochondral allografts, microfracture, autologous chondrocyte and mesenchymal stem cell-based therapies [4,5]. However, the results reported in this field showed limited satisfactory results and the management of chondral defects remains a big challenge. This is mostly due to the biochemical and mechanical properties of the obtained engineered cartilage, which often do not match those of the native tissue [6]. Tissue engineering for regenerative approaches emerges as one of the most promising biomedical applications for cartilage tissue regeneration. The latter is based on the use of innovative biomaterials, which act as scaffolds, mimicking a three-dimensional (3D) extracellular matrix (ECM) microenvironment, with or without the use of chondrocytes or mesenchymal stem cells from different sources [7–10]. Over the past decades, several advances in this field have arisen, based on the innovative techniques used for biomaterial characterization, design and functionalization [11,12]. The biomaterials used in cartilage engineering approaches should provide mechanical support, shape, and cell-scale architecture for neo-tissue formation as cells expand and organize. In addition to defining the 3D architecture for the neo-tissue, the scaffold provides the microenvironment (synthetic temporary ECM) for regenerative cell recruitment, support, proliferation, differentiation and, finally, neo-tissue formation [13]. The most commonly used degradable biomaterials nowadays include some synthetic polyesters such as poly(l-glycolic acid) (PLGA) and poly(l-lactic acid) (PLLA) and natural biopolymers such as collagen, alginate, fibrin and chitosan [14,15]. The natural polymers show better biological properties that are more suitable for the native cartilage microenvironment, promoting required biocompatibility, cellular responses and biodegradability [16]. Among them, collagen type I is widely used for scaffold construction and cartilage tissue engineering approaches, due to its high biocompatibility and widespread clinical usage [17–20]. Although there are many scaffolds

based on collagen, its long-term performance still shows an inferior mechanical property and limited chondrogenic capacity. For this reason, improvements of the physical and structural properties of collagen I-based scaffolds are still required, as stated and highlighted by Irawan et al., in the recently published review [21]. Recently, the biocompatibility and the chondrogenic potential of a new 3D collagen type I-based scaffold has been evaluated by our research group both in vitro and in vivo (etherotopic implantation) [22,23]. Our in vitro results performed using this scaffold in combination with human adipose-tissue derived mesenchymal stem cells (hADMSCs) showed that the scaffold is able to promote the early stages of chondrogenic cell differentiation and that the addiction of specific inductive factors induces complete differentiation as highlighted both by specific cartilage markers expression and typical chondrocyte morphology [22]. The most important cartilage markers are represented by glycosaminoglycans (GAGs), collagen type II and aggrecan, which are typical ECM components of hyaline cartilage that characterise the articular cartilage of diarthrodial joints. Collagen type I, instead represents the main constituent of the fibrocartilage matrix, which possesses completely different mechanical properties compared to hyaline cartilage [1,6]. Another important chondrogenic marker is represented by SOX9, a transcription factor expressed by chondrocytes, which are the only cell type present within the cartilage tissue. It has been identified as a regulator of the chondrocyte lineage, essential for chondrocyte differentiation and cartilage formation. It is associated with the enhancement of collagen II and aggrecan synthesis within the cartilage matrix [24]. In vivo data obtained by subcutaneous implantation (heterotopic model) of a cell free scaffold showed that it is biocompatible and able to recruit host cells and to guide them towards the chondrogenic differentiation [22]. Furthermore, the cartilage-like microstructural properties of this biomaterial, in terms of density and elasticity, were combined in a simple production process [25], which makes this scaffold even very interesting to be evaluated for cartilage regenerative approaches. For this reason, to further evaluate and emphasize the data obtained in our previous studies, the aim of the present work was to continue the validation of this cell-free collagen I-based scaffold in an articular cartilage lesion (ACL) orthotopic model in terms of host cells recruitment, ECM deposition and cartilaginous repair promotion. The results of the present study complete the multi-step evaluation process of the 3D collagen I-

based scaffold and may pave the way to the use of the latter in the cartilage regeneration approaches.

3.2. Materials and Methods

3.2.1. Scaffold Features

Collagen I-based scaffolds used in the present study were manufactured by Fin-Ceramica Faenza SpA (Faenza, Italy). The characterization and process of manufacturing were already widely defined in our previous study [22] and summarised below. These supports present a cylindrical form (8 mm diameter and 5 mm height) and are made up of equine type I collagen gel (1wt%) furnished in aqueous acetic buffer solution (pH = 3.5) (Opocrin SpA, Modena, Italy). The development process and physical and chemical features have been explained previously [22,23]. In Brief, collagen gel was diluted in water and supplied by 0.1 M NaOH solution, up to the isoelectric point (pH = 5.5), in which it precipitated in fibres. Subsequently, it was crosslinked at 37◦C by 48 h long immersion of the fibres in NaHCO3 /Na2CO3 (Sigma Aldrich, Milan, Italy) and Merck Millipore, aqueous solution with a 1,4-butanediol-diglycidyl-ether (BDDGE) and freeze-dried for 25 h under vacuum conditions (P = 0.29 mbar) to obtain a porous 3D structure. Finally, the collagen constructs were treated with gamma-rays at a minimum of 25 kGy. The characterisation of 3D collagen scaffolds from a morphological and microstructural point of view was performed by scanning electron microscopy (SEM) by using an SEM-LEO 438 VP (Carl Zeiss AG, Oberkochen, Germany). Before the analysis, 3D scaffolds were sputter-coated with gold. SEM images were assessed by image J software by calculating the mean pore diameter (mean value of 67 ± 31 microns on a total of 327 pores) (Figure 1). The swelling ability of the material was estimated on 20 cartilaginous cylindrical constructs (ø = 10 mm, h = 4 mm) and determined by evaluating the weight increase and the percent increase in both dimensions [26], as already reported in our previous study [22]. The data analysis did not include the outlier values (Huber test). The porosity and density of collagen constructs were assessed with a glass pycnometer full of highly purified water on n. 20 scaffolds (d = 18 mm; h = 4 30mm) [27]. Pore diameter was then calculated using the geometric volume of the scaffolds and the mean value of the achieved densities [22].

3.2.2. Breeding and Housing of Animals, Experimental Design and Surgery Procedure

Twenty-seven 2-month-old healthy female Wistar outbred rats (Charles River Laboratories, Milan, Italy), with a bodyweight of 300 ± 20 g, were used in the present study. The animals were kept in polycarbonate cages (10.25”W × 18.75”D × 8”H) at controlled humidity and temperature (20–23 ◦C) throughout the whole period of the experiment, with free access to food and water and a 12 h light/dark photoperiod. The 27 animals were divided into three groups at three different time points as shown in Table 1. The ACL groups consisted of rats submitted to surgical treatment to create defects inducing the ACL model. In the CTRL group, only 4-week samples were taken into account for the analysis.

Table 1. Experimental groups.

Study Groups	Time Points	Number of Rats
CTRL	4, 8, 16 weeks	n. 9 (3 × each time point)
ACL (only lesion)	4, 8, 16 weeks	n. 9 (3 × each time point)
ACL-S (lesion + scaffold)	4, 8, 16 weeks	n. 9 (3 × each time point)

Total anaesthesia (30 mg/kg Zoletil 100 + altadol 5 mg/kg + maintenance mixture of O2 and isoflurane 2%–2.5%, Vibrac, Milan, Italy) was used for the surgery procedure. The electric clipper was used to shave the right limb anterior portion, which was then cleaned with povidone iodine (Sceptre Medical, New Delhi, India). The vertical incision was made through the medial border of the skin around the knee cap and, subsequently, through the articular capsule. Afterwards, the patella was moved laterally to expose the right limb femorotibial joint. By flexing the knee the femoral condyles were exposed and a 1 mm × 1.5 mm sharp surgical forceps and needles were used to make a hole within the articular cartilage at the level of the femoropatellar groove of the right limb. Each rat from the ACL-S group received the same treatment, i.e., the collagen scaffolds were sterilely cut into 1 mm × 1.5 mm pieces and implanted into the femoral condyle hole on the right leg while no material was implanted in rats from the ACL group. The implantation was made using press-fit fixation, without supplementary fixation devices. The patella was then removed back, and the articular capsule and skin were sutured by using a 3–0 polydioxanone suture (Figure 1). Post-surgery, one dose of antibiotic Convenia ® 0.1 mL/kg, (Vibrac, Milan, Italy), anti-inflammatory (Meloxicam 1 mg/kg) and analgesic (Tramadol 5 mg/kg) drugs, was administered for 3 days. After surgery, the animals were free to move in the cages without joint immobilization. During all the experimental period the suffering of animals was monitored through their observation (weight, lameness, fur appearance, consumption of food and water), performed once a day. The animals from all groups (CTRL, ACL and ACL-S) and all the sub-groups (4-, 8- and 16-weeks) after the surgical procedures were sacrificed by carbon dioxide (CO2) overdose. After euthanasia, femurs were explanted, cleaned of soft tissues and the samples were processed for histological, immunohistochemical and gene expression analyses. All the procedures were carried out at the Center for Advanced Preclinical In Vivo Research (CAPIR), University of Catania, conformed to the guidelines of the Institutional Animal Care and Use Committee (I.A.C.U.C.) of the University of Catania (Protocol n. 2112015-PR of the 14.01.2015, Italian Ministry of Health). The experiments were conducted in accordance with the Italian Animal Protection Law (116/1992) and the European Community Council Directive (86/609/EEC).

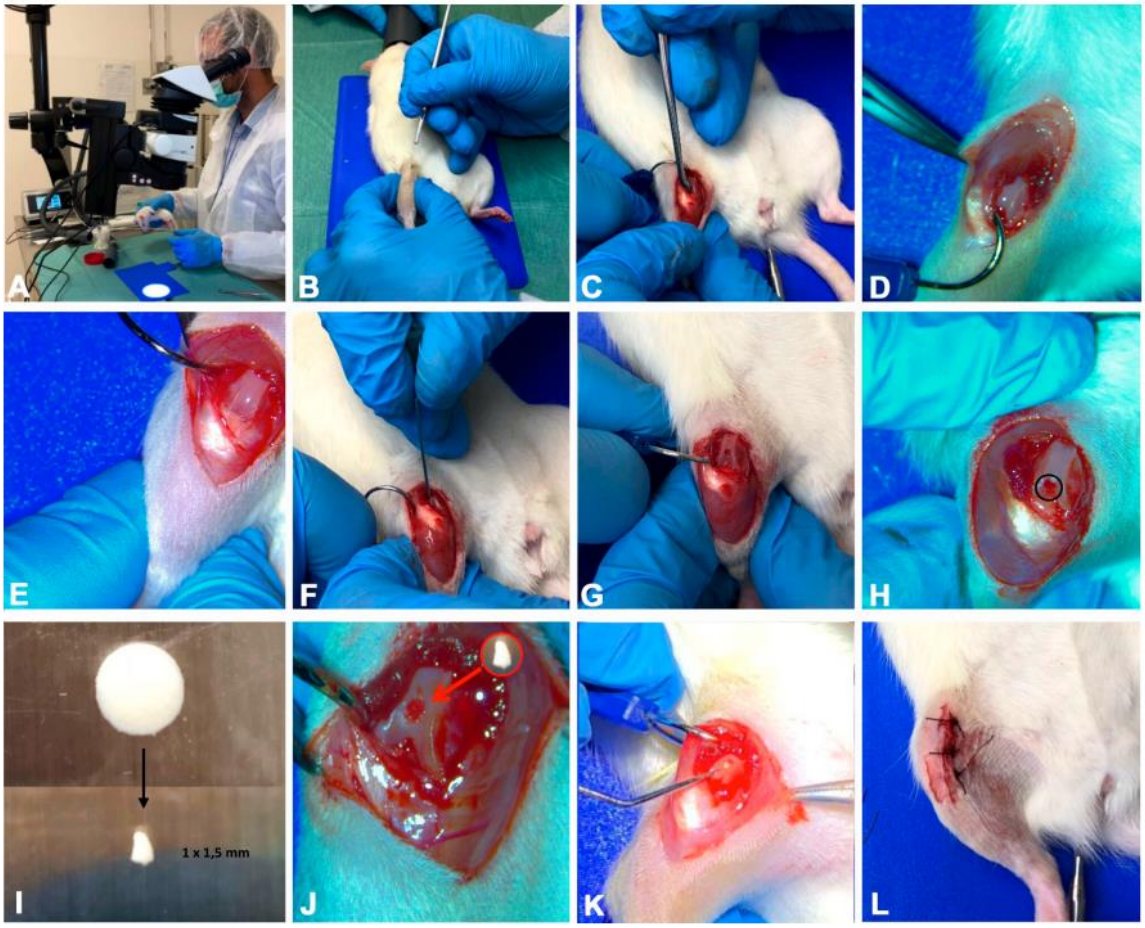

Figure 1. The photographs representing the surgical procedure performed to create defects (ACL induction) and to implant a collagen I-based scaffold. (A) total anaesthesia induction; (B) knee joint preparation for the incision; (C–E) vertical incision through the skin and articular capsule along the medial border and lateral displacement of the patella; (F–H) hole formation at the level of the femoropatellar groove in both ACL and ACL-S groups; (I) collagen I-based scaffold preparation and cutting; (J) collagen I-based scaffold implantation into the hole in the ACL-S group only; (K,L) patella replacement and the articular capsule and skin suture.

3.2.3. Histology Analysis

Cartilage samples were washed in phosphate-buffered saline (PBS, Bio-Optica, Milano, Italy), fixed in 10% buffered-formalin (Bio-Optica, Milan, Italy) for 24 h at room temperature. Afterwards, the samples were dehydrated in graded ethanol (Bio-Optica, Milan, Italy), cleaned in xylene (Bio-Optica, Milan, Italy) and paraffin-embedded (Bio-Optica, Milan, Italy), being careful to preserve the desired anatomical orientation. For the general evaluation of the morphological structure of the cartilage, the slides of 4–5 µm thickness were cut from the obtained paraffin blocks and haematoxylin and eosin-stained (H&E; Bio-Optica, Milan, Italy). The samples were then examined with a Zeiss Axioplan light microscope (Carl Zeiss, Oberkochen, Germany) and by a digital camera (AxioCam MRc5, Carl Zeiss), used to take images. For qualitative histological analysis the following parameters were analysed:

• The type of repaired tissue on the lesion surface (cartilaginous, fibrous or calcified);
• Capability of the collagen I-based scaffold to recruit host cells and promote cartilaginous matrix deposition;
• The scaffold biocompatibility and reabsorption of the collagen I-based scaffold.

3.2.4. Analysis of sGAGs by Histochemistry

The samples were obtained as described above. Alcian Blue staining (Bio-Optica, Milan, Italy) was used to evaluate the expression of glycosaminoglycans (GAGs). The evaluation was made by computerised densitometric measurements. The samples were observed with a Zeiss Axioplan light microscope (Carl Zeiss, Oberkochen, Germany) and the images were taken using a digital camera (AxioCam MRc5, Carl Zeiss, Oberkochen, Germany).

3.2.5. Immunohistochemistry (IHC)

Analysis Articular cartilage samples were processed for immunohistochemical analysis as previously described [28]. In brief, the sections were de-waxed in xylene, hydrated in graded ethanol scale and incubated in 0.3% H2O2 /PBS to stop endogenous peroxidase activity for 30 min. Afterwards, the slides were cleaned for 20 min with PBS (Bio-Optica, Milan, Italy). The slides were heated in a microwave oven (5min×3, 750W, LG Electronics Italia S.p.A., Milan, Italy) in Tris-EDTA buffer (pH 8.0; Bio-Optica, Milan, Italy) or in citrate buffer–pH 6 (pH 6.0; Bio-Optica, Milan, Italy), for the antigenic retrieval [29]. Afterwards, the slides were incubated overnight at 4 °C with diluted rabbit polyclonal antibodies against types I collagen (ab34710; Abcam, Cambridge, UK) and type II collagen (ab34712; Abcam, Cambridge, UK); rabbit monoclonal anti-SOX9 (ab185966; Abcam, Cambridge, UK) and anti-aggrecan (ab3778; Abcam, Cambridge, UK) antibodies, diluted 1:100 in PBS (Sigma-Aldrich, Milan, Italy). Immune-complexes were then incubated with biotinylated link antibodies (HRP-conjugated anti-rabbit and anti-mouse were used as secondary antibodies) and detected with peroxidase-labelled streptavidin (LSAB + System-HRP, K0690, Dako, Glostrup, Denmark). Immunoreactivity was labelled using 0.1% 3,3 0 -diaminobenzidine (DAB) (DAB substrate Chromogen System; Dako, Glostrup, Denmark). The Mayer's hematoxylin (Histolab Products AB, Göteborg, Sweden) was used for the counterstain and then the sections were mounted in GVA (Zymed Laboratories, San Francisco, CA, USA), observed with an Axioplan Zeiss light microscope (Carl Zeiss, Oberkochen, Germany) and captured with a digital camera (AxioCam MRc5, Carl Zeiss, Oberkochen, Germany).

3.2.6. Computerized Morphometric Measurements and Image Analysis

One field of about 550,000 μm^2, corresponding to the defect area, carefully selected from each section (three sections for each time point), was analysed for histochemical assessment of Alcian Blue staining, detecting GAGs expression, and to quantify the level of positive anti-Collagen I, anti-Collagen II, anti-Aggrecan and anti-SOX9 antibodies immunoexpression. The image analysis software (AxioVision Release 4.8.2-SP2 Software, Carl Zeiss Microscopy GmbH, Jena, Germany), which quantifies the staining level as the densitometric count ($pixel^2$) normalized to the defect area of each sample, was used. The samples were analysed

by using the Zeiss Axioplan light microscope (Carl Zeiss, Oberkochen, Germany) and the pictures were taken with a digital camera (AxioCam MRc5, Carl Zeiss, Oberkochen, Germany). Two investigators (one anatomical morphologist and one histologist) made the morphological assessment. If disputes occurred, a unanimous agreement was reached after section re-evaluation and before proceeding with data interpretation.

3.2.7. Quantitative Real-Time Polymerase Chain Reaction (q-PCR)

Total RNA was isolated from paraffin-embedded tissue sections by using the RNeasy FFPE Kit (Qiagen, Germantown, MD, USA). cDNA was synthesised from 1 µg of total RNA using a High-Capacity cDNA Reverse Transcription Kit (Applied Biosystems). Quantitative RT-PCR was performed using the SYBR Green method on a 7900HT Real Time PCR (Applied Biosystems). Specific primers for chondral genes, including COL1A1, COL2A1, aggrecan and SOX9, were designed using Primer Blast [30] and selecting exon-exon junctions on mRNA as a target region for annealing. Gene expression was assessed using the $2 - \Delta\Delta Ct$ method [31]. Oligonucleotide sequences are reported in Table 2. Results were normalised to the levels of Beta-Tubulin (TUBB), used as an endogenous control.

Table 2. Primer sequences.

Target Gene	Forward	Reverse
COL1A1	CCGGAAACAGACAAGCAACCCAAA	AAAGGAGCAGAAAGGGCAGCATTG
COL2A1	TGGTCTTGGTGGAAACTTTGCTGC	AGGTTCACCAGGTTCACCAGGATT
Aggrecan	TGTGGTGATGATCTGGCACGAGAA	CGGCGGACAAATTAGATGCGGTT
Sox9	AACAACCCGTCTACACACAGCTCA	TGGGTAATGCGCTTGGATAGGTCA
TuBB4a	GACGTGAGTACTGCTCCGC	CTTGCAGGTGCACGATTTCC

3.2.8. Statistical Analysis

The statistical evaluation was carried out by using GraphPad Instat ® Biostatistics version 3.0 software (GraphPad Software, Inc., La Jolla, CA, USA), as previously described [32]. Differences between experimental groups were evaluated by using a two-way ANOVA followed by Tukey's multiple comparison post hoc test. Datasets were tested for normal distribution with the Kolmogorov–Smirnov test. All variables were normally distributed. For all experiments, p-values of less than 0.05 were considered statistically significant (*$p < 0.05$; **$p < 0.01$; ***$p < 0.001$; ****$p < 0.0001$ and ns, not significant). The data are presented as the mean value ± SD, as previously described [33].

3.3. Results

3.3.1. 3D Scaffold Characterization before Implantation

The microstructural and morphological properties of the 3D ColI-based scaffold were evaluated by SEM analysis as previously indicated [22,23]. Briefly, Figure 2 shows SEM images of the 3D scaffold at different magnifications, displaying a high porosity of the scaffold with 3D intersected pores without any defined alignment of the collagen fibers. Pore distribution analysis indicated a frequency (> 65%) of pores between 40 and 100 µm in size. The swelling test was performed to assess the change of material structure clearly demonstrating that the collagen I-based scaffold is highly hydrophilic and reaches a steady-state in less than 1 min. The volume of absorbed PBS was quantified to evaluate the capability of the collagen scaffold to maintain the liquid assigned to the support of the 3D structure. After swelling, both diameter (6 ± 1%) and thickness (27 ± 9%) of the scaffold appeared significantly increased.

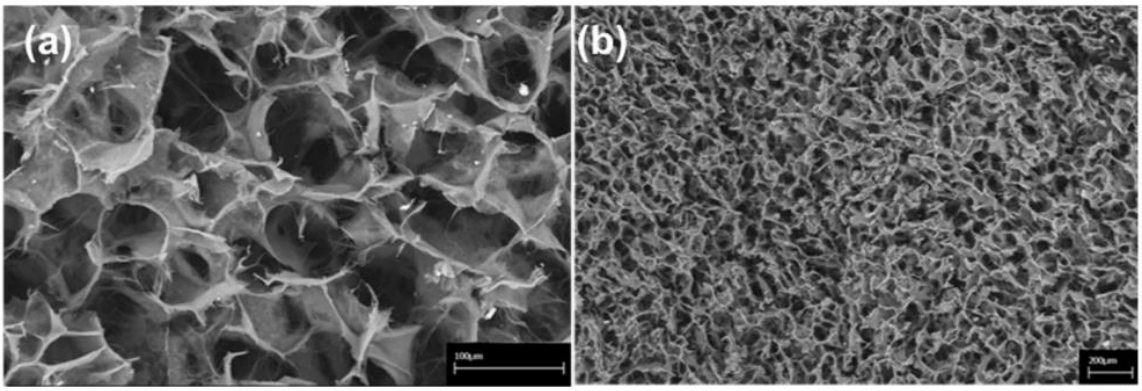

Figure 2. Scanning Electron Microscopy (SEM) images of the collagen-based scaffold. At higher magnification, interconnected collagen fibres are detectable within the scaffold. Scale bars: 100 µm in (a); 200 µm in (b).

3.3.2. Morphological Evaluation of Explanted Femurs

To assess the capability of the collagen I-based scaffold to promote cartilage restoration we performed macroscopic (Figure 3A) and microscopic (Figure 3B) evaluation on the explanted femurs at 4-, 8-, and 16-weeks post-surgery and orthotopic implantation. The hematoxylin and eosin (H&E) staining was used to study the microscopic morphology of the femoral articular cartilage in both groups (femurs with implanted collagen I-scaffolds: ACL-S group, and femurs without scaffolds: ACL group) in order to detect alterations. In the

control group, articular cartilage showed a normal cytoarchitecture. In the superficial zone, cells appeared flat and small; in the middle and deep zone, chondrocytes were organised in columns; the tidemark was very strong and evident (Figure 3Ba). In the articular cartilage of the ACL group, the general tissue organization was completely altered due to the defect induction. The superficial, middle and deep zones, as well as the tidemark, were not observable anymore at all the time points (Figure 3Bb–d). At 4 weeks post-surgery, the H&E staining revealed a newly formed fibrous tissue (scar tissue) in the superficial zone at the surface of the subchondral bone, corresponding to the defect repair (Figure 3Bb). At 8- and 16-weeks the scar tissue tended to be progressively replaced by a tissue that appeared to be calcified, suggested by the morphological aspect of the tissue and poor proteoglycans deposit, further evidenced by Alcian Blue staining (Figure 4). The peri-native cartilage features appeared totally altered (Figure 3Bc,d). In the articular cartilage of the implanted group (ACL-S), at 4-weeks post-surgery, the H&E staining showed the presence of newly formed tissue at the interface between the subchondral bone and collagen scaffold, which presented morphological features resembling a prechondrogenic mesenchymal-like tissue, characterised by the spindle-shaped cells growing without any apparent internal organisation (Figure 3Be). However, this observation has not been validated by specific stainings and would need to be confirmed. Afterwards, the samples revealed the capacity of the biomaterial to recruit host cells that infiltrated, adhered and grown within the scaffold (8-weeks, Figure 3Bf). A progressive integration and replacement of the degradable collagen scaffold with the reparative newly formed cartilage-like tissue were shown (16-weeks, Figure 3Bg).

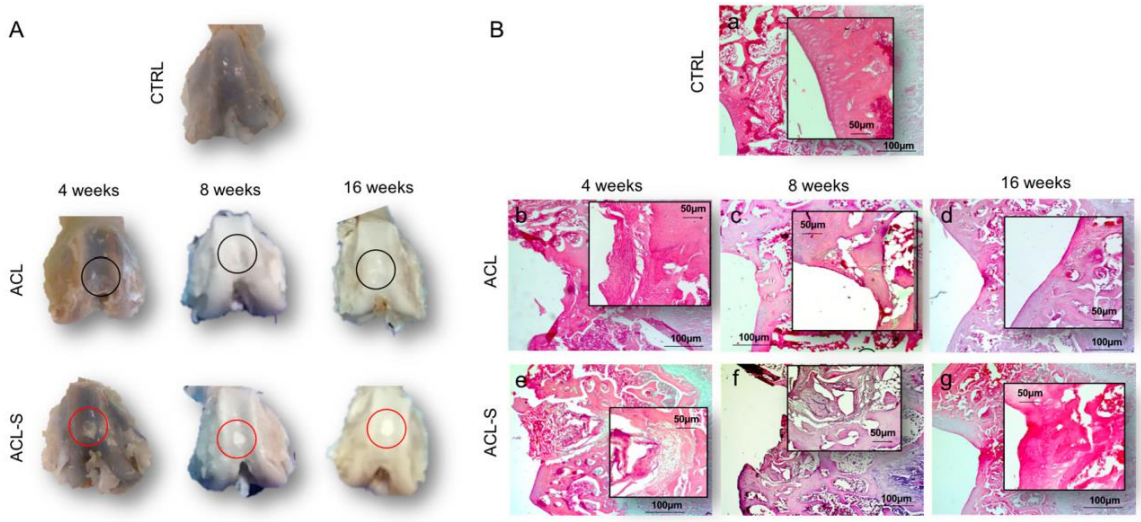

Figure 3. Cartilage repair evaluation through macroscopic and microscopic evaluation. (A) Macroscopic evaluation of repair capacity of femoral articular cartilage explants after defect creation indicated with black circles (ACL group) and in vivo scaffold implantation indicated with red circles (ACL-S group) at 4-, 8- and 16-weeks; (B) Histological evaluation by H&E staining of femoral articular cartilage samples after defect creation (ACL group) and in vivo scaffold implantation (ACL-S group) at 4-, 8- and 16-weeks: (a) control sample presenting a normal cartilage cytoarchitecture; (b) ACL group sample at 4-weeks presenting fibrocartilage formation at the defect area level; (c,d) ACL group sample at 8- and 16-weeks presenting cartilage calcification corresponding to the defect area level; (e) ACL-S group sample at 4-weeks presenting a prechondrogenic mesenchyme-like tissue features at the interface between scaffold and the peri-native tissue; (f) ACL-S group sample at 8-weeks presenting matrix deposition within the scaffold, suggesting host cell recruitment and their chondrogenic differentiation; (g) ACL-S group sample at 16-weeks presenting a total scaffold reabsorption and replacement with a newly formed cartilage-like tissue. Scale bar: 100 µm. The inserts represent the image magnifications (scale bar: 50 µm) to evidence the morphology changes observed in a time-dependent manner.

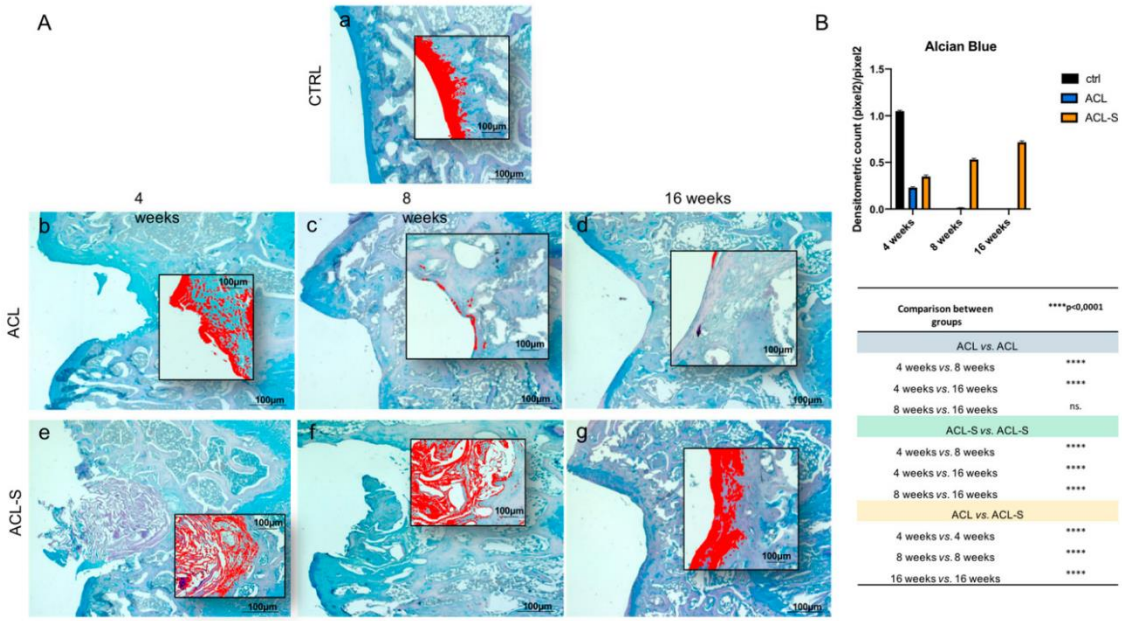

Figure 4. Histochemical evaluation of the deposition of sGAGs in femoral articular cartilage samples at 4-, 8- and 16-weeks post-surgery revealed by the intensity of Alcian Blue staining through computerised densitometric measurements and image analysis. (A) The inserts represent the image magnifications (scale bar: 100 µm) analysed by the software: the red colour corresponds to high intensity Alcian Blue staining. (a) control sample of articular cartilage; (b–d) ACL group samples at 4-, 8- and 16-weeks; (e–g) ACL-S group samples at 4-, 8- and 16-weeks. Scale bars: 100 µm. (B) Graph representing staining level expressed as densitometric count (pixel^2) normalized to the area of each section expressed in pixel^2. Results are presented as the mean ± SD. Two-way ANOVA test followed by Tukey's multiple comparison test reported that all pairwise comparisons were significantly different (p-value < 0.0001) except for ACL 8-weeks vs. ACL 16-weeks, which was not significant (ns.).

The evaluation of cartilage repair was also assessed by the deposition of sulfated glycosaminoglycans (sGAGs) revealed by the intensity of Alcian Blue staining (Figure 4). In the ACL group at 4-weeks, the newly formed fibrous tissue showed a low-intensity blue staining (Figure 4Ab), which diminished progressively and in a significant way with the supposed calcification of the cartilage tissue through the time points and, especially, at 16-weeks (p-value < 0.0001, Figure 4Ad,B). In the ACL-S group (Figure 4Ae–g), the Alcian Blue staining was much stronger than in the defect control group (ACL group). The internal repair integrity was underlined by the higher ECM deposition within the scaffolds due to the recruitment of host cells, moreover, it appeared progressive through the time points, especially at 16-weeks post-implantation (p-value < 0.0001, Figure 4Af,B).

3.3.3. Ex Vivo Evaluation of Cartilage Regeneration

Immunohistochemical staining with statistical analysis was carried out in all groups to evaluate cartilage repair through the expression level of SOX9 (Figure 5A), a pivotal transcription factor for cartilage formation and ECM cartilaginous structural molecules, Aggrecan (Figure 5A'), Collagen type I (Figure 6A), and Collagen type II (Figure 6A').

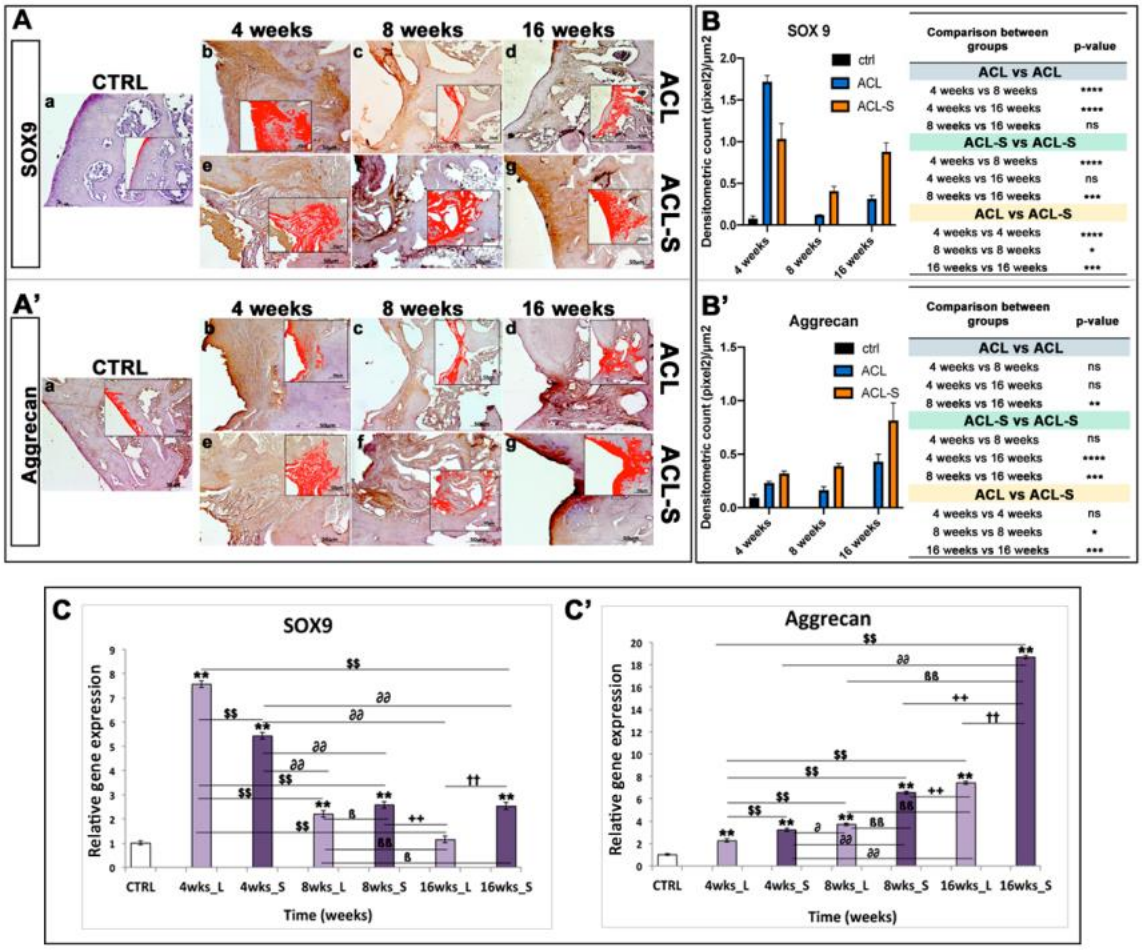

Figure 5. Sox9 and aggrecan evaluation in femoral articular cartilage samples at 4-, 8- and 16-weeks post-surgery. (A–A') Immunohistochemical analyses: (a) control sample of articular cartilage; (b–d) ACL group samples at 4-, 8- and 16-weeks; (e–g) ACL-S group samples at 4-, 8- and 16-weeks. In the inserts, the red colour corresponds to brown staining (immune complexes labelled with chromogen); scale bars 50 µm. (B–B') Graph representing staining level expressed as densitometric count (pixel^2) normalized to the area of each section expressed in µm^2. (C–C') Relative quantitation (RQ) of gene expression showing the time-course of Sox9 and Aggrecan in ACL (L) and ACL-S (S) groups, after 4-, 8-, and 16-weeks from surgery. TUBB4a has been used as endogenous controls. Results are presented as the mean ± SD. Differences between groups were evaluated by using a two-way ANOVA followed by Tukey's multiple comparison post-hoc test (* $p < 0.05$; ** $p < 0.01$;

*** p < 0.001; **** p < 0.0001; ns, not significant). * CTRL vs 4-, 8-, 16- wks_L and 4-, 8-, 16-wks_S; $ 4-wks_L vs 8-, 16-wks_L and 4-, 8-, 16-wks_S; ∂ 4-wks_S vs 8-, 16-wks_L and 8-, 16-wks_S; β 8-wks_L vs 16-wks_L and 8-, 16-wks_S; + 8-wks_S vs 16-wks_L and 16-wks_S; † 16-wks_L vs 16-wks_S.

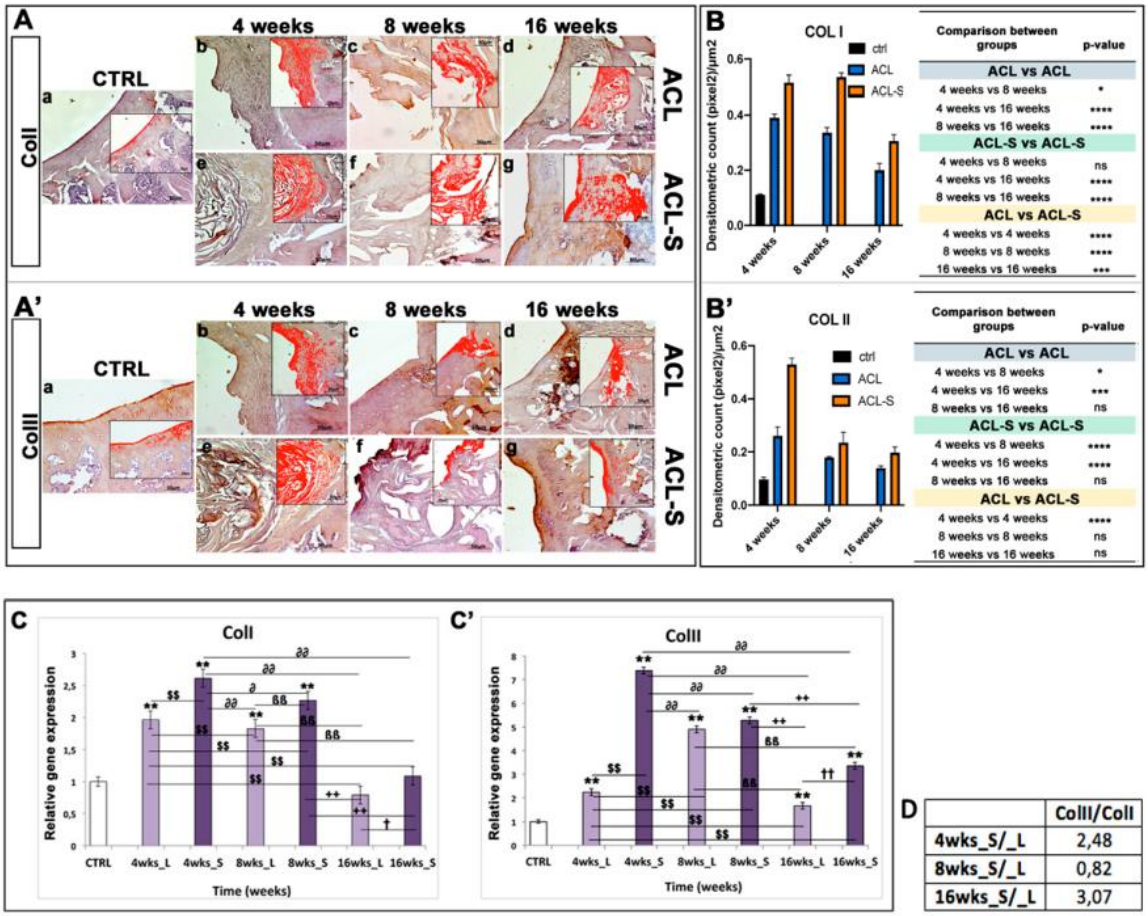

D

	ColII/ColI
4wks_S/_L	2,48
8wks_S/_L	0,82
16wks_S/_L	3,07

Figure 6. Collagen type I and collagen type II evaluation in femoral articular cartilage samples at 4-, 8- and 16-weeks post-surgery. (A–A') Immunohistochemical analyses: (a) control sample of articular cartilage; (b–d) ACL group samples at 4-, 8- and 16-weeks; (e–g) ACL-S group samples at 4-, 8- and 16-weeks. In the inserts, the red colour corresponds to brown staining (immune complexes labelled with chromogen); scale bars 50 µm. (B–B') Graph representing staining level expressed as densitometric count (pixel^2) normalized to the area of each section expressed in µm^2. (C–C') Relative quantitation (RQ) of gene expression showing the time-course of ColI and ColII in ACL (L) and ACL-S (S) groups, after 4-, 8-, and 16-weeks from surgery. TUBB4a has been used as endogenous controls. Results are presented as the mean ± SD. Differences between groups were evaluated by using a two-way ANOVA followed by Tukey's multiple comparison post-hoc test (*p < 0.05; **p < 0.01; ***p < 0.001; ****p < 0.0001; ns, not significant). (D) Table showing the ratio of collagen II/collagen I (ColII/ColI). * CTRL vs 4-, 8-, 16-wks_L and 4-, 8-, 16-wks_S; $ 4-wks_L vs 8-, 16-wks_L and 4-, 8-, 16-wks_S; ∂ 4-wks_S vs 8-, 16-wks_L and 8-, 16-wks_S; β 8-wks_L vs 16-wks_L and 8-, 16-wks_S; + 8-wks_S vs 16-wks_L and 16-wks_S; † 16-wks_L vs 16-wks_S.

A very strong expression of SOX9 was seen at 4-weeks post-surgery, especially in the ACL group (Figure 5Ab). It decreased significantly at 8-weeks in both ACL (p-value < 0.0001, Figure 5Ac,B) and ACL-S (p-value < 0.0001, Figure 5Af,B) groups, to increase again at 16-weeks especially in ACL-S group (p-value < 0.001, Figure 5Ag,B). Overall, the SOX9 expression was significantly higher in ACL-S group when compared to defect control group (ACL group), both at 8- (p-value < 0.05, Figure 5Af,B) and 16-weeks (p-value < 0.0001, Figure 5Ag,B). The expression profile of aggrecan showed a progressive increase through the time points, with the highest peak at 16-weeks in the ACL-S group (Figure 5A'g). Overall, aggrecan expression was always higher in the ACL-S group when compared to the defect control group and it was significant at 8- (p-value < 0.05, Figure 5A'f,B') and 16-weeks (p-value < 0.001, Figure 5A'g,B'). Collagen type I expression was strong at 4-weeks (Figure 6Ae) and 8-weeks (Figure 6Af), in the ACL-S group, decreasing significantly at 16-weeks post-surgery (p-value < 0.0001, Figure 6Ag,B). However, the collagen I expression resulted significantly higher in the ACL-S group when compared to the defect control (ACL group) at all time points: 4-weeks (p-value < 0.0001, Figure 6Ae,B), 8-weeks (p-value < 0.0001, Figure 6Af,B), 16-weeks (p-value < 0.001, Figure 6Ag,B). A very strong expression of collagen type II was seen at 4-weeks post-surgery, especially in the ACL-S group in which it was significantly higher when compared to the defect control group (ACL group) (p-value < 0.0001, Figure 6A'e,B') and it decreased progressively through the time points (Figure 6A'f,g). The expression profile of collagen II demonstrated a significant difference between the ACL and ACL-S groups at 4-weeks (p-value < 0.0001, Figure 6A'b,e,B') but not at 8- and 16-weeks (p-value < 0.05, Figure 6A'c,d,f,g,B'). A qRT-PCR analysis was performed on total RNA isolated from explanted scaffolds to evaluate the expression of specific genes correlated to cartilage phenotype. The expression profiles of cartilaginous genes, including ColI, ColII, Aggrecan and Sox9 at 4-, 8-, and 16-weeks were compared to control mRNA levels. Logarithmic RQ values are reported in Figures 4 and 5. Sox9 displayed a characteristic peak of expression at 4-weeks both in the ACL (RQ = 7.563) and in ACL-S groups (RQ = 5.432) that decreased progressively over time (ACL group: 8-weeks, RQ = 2.199 and 16-weeks RQ = 1.143; ACL-S group: 8-weeks RQ = 2.580, 16-weeks RQ = 2.528), even if the ACL-S group maintained a higher expression of Sox9 when compared to the ACL group (Figure 5C). Aggrecan exhibited a lower expression until the 8th week with a peak of

expression at the 16th week in both groups, although the ACL-S group (RQ = 18.687) displayed a more pronounced expression than the ACL group (RQ = 7.433) (Figure 5C'). ColI showed an increased expression during the fourth week in both groups, RQ = 1.965 in the ACL group and RQ = 2.612 in the ACL-S group, that decreased down to 0.792 and 1.085 at 16-weeks, respectively for the ACL and ACL-S groups (Figure 6C). Finally, ColII showed a distinctive peak of expression at 4-weeks for ACL-S (RQ = 7.388) with a subsequent decrease and reduced modulation (3.355 orders of magnitude) until week 16; in contrast, the ACL group showed a higher ColII expression at 8-weeks (RQ = 4.905) that subsequently decreased to 1.671 orders of magnitude at week 16 (Figure 6C'). Moreover, the gene expression profile data showed a ratio of ColII/ColI for ACL-S/ACL groups of 2.48 fold at 4-weeks, 0.82 at 8-weeks and 3.07 at 16-weeks post-surgery (Figure 6D).

3.4. Discussion

The aim of the present study was to evaluate the extent to which the cell-free collagen I-based 3D scaffold might support hyaline cartilage repair of femoral articular cartilage defects, created to reproduce the ACL model, at 16-weeks post-surgery. The concept of using cell-free scaffolds in tissue engineering is widely accepted and has been advanced by Omori et al., in 2008, in an interesting study on laryngeal cartilage reconstruction in a canine model [34], where the authors suggested the successful cartilage reconstruction by the in situ tissue engineering approach. In the present study, the collagen I-based scaffolds were confirmed to be biocompatible, as already demonstrated in our previous study [23] and as evidenced by the histological analysis of the present study, showing total biodegradation and replacement of the biomaterial with the newly formed cartilage-like tissue at 16-weeks post-implantation (Figure 3B). Moreover, as previously revealed [22,35,36], the scaffolds showed good immune tolerance by the animals, as suggested by the absence of scar-like tissue formation and inflammatory cell infiltration at the interface between the scaffold and peri-native cartilage tissue (Figure 3B). Furthermore, the H&E and Alcian Blue staining demonstrated that the collagen-based scaffold allowed the formation of an articular cartilage-like tissue corresponding to the defect area at the femoropatellar groove level. It was underlined by the significantly higher deposition of sGAGs at 16-weeks post-implantation (Figure 4g) when compared to the defect control group (Figure 4d). The latter showed, instead, newly formed

tissue resembling calcified tissue in the area corresponding to the defect, at the same time point. These data were confirmed by immunohistochemical analysis, which showed a higher expression of cartilage markers in ACL-S group samples, when compared to the ACL group samples (Figures 5 and 6), at all the time points. The only exception regards the SOX9 expression, which at its highest peak, corresponded to the ACL group sample at 4-weeks post-surgery (Figure 5Ab). The latter was probably due to the fact that, at 4-weeks, we expected that the formation of fibrous tissue might be preceded by mesenchymal tissue formation, characterized by a high SOX9 expression [37,38]. Afterwards, along with the probably observed calcification-unlike process (8- and 16-weeks post-surgery) in the ACL group, a significant decrease of SOX9 expression was observed (Figure 5Ac,d,B). It probably happened because the recruited host cells were not supported by any 3D structure, like that given by the collagen I-based scaffold (ACL-S group, Figure 5Ae–g). Indeed, it has been widely shown that the 3D architectural support enhances and improves the cartilaginous matrix formation and stability [39–41]. SOX9 is a transcription factor that plays a key role in chondrogenesis, both by driving the collagen type II and aggrecan expression and by supporting the survival of chondrocyte [37,42]. Apart from the exception of week 4, the results of immunohistochemistry demonstrated that SOX9 expression was maintained always higher in the ACL-S group, especially at 16-weeks post-implantation. These results were observed also in the expression profiles of collagen II (Figure 6) and, especially, of aggrecan, which the highest peak corresponded to the the ACL-S group at 16-weeks (Figure 5A'g). Another important observation regards the expression profiles of collagen type I and II, which the highest peaks corresponded to the ACL-S group at week 4, as seen in Figure 6Ae,A'e. This was probably due to the fact that at this time point, the collagen I-based scaffolds still conserved their integrity, and have not yet undergone the biodegradation process, which was observable at 8- and, even more, at 16-weeks after implantation (Figures 3 and 4). However, the scaffold has not been specifically labelled and this observation would need to be further confirmed. The collagen II high expression was also justified by the infiltrated cells within the scaffolds, already synthesising this cartilage marker, and occupying a bigger area when compared to the cartilage repair tissue at 8- and 16-weeks (Figure 3). The immunohistochemistry results were further confirmed by the gene expression analysis, which presented the same expression profiles of all the chondrogenic markers, as seen in Figures

5C and 6C. Overall, the results of histological, histochemical, immunohistochemical and gene expression analysis confirmed that implantation of collagen I-based scaffold within the cartilage defects of rats, improved the cartilage tissue regeneration when compared to the group without the scaffolds.

3.5. Conclusions

In conclusion, our data support the high biocompatibility of the collagen I-based scaffold, which is able to efficaciously integrate into the host articular cartilage and to promote the development of new cartilage-like tissue by recruiting the host cells and driving them towards the chondrogenic differentiation. Moreover, thanks to the good biodegradability over time (up to 16-weeks), this scaffold represents a promising tool for cartilage tissue engineering and repair approaches.

Author Contributions

M.A.S. and G.C. conceived, wrote and designed the experiments; S.R., A.D., G.L., performed the experiments and edited the manuscript; P.C., C.P., A.C. and M.D.R. analysed the data; C.F., R.P. contributed reagents/materials/analysis tools, data interpretation and reviewed the manuscript; R.P. conceived the study design and reviewed the manuscript; G.M. conceived the study design, reviewed the final proof of paper, provided financial support and correspondence. All authors have read and agreed to the published version of the manuscript.

Funding

This research was sustained by the University Research Project Grant (Triennial Research Plan 2016–2018) at the Department of Biomedical and Biotechnological Sciences, University of Catania, Catania, Italy.

Acknowledgments

We thank Marco Abbate for surgical procedure support and Elisabetta Pricoco for technical support and for careful help concerning the histological and histochemical evaluation and interpretation of data.

Conflicts of Interest

The authors declare no conflict of interest.

3.6. References

1. Karuppal, R. Current concepts in the articular cartilage repair and regeneration. *J. Orthop.* **2017**, *14*, A1–A3.
2. Di Rosa, M.; Szychlinska, M.; Tibullo, D.; Malaguarnera, M.; Musumeci, G. Expression of CHI3L1 and CHIT1 in Osteoarthritic Rat Cartilage Model. A Morphological Study. *Eur. J. Histochem.* **2014**, *58*, 2423.
3. Szychlinska, M.A.; Trovato, F.M.; Di Rosa, M.; Malaguarnera, L.; Puzzo, L.; Leonardi, R.; Castrogiovanni, P.; Musumeci, G. Co-Expression and Co-Localization of Cartilage Glycoproteins CHI3L1 and Lubricin in Osteoarthritic Cartilage: Morphological, Immunohistochemical and Gene Expression Profiles. *Int. J. Mol. Sci.* **2016**, *17*, 359.
4. Redondo, M.; Beer, A.; Yanke, A. Cartilage Restoration: Microfracture and Osteochondral Autograft Transplantation. *J. Knee Surg.* **2018**, *31*, 231–238.
5. Richter, D.; Schenck, R.C.; Wascher, D.C.; Treme, G. Knee Articular Cartilage Repair and Restoration Techniques: A Review of the Literature. *Sports Health* **2015**, *8*, 153–160.
6. Armiento, A.R.; Stoddart, M.; Alini, M.; Eglin, D. Biomaterials for articular cartilage tissue engineering: Learning from biology. *Acta Biomater.* **2018**, *65*, 1–20.
7. Sharma, P.; Kumar, P.; Sharma, R.; Bhatt, V.D.; Dhot, P.S. Tissue Engineering; Current Status & Futuristic Scope. *J. Med. Life* **2019**, *12*, 225–229.
8. Eftekharid, A.; Dizaj, S.M.; Sharifi, S.; Salatin, S.; Saadat, Y.R.; Vahed, S.Z.; Samiei, M.; Ardalan, M.R.; Rameshrad, M.; Ahmadian, E.; et al. The Use of Nanomaterials in Tissue Engineering for Cartilage Regeneration; Current Approaches and Future Perspectives. *Int. J. Mol. Sci.* **2020**, *21*, 536.
9. Huang, B.J.; Hu, J.C.; Athanasiou, K.A. Cell-based tissue engineering strategies used in the clinical repair of articular cartilage. *Biomaterials* **2016**, *98*, 1–22.
10. Kwan, H.; Chisari, E.; Khan, W.S. Cell-Free Scaffolds as a Monotherapy for Focal Chondral Knee Defects. *Materials* **2020**, *13*, 306.
11. Campos, Y.; Almirall, A.; Fuentes, G.; Bloem, H.L.; Kaijzel, E.L.; Cruz, L.J. Tissue Engineering: An Alternative to Repair Cartilage. *Tissue Eng. Part B Rev.* **2019**, *25*, 357–373.
12. Szychlinska, M.A.; D'Amora, U.; Ravalli, S.; Ambrosio, L.; Di Rosa, M.; Musumeci, G. Functional Biomolecule Delivery Systems and Bioengineering in Cartilage Regeneration. *Curr. Pharm. Biotechnol.* **2019**, *20*, 32–46.
13. Im, G. Biomaterials in orthopaedics: The past and future with immune modulation. *Biomater. Res.* **2020**, *24*, 7.
14. Dai, Y.; Shen, T.; Ma, L.; Wang, D.-A.; Gaoa, C. Regeneration of osteochondral defects in vivo by a cell-free cylindrical poly(lactide-co-glycolide) scaffold with a radially oriented microstructure. *J. Tissue Eng. Regen. Med.* **2017**, *12*, 1647–1661.
15. Szychlinska, M.; Castrogiovanni, P.; Nsir, H.; Di Rosa, M.; Guglielmino, C.; Parenti, R.; Calabrese, G.; Pricoco, E.; Salvatorelli, L.; Magro, G.; et al. Engineered cartilage regeneration from adipose tissue derived-mesenchymal stem cells: A morphomolecular study on osteoblast, chondrocyte and apoptosis evaluation. *Exp. Cell Res.* **2017**, *357*, 222–235.
16. Dang, J.; Leong, K.W. Natural polymers for gene delivery and tissue engineering. *Adv. Drug Deliv. Rev.* **2006**, *58*, 487–499.
17. Gavenis, K.; Schneider, U.; Maus, U.; Mumme, T.; Muller-Rath, R.; Schmidt-Rohlfing, B.; Andereya, S. Cell-free repair of small cartilage defects in the Goettinger minipig: Which defect size is possible? *Knee Surg. Sports Traumatol. Arthrosc.* **2011**, *20*, 2307–2314.
18. Efe, T.; Theisen, C.; Fuchs-Winkelmann, S.; Stein, T.; Getgood, A.; Rominger, M.B.; Paletta, J.R.J.; Schofer, M.D. Cell-free collagen type I matrix for repair of cartilage defects—Clinical and magnetic resonance imaging results. *Knee Surg. Sports Traumatol. Arthrosc.* **2011**, *20*, 1915–1922.
19. Schüttler, K.F.; Schenker, H.; Theisen, C.; Schofer, M.D.; Getgood, A.; Roessler, P.P.; Struewer, J.; Rominger, M.B.; Efe, T. Use of cell-free collagen type I matrix implants for the treatment of small cartilage defects in the knee: Clinical and magnetic resonance imaging evaluation. *Knee Surg. Sports Traumatol. Arthrosc.* **2013**, *22*, 1270–1276.
20. Roessler, P.P.; Pfister, B.; Gesslein, M.; Figiel, J.; Heyse, T.J.; Colcuc, C.; Lorbach, O.; Efe, T.; Schüttler, K.F. Short-term follow up after implantation of a cell-free collagen type I matrix for the treatment of large cartilage defects of the knee. *Int. Orthop.* **2015**, *39*, 2473–2479.

21. Irawan, V.; Sung, T.-C.; Higuchi, A.; Ikoma, T. Collagen Scaffolds in Cartilage Tissue Engineering and Relevant Approaches for Future Development. *Tissue Eng. Regen. Med.* **2018**, *15*, 673–697.
22. Calabrese, G.; Forte, S.; Gulino, R.; Cefalì, F.; Figallo, E.; Salvatorelli, L.; Maniscalchi, E.T.; Angelico, G.; Parenti, R.; Gulisano, M.; et al. Combination of Collagen-Based Scaffold and Bioactive Factors Induces Adipose-Derived Mesenchymal Stem Cells Chondrogenic Differentiation In vitro. *Front. Physiol.* **2017**, *8*, 50.
23. Calabrese, G.; Gulino, R.; Giuffrida, R.; Forte, S.; Figallo, E.; Fabbi, C.; Salvatorelli, L.; Memeo, L.; Gulisano, M.; Parenti, R. In Vivo Evaluation of Biocompatibility and Chondrogenic Potential of a Cell-Free Collagen-Based Scaffold. *Front. Physiol.* **2017**, *8*, 984.
24. Lefebvre, V.; Dvir-Ginzberg, M. SOX9 and the many facets of its regulation in the chondrocyte lineage. *Connect. Tissue Res.* **2016**, *58*, 2–14.
25. Deponti, D.; Di Giancamillo, A.; Gervaso, F.; Domenicucci, M.; Domeneghini, C.; Sannino, A.; Peretti, G.M. Collagen Scaffold for Cartilage Tissue Engineering: The Benefit of Fibrin Glue and the Proper Culture Time in an Infant Cartilage Model. *Tissue Eng. Part A* **2014**, *20*, 1113–1126.
26. Ma, L.; Gao, C.; Mao, Z.; Zhou, J.; Shen, J.; Hu, X.; Han, C. Collagen/chitosan porous scaffolds with improved biostability for skin tissue engineering. *Biomaterials* **2003**, *24*, 4833–4841.
27. She, H.; Xiao, X.; Liu, R. Preparation and characterization of polycaprolactone-chitosan composites for tissue engineering applications. *J. Mater. Sci.* **2007**, *42*, 8113–8119.
28. Szychlinska, M.A.; Castrogiovanni, P.; Trovato, F.M.; Nsir, H.; Zarrouk, M.; Furno, D.L.; Di Rosa, M.; Imbesi, R.; Musumeci, G. Physical activity and Mediterranean diet based on olive tree phenolic compounds from two different geographical areas have protective effects on early osteoarthritis, muscle atrophy and hepatic steatosis. *Eur. J. Nutr.* **2018**, *58*, 565–581.
29. Szychlinska, M.; Imbesi, R.; Castrogiovanni, P.; Guglielmino, C.; Ravalli, S.; Di Rosa, M.; Musumeci, G. Assessment of Vitamin D Supplementation on Articular Cartilage Morphology in a Young Healthy Sedentary Rat Model. *Nutrients* **2019**, *11*, 1260.
30. Ye, J.; Coulouris, G.; Zaretskaya, I.; Cutcutache, I.; Rozen, S.G.; Madden, T. Primer-BLAST: A tool to design target-specific primers for polymerase chain reaction. *BMC Bioinform.* **2012**, *13*, 134.
31. Livak, K.J.; Schmittgen, T.D. Analysis of relative gene expression data using real-time quantitative PCR and the 2(-Delta Delta C(T)) Method. *Methods* **2001**, *25*, 402–408.
32. Szychlinska, M.A.; Calabrese, G.; Ravalli, S.; Parrinello, N.L.; Forte, S.; Castrogiovanni, P.; Pricoco, E.; Imbesi, R.; Castorina, S.; Leonardi, R.; et al. Cycloastragenol as an Exogenous Enhancer of Chondrogenic Differentiation of Human Adipose-Derived Mesenchymal Stem Cells. A Morphological Study. *Cells* **2020**, *9*, 347.
33. Castrogiovanni, P.; Di Rosa, M.; Ravalli, S.; Castorina, A.; Guglielmino, C.; Imbesi, R.; Vecchio, M.; Drago, F.; Szychlinska, M.A.; Musumeci, G. Moderate Physical Activity as a Prevention Method for Knee Osteoarthritis and the Role of Synoviocytes as Biological Key. *Int. J. Mol. Sci.* **2019**, *20*, 511.
34. Omori, K.; Nakamura, T.; Kanemaru, S.; Magrufov, A.; Yamashita, M.; Shimizu, Y. In Situ Tissue Engineering of the Cricoid and Trachea in a Canine Model. *Ann. Otol. Rhinol. Laryngol.* **2008**, *117*, 609–613.
35. Calabrese, G.; Giuffrida, R.; Forte, S.; Salvatorelli, L.; Fabbi, C.; Figallo, E.; Gulisano, M.; Parenti, R.; Magro, G.; Colarossi, C.; et al. Bone augmentation after ectopic implantation of a cell-free collagen-hydroxyapatite scaffold in the mouse. *Sci. Rep.* **2016**, *6*, 36399.
36. Calabrese, G.; Giuffrida, R.; Forte, S.; Fabbi, C.; Figallo, E.; Salvatorelli, L.; Memeo, L.; Parenti, R.; Gulisano, M.; Gulino, R. Human adipose-derived mesenchymal stem cells seeded into a collagen-hydroxyapatite scaffold promote bone augmentation after implantation in the mouse. *Sci. Rep.* **2017**, *7*, 7110.
37. Lefebvre, V.; Angelozzi, M.; Haseeb, A. SOX9 in cartilage development and disease. *Curr. Opin. Cell Biol.* **2019**, *61*, 39–47.
38. Akiyama, H.; Kim, J.E.; Nakashima, K.; Balmes, G.; Iwai, N.; Deng, J.M.; Zhang, Z.; Martin, J.F.; Behringer, R.R.; Nakamura, T.; et al. Osteo-chondroprogenitor cells are derived from Sox9 expressing precursors. *Proc. Natl. Acad. Sci. USA* **2005**, *102*, 14665–14670.
39. Jin, G.Z.; Kim, H.W. Chondrogenic Potential of Dedifferentiated Rat Chondrocytes Reevaluated in Two- and Three-Dimensional Culture Conditions. *Tissue Eng. Regen. Med.* **2017**, *15*, 163–172.
40. Ng, J.; Wei, Y.; Zhou, B.; Burapachaisri, A.; Guo, X.E.; Vunjak-Novakovic, G. Extracellular matrix components and culture regimen selectively regulate cartilage formation by self-assembling human mesenchymal stem cells in vitro and in vivo. *Stem Cell Res. Ther.* **2016**, *7*, 183.

41. Estes, B.; Guilak, F. Three-Dimensional Culture Systems to Induce Chondrogenesis of Adipose-Derived Stem Cells. *Breast Cancer* **2011**, *702*, 201–217.
42. Liu, C.F.; Angelozzi, M.; Haseeb, A.; Lefebvre, V. SOX9 is dispensable for the initiation of epigenetic remodeling and the activation of marker genes at the onset of chondrogenesis. *Development* **2018**, *145*, 164459.

4. ASSESSMENT OF VITAMIN D SUPPLEMENTATION ON ARTICULAR CARTILAGE MORPHOLOGY IN A YOUNG HEALTHY SEDENTARY RAT MODEL

Marta Anna Szychlinska[1,†], Rosa Imbesi[1,†], Paola Castrogiovanni[1], Claudia Guglielmino[1], Silvia Ravalli[1], Michelino Di Rosa[1,‡] and Giuseppe Musumeci[1,2,, ‡]*

[1]Department of Biomedical and Biotechnological Sciences, Anatomy, Histology and Movement Sciences Section, School of Medicine, University of Catania, 95123 Catania, Italy;

[2]Research Center on Motor Activities (CRAM), University of Catania, 95123 Catania, Italy

[*]Correspondence: g.musumeci@unict.it; Tel.: +095-378-2036

[†]Co-first authorship

[‡] Co-last authorship

Nutrients 2019, 11(6), 1260; DOI: 10.3390/nu11061260

4.1. Introduction

The importance of vitamin D (Vit D) in the musculoskeletal system development and function, is well known, as reported in several studies testifying a range of effects of Vit D deficiency on cartilage, bone and muscle tissues [1,2,3].

Articular cartilage is an avascular tissue characterized by chondrocytes surrounded by an ECM, rich in water and consisting of collagen type II and proteoglycans with sulfated glycosaminoglycan (GAG) side chains. When an imbalance between catabolism and anabolism occurs in the articular cartilage, joint impairment may manifest as a typical condition of some diseases such as osteoarthritis (OA), characterized by cartilage degeneration and progressive loss [4,5].

Healthy cartilage turnover depends on suitable accessibility of Vit D [1]. Suboptimal levels may lead to OA via its adverse effects on cartilage metabolism [6,7]. Indeed, it has been demonstrated that adequate levels of Vit D stimulate mature chondrocytes to synthesize proteoglycan matrix proteins [8,9]. On the other hand, its low levels increase MMP activity [10]. Therefore, low levels of exogenous Vit D may alter the stability of cartilage metabolism by reducing the synthesis of proteoglycan and/or increasing the MMPs activity, leading to cartilage loss. Data from the literature show that Vit D deficiency is responsible for proteoglycans and matrix loss in the animal model [11] and it is also associated with progression of OA, in humans [6,7,12]. Scientific data support the beneficial effects of Vit D as an immunomodulatory and anti-inflammatory agent in OA [7,13], even if the reported data are controversial [14,15]. It has been shown that Vit D influences the state of the joints through the action of VDR, whose polymorphism has been associated with OA [16,17]. Deficiency in Vit D has been associated with several other musculoskeletal diseases, such as osteomalacia, osteopenia, osteoporosis, increased risk of fracture and muscle weakness [18]. However, the exogenous Vit D supplementation with diet has been quite poorly studied and it is still unclear whether it has beneficial effects in the prevention of Vit D-deficiency related diseases of musculoskeletal tissues, especially during the developmental period.

From the mentioned above scientific data, it is evident how complex is the relation between the musculoskeletal system and molecular action of Vit D. For this reason, the aim of the present study was to evaluate the effects of exogenous Vit D supplementation and restriction on morphology and expression of some chondrocyte markers such as lubricin, Col II and

hypertrophic marker collagen type X (Col X), in tibial articular cartilage of young healthy sedentary rats. The hypothesis of the present study was that Vit D supplementation may support the development of the articular cartilage morphology during its developmental period by determining the increase in its thickness, which may better support the mechanical loading and permit in this way to perform the native function of articular cartilage.

4.2. Materials and Methods

4.2.1. Breeding and Housing of Animals

Twelve nine-week-old healthy Sprague–Dawley male rats (Envigo RMS S.r.l., Udine, Italy), with an average body weight of 271 ± 25 g, were housed in polycarbonate cages (cage dimensions: 10.25″ W × 18.75″ D × 8″ H) at controlled temperature (20–23 °C) and humidity. Only male rats were used to avoid different results related to different genders. During the whole period of the research, with free access to water and food and a photoperiod of 12 h light/dark at the "Center for Advanced Preclinical In Vivo Research (CAPIR)". Rats were allowed to adopt one week to their environment before the experiments began. At the end of the experimental period (10 weeks), the animals were humanely sacrificed by exposure to a chamber filled with carbon dioxide until one minute after breathing stopped and then were decapitated. After euthanasia, articular cartilage samples from tibia were used to perform the histological, histochemical, histomorphometric and immunohistochemical evaluation. In order to maximize the information obtained from the minimum resource and to generate statistically robust data, the power analysis sample size was performed using the G*Power3.1 calculator software (Düsseldorf University, Düsseldorf, Germany) [19]. All of the experiments were designed to minimize animal suffering and to use the minimum number of animals required to achieve a valid statistical evaluation according to the principles of the 3R's (replacement, reduction and refinement). All of the procedures conformed to the guidelines of the Institutional Animal Care and Use Committee (I.A.C.U.C.) at the Center for Advanced Preclinical In Vivo Research (CAPIR), University of Catania, and approved by Italian Ministry of Health, Protocol n. 2112015-PR of the 14.01.2015 (14 January 2015). The experiments were conducted in accordance with the European Community Council Directive (86/609/EEC) and the Italian Animal Protection Law (116/1992).

4.2.2. Experimental Design

Three different diets were used for the experiment, provided by Mucedola s.r.l. (Settimo Milanese, Milan, Italy) by adding different contents of cholecalciferol (Vit D_3) in a standard chow. In particular, a regular diet with a content in Vit D_3 of 1400 IU/kg (R), a regular diet with Vit D_3 supplementation (4000 IU/kg) (R-DS) and a regular diet with Vit D_3 restriction (0 IU/kg) (R-DR). The composition of the experimental diets is reported in Table 1. The 12 animals were divided into three groups: R, control rats, fed with R diet (n = 4); R-DS, rats fed with R-DS diet (n = 4); R-DR, rats fed with R-DR diet (n = 4). The experimental protocol was carried out for a period of 10 weeks and body weights, food and drink consumptions were monitored three days per week

throughout the experiment. At the end of the experiment, rats were sacrificed, as above reported, in order to obtain cartilage tissue in which evaluations were performed.

Table 1. The composition of the experimental diets

Compound	R	R-DS	R-DR
Water (% *w/w*)	10.69	10.69	10.69
Protein (% m/m)	22.90	22.90	22.90
Fat (% m/m)	3.54	3.54	3.54
Fiber (% m/m)	3.63	3.63	3.63
Ash (% m/m)	7.55	7.55	7.55
FNE (% m/m)	51.44	51.44	51.44
Carbohydrates (% m/m)	55.07	55.07	55.07
M.E. (kcal/kg)	2757	2757	2757
Vitamin A (IU/kg)	16,000	16,000	16,000
Vitamin D_3 (IU/kg)	1400	4000	0
Vitamin B1 (mg/kg)	19.1	19.1	19.1
Vitamin B2 (mg/kg)	19.1	19.1	19.1
Vitamin B6 (mg/kg)	10.9	10.9	10.9
Vitamin B12 (mg/kg)	0.03	0.03	0.03
Vitamin E (α-tocopherol) (mg/kg)	68.5	68.5	68.5
Vitamin PP (mg/kg)	95.2	95.2	95.2
Iron (mg/kg)	599	599	599
Calcium (mg/kg)	10,575	10,575	10,575
Magnesium (mg/kg)	2485	2485	2485
Phosphorus (mg/kg)	9619	9619	9619
Potassium (mg/kg)	9782	9782	9782
Zinc (mg/kg)	106.9	106.9	106.9
Sodium (mg/kg)	3033	3033	3033

M.E.: Metabolizable Energy; R: Regular diet; R-DS: Regular diet with vitamin D supplementation; R-DR: Regular diet with vitamin D restriction.

4.2.3. Histology

The tibias explantation procedure and the subsequent cleaning of soft tissues were performed as previously described [20]. Specimens were incubated in a decalcifying solution (14% EDTA, PH: 7,2) for 7–10 days, washed for one h and then were fixed in 10% neutral buffered formalin (Bio-Optica, Milan, Italy). After overnight washing, they were embedded in paraffin as previously described [21]. The samples were placed in the cassettes in longitudinal and cross directions after wax infiltration. Tissue samples (4–5 μm) were cut from paraffin blocks by a rotary manual microtome (Leica RM2235, Milan, Italy) and then mounted on silane-coated slides (Menzel-Gläser, Braunschweig, Germany) and preserved at room temperature. Afterwards, the sections were dewaxed in xylene, hydrated by graded ethanol, and stained by Hematoxylin and Eosin (H&E), Alcian Blue and Mallory's trichrome stainings for detection of structural alterations, histochemical evaluation and histomorphometric measurements (thickness of the articular cartilage). The slides were examined with a Zeiss Axioplan light microscope (Carl Zeiss, Oberkochen, Germany), and pictures were taken with a digital camera (AxioCam MRc5, Carl Zeiss, Oberkochen, Germany).

4.2.4. Histomorphometric Analysis

Four fields, the area of which was about 550,000 μm^2, randomly selected from sections (four from each rat), were analysed for morphometric analysis. The thickness of the articular cartilage was considered and calculated using software for image acquisition (AxioVision Release 4.8.2-SP2 Software, Carl Zeiss Microscopy GmbH, Jena, Germany). The data were expressed as mean ± standard deviation (SD). The statistical significance of the results was then evaluated. Digital micrographs were taken using the Zeiss Axioplan light microscope (Carl Zeiss, Oberkochen, Germany), using a lens with a magnification of ×10, i.e., total magnification 100) fitted with a digital camera (AxioCam MRc5, Carl Zeiss, Oberkochen, Germany). Three blinded investigators (two anatomical morphologists and one histologist) made the evaluations that were assumed to be correct if the recorded values had no statistically significant difference. In case of a dispute concerning interpretation, the case was reconsidered to reach a unanimous agreement.

4.2.5. Immunohistochemistry (IHC)

Articular cartilage samples were processed for immunohistochemical analysis as previously described [22]. In detail, the slides were dewaxed in xylene, hydrated by graded ethanol, incubated for 30 min in 0.3% hydroperoxyl (H_2O_2)/methanol to remove endogenous peroxidase activity and then rinsed in phosphate-buffered saline (PBS; Bio-Optica, Milan, Italy) for 20 min. In order to unmask the antigenic sites, the samples were stored in capped polypropylene slide holders with citrate buffer (10 mM citric acid, 0.05% Tween 20, pH 6.0; Bio-Optica, Milan, Italy) and heated for 5 min for three times through a microwave oven (750 W, LG Electronics Italia S.p.A., Milan, Italy). In order to prevent non-specific binding of the antibodies, a blocking step with 5% bovine serum albumin (BSA, Sigma, Milan, Italy) in PBS for one h in a moist chamber was performed before the application of the primary antibodies. The sections were then incubated overnight at 4 °C with the following antibodies: Rabbit polyclonal Anti-Col II antibody (ab34712; Abcam, Cambridge, UK), work dilution in PBS (Bio-Optica, Milan, Italy) 10 μg/mL; rabbit polyclonal Anti-Col X antibody (ab58632; Abcam, Cambridge, UK), work dilution in PBS (Bio-Optica, Milan, Italy) 10 μg/mL; rabbit polyclonal anti-lubricin antibody (ab28484; Abcam, Cambridge, UK), work dilution in PBS (Bio-Optica, Milan, Italy) 4 μg/mL; rat monoclonal anti-VDR (ab115495; Abcam, Cambridge, UK), work dilution in PBS (Bio-Optica, Milan, Italy) 10 μg/mL. The samples were then coated with a biotinylated antibody (horseradish peroxidase (HRP)-conjugated anti-goat and anti-rabbit were used as secondary antibodies), and the immune complexes were detected with peroxidase-labeled streptavidin (labelled streptavidin-biotin (LSAB) + System-HRP, K0690, Dako, Glostrup, Denmark), after incubation for 10 min at room temperature. The immunoreaction was detected by incubating the sections for 2 min in a 0.1% 3,3′-diaminobenzidine, 0.02% hydrogen peroxide solution (DAB substrate Chromogen System; Dako, Denmark). The slides were lightly counterstained with Mayer's Hematoxylin (Histolab Products AB, Goteborg, Sweden) and mounted in GVA mount (Zymed, Laboratories Inc., San Francisco, CA, USA).

4.2.6. Computerised Densitometric Measurements and Image Analysis

Four fields, the area of which was about 550,000 μm^2, randomly selected from each section, were analysed for histochemical evaluation of Alcian Blue staining which detects mucosubstance content (GAGs) and Mallory's trichrome staining which detects the fibrous component (collagen fibres). It was used as an image analysis software (AxioVision Release 4.8.2-SP2 Software, Carl Zeiss Microscopy GmbH, Jena, Germany), which quantifies the level of staining in the densitometric count ($pixel^2$)/μm2 of articular cartilage.

To quantify the level of immunostaining of positive anti-Col II, anti-Col X, anti-lubricin and anti-VDR antibodies immunolabelling, the same software was used for calculating the densitometric count ($pixel^2$)/μm^2 of the immunostained articular cartilage area in four fields, the area of which was about 550.000 μm^2, randomly selected from slides. Digital micrographs were taken using the Zeiss Axioplan light microscope (Carl Zeiss, Oberkochen, Germany), using a lens with a magnification of ×10, i.e., total magnification 100) fitted with a digital camera (AxioCam MRc5, Carl Zeiss, Oberkochen, Germany). Three blinded investigators (two anatomical morphologists and one histologist) made the evaluations that were assumed to be correct if the recorded values had no statistically significant difference. If disputes concerning interpretation occurred, a unanimous agreement was reached after sample re-evaluation [23].

4.2.7. Statistical Analysis

The statistical analysis was performed using GraphPad Instat® Biostatistics version 3.0 software (GraphPad Software, Inc., La Jolla, CA, USA) [21,22]. Datasets were tested for normal distribution with the Kolmogorov–Smirnov test. All variables were normally distributed. Two-way-ANOVA (Tukey's multiple comparisons test) was used for comparisons between more than two groups. p-values of less than 0.05 were considered statistically significant; more than 0.05, they were considered not significant (ns). The data are presented as the mean ± SD.

4.3. Results

4.3.1. Histology and Histomorphometric Analysis

The H&E staining was used to study the general morphology of the tibial articular cartilage in all groups in order to detect eventual alterations and to make a histomorphometric evaluation on the thickness of the articular cartilage. In the R group (control), articular cartilage showed a normal cytoarchitecture. In the superficial zone, cells were flat and small; in the middle and deep zone, chondrocytes were organised in columns; the tidemark was very strong and evident; thickness of articular cartilage in the R group measured 235.7 ± 12.20 μm (Figure 1A). In the articular cartilage of the R-DS group, a general tissue preservation was observed in the superficial, middle and deep zones even if the tidemark was a little bit less evident and the deeper zone above the tidemark was very thick, thus determining a

greater overall thickness of the articular cartilage in the R-DS group, measuring 301.6 ± 19.25 µm (Figure 1B). In the R-DR group, though the articular cartilage did not show evident alterations, in its middle and deep zones the chondrocytes were poorly organised in columns, and the tidemark was not always perceptible; moreover, articular cartilage in the R-DR group showed an apparent reduction of thickness, measuring 130.00 ± 13.19 µm (Figure 1C). In the statistical analysis, it emerged that the differences in articular cartilage thickness among groups were statistically significant. In the R-DS group the thickness was greater than both the R group ($p = 0.0071$) and the R-DR group ($p < 0.0001$). The R-DR group had a thickness of articular cartilage lower even if compared to the R group ($p < 0.0001$) (Table 2).

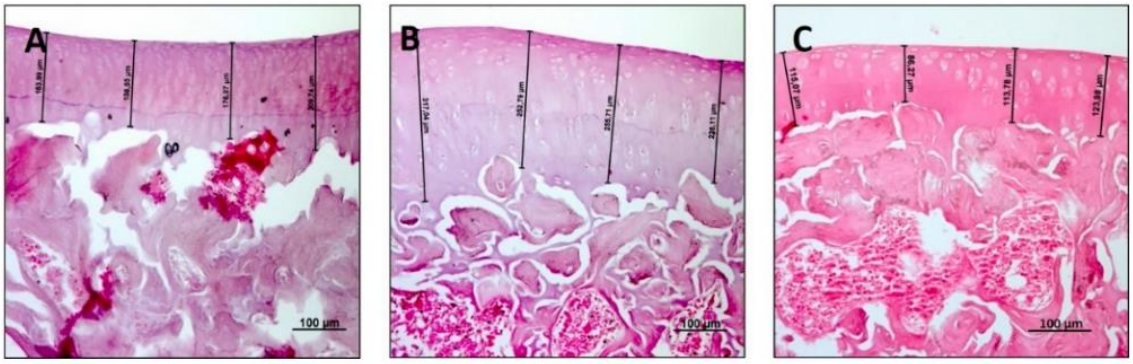

Figure 1. Histological evaluation and histomorphometric analysis of articular cartilage by hematoxylin and eosin (H&E) staining. (A) R group (control). In the superficial zone of the articular cartilage, chondrocytes were flat and small; in the middle and deep zone, cells were organised in columns; the tidemark was very strong and evident; (B) R-DS group. General tissue preservation was observed in the superficial, middle and deep zones; the tidemark was a little bit less evident, and the deeper zone above the tidemark was very thick; (C) R-DR group. Articular cartilage did not show evident alterations; in middle and deep zones the chondrocytes were poorly organised in columns, and the tidemark was not always perceptible. (A–C) Objective lens, 10; scale bars: 100 µm. These are the most representative images of articular cartilage from rats of each group (R, R-DS and R-DR).

Table 2. THICKNESS—Articular cartilage

	R (Mean ± SD)	R-DS (Mean ± SD)	R-DR (Mean ± SD)	*p*-Value
Thickness (µm)	235.7 ± 12.20	301.6 ± 19.25	130.00 ± 13.19	R vs. R-DS: 0.0071 R vs. R-DR: < 0.0001 R-DS vs. R-DR: < 0.0001

The Alcian Blue staining was used to detect and quantify the mucosubstance content (GAGs) in the articular cartilage of all groups. Experimental data obtained using an image analysis software which quantifies the level of Alcian Blue staining expressed as densitometric count (pixel^2)/μm^2 of articular cartilage, showed a decreased staining in the R-DR group and increased staining in the R-DS group (Figure 2A–C). In statistical analysis, the difference between R-DS (3.009 ± 0.44) compared to the R group (1.940 ± 0.34) was statistically significant ($p = 0.0175$); the same for the comparison between R-DS compared to the R-DR group (0.980 ± 0.35) ($p < 0.0001$). The R-DR group had a lower value also when compared to the R group ($p = 0.0359$) (Table 3).

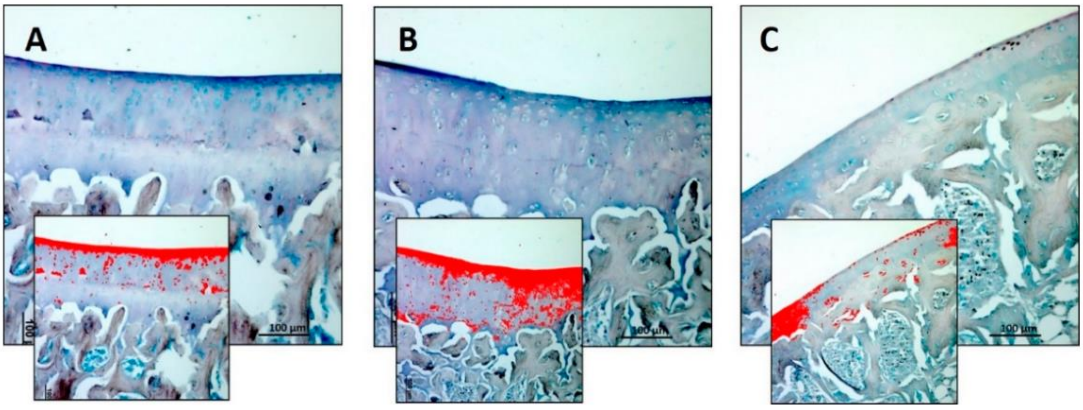

Figure 2. Histochemical evaluation of the mucosubstance content glycosaminoglycan (GAGs) in the articular cartilage by Alcian Blue staining through computerised densitometric measurements and image analysis. (A) R group; (B) R-DS group; (C) R-DR group. In inserts are the image analyses by the software in which the red colour represents Alcian Blue staining, showing a decreased staining in the R-DR group and increased staining in the R-DS group. For details, see the text. (A–C) Objective lens, 10; scale bars: 100 µm. These are the most representative images of articular cartilage from rats of each group (R, R-DS and R-DR).

Table 3. ALCIAN BLUE Staining—Articular cartilage

	R (Mean ± SD)	R-DS (Mean ± SD)	R-DR (Mean ± SD)	*p*-Value
Densitometric count (pixel^2)/μm^2	1.940 ± 0.34	3.009 ± 0.44	0.980 ± 0.35	R vs. R-DS: 0.0175 R vs. R-DR: 0.0359 R-DS vs. R-DR: < 0.0001

The Mallory's trichrome staining was used to highlight the fibrous component (collagen fibres, in blue) of articular cartilage in the experimental groups. Experimental data obtained using an image analysis software which quantifies the level of blue staining, expressed as densitometric count (pixel^2)/μm^2 of articular cartilage, showed a decreased staining in the R-DR group when compared to both the R group and R-DS one, and none significant difference between the R-DS group and R one (Figure 3A–C). In statistical analysis, the difference between R-DS (4.834 ± 0.74) compared to the R group (4.246 ± 0.77) was not statistically significant (p = ns); not the same for the comparison R-DS compared to the R-DR group (2.925 ± 0.31) (p = 0.0003). The R-DR group had a lower value also when compared to the R group (p = 0.0120) (Table 4).

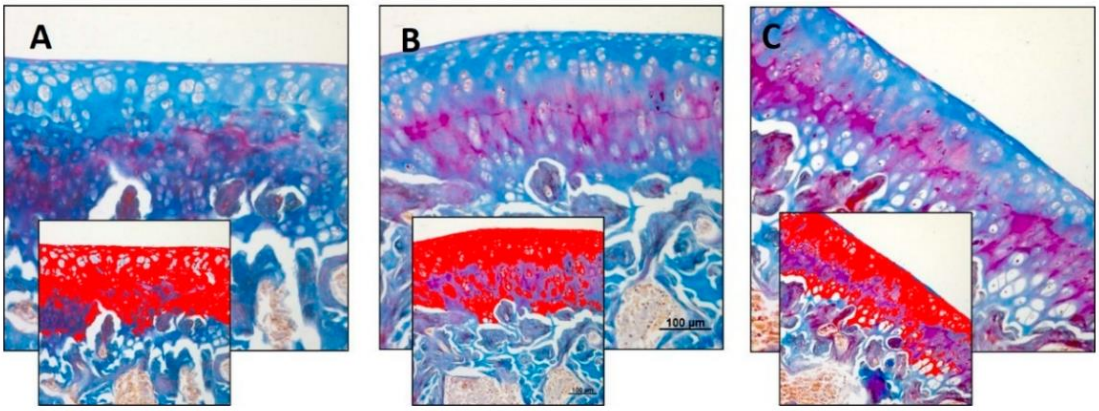

Figure 3. Histochemical evaluation of the fibrous component (collagen fibres) in the articular cartilage by Mallory's trichrome staining through computerised densitometric measurements and image analysis. (A) R group; (B) R-DS group; (C) R-DR group. In inserts are the image analyses by the software in which the red colour represents blue staining (collagen fibres), showing a decreased staining in the R-DR group. For details, see the text. (A–C) Objective lens, 10; scale bars: 100 μm. These are the most representative images of articular cartilage from rats of each group (R, R-DS and R-DR).

Table 4. MALLORY'S Trichrome Staining—Articular cartilage

	R (Mean ± SD)	R-DS (Mean ± SD)	R-DR (Mean ± SD)	*p*-Value
Densitometric count (pixel^2)/μm^2	4.246 ± 0.77	4.834 ± 0.74	2.925 ± 0.31	R vs. R-DS: ns R vs. R-DR: 0.0120 R-DS vs. R-DR: 0.0003

4.3.2. Immunohistochemistry (IHC)

Immunohistochemical staining with statistical analysis was used to verify the greater or lesser expression of structural molecules, such as Col II and X, and functional molecules, such as lubricin and VDR. Data were obtained using an image analysis software which quantifies the level of brown staining, expressed as densitometric count (pixel^2)/μm^2 of articular cartilage. In Col II immunostaining, it was observed that a significant decrease was only in the R-DR group if compared to other experimental groups (R and R-DS groups) (Figure 4A–C). In statistical analysis, the difference between R-DS (0.889 ± 0.15) compared to the R group (0.793 ± 0.20) was not statistically significant (p = ns); the difference between R-DS compared to the R-DR group (0.247 ± 0.09) was statistically significant (p = 0.0016); also, the difference between R-DR compared to the R group was statistically significant (p = 0.0076) (Table 5).

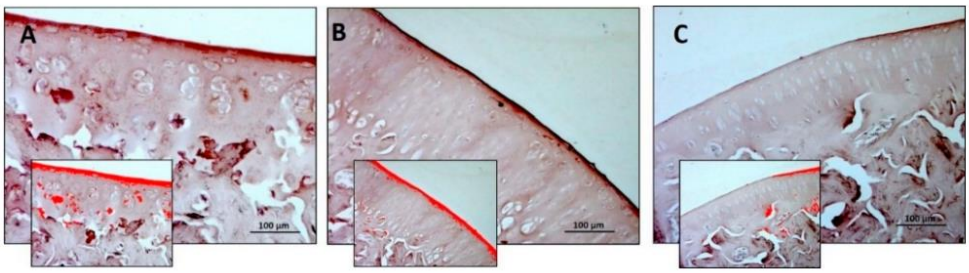

Figure 4. Collagen II (Col II) immunohistochemical evaluation in the articular cartilage through computerised densitometric measurements and image analysis. (A) R group; (B) R-DS group; (C) R-DR group. In inserts are the image analyses by the software in which the red colour represents brown staining (immune complexes labelled with chromogen). For details, see the text. (A–C) Objective lens, 10; scale bars: 100 μm. These are the most representative images of articular cartilage from rats of each group (R, R-DS and R-DR).

Table 5. COL II Immunostaining—Articular cartilage

	R (Mean ± SD)	R-DS (Mean ± SD)	R-DR (Mean ± SD)	*p*-Value
Densitometric count (pixel^2)/μm^2	0.793 ± 0.20	0.889 ± 0.15	0.247 ± 0.09	R vs. R-DS: ns R vs. R-DR: 0.0076 R-DS vs. R-DR: 0.0016

In Col X immunostaining, a higher immunoexpression was evidenced in the R-DR group compared to both R and R-DS groups (Figure 5A–C). In statistical analysis, the difference between R-DR (0.517 ± 0.03) compared to the R group (0.236 ± 0.04) was statistically

significant ($p < 0.0001$); also the difference between R-DR compared to the R-DS group (0.300 ± 0.06) was significant ($p < 0.0001$); instead, the difference between R-DS compared to the R group was not statistically significant (p = ns) (Table 6).

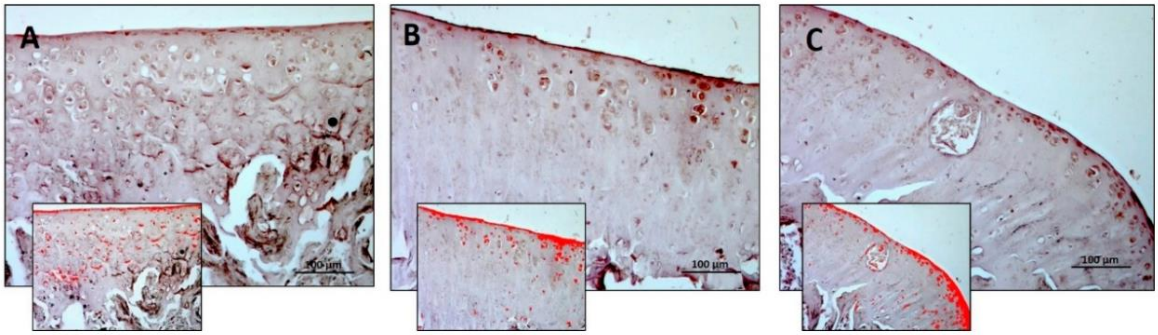

Figure 5. Collagen X (Col X) immunohistochemical evaluation in the articular cartilage through computerised densitometric measurements and image analysis. (A) R group; (B) R-DS group; (C) R-DR group. In inserts are the image analyses by the software in which the red colour represents brown staining (immune complexes labelled with chromogen). For details, see the text. (A–C) Objective lens, 10; scale bars: 100 µm. These are the most representative images of articular cartilage from rats of each group (R, R-DS and R-DR).

Table 6. COL X Immunostaining—Articular cartilage

	R (Mean ± SD)	R-DS (Mean ± SD)	R-DR (Mean ± SD)	*p*-Value
Densitometric count (pixel^2)/µm^2	0.236 ± 0.04	0.300 ± 0.06	0.517 ± 0.03	R vs. R-DS: ns R vs. R-DR: < 0.0001 R-DS vs. R-DR: < 0.0001

In lubricin immunostaining, the R-DS group showed higher immunostaining in comparison to both R and R-DR groups (Figure 6A–C). In statistical analysis, the difference between R-DS (2.427 ± 0.35) compared to the R group (1.283 ± 0.34) was statistically significant ($p = 0.001$); the same for comparison between R-DS compared to the R-DR group (1.240 ± 0.50) ($p = 0.0008$); on the contrary, the difference between R-DR compared to the R group was not statistically significant (p = ns) (Table 7).

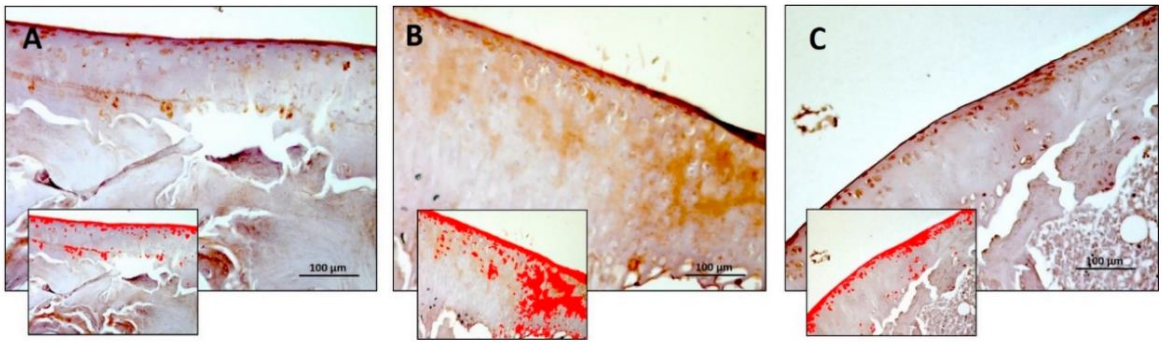

Figure 6. Lubricin immunohistochemical evaluation in the articular cartilage through computerised densitometric measurements and image analysis. (A) R group; (B) R-DS group; (C) R-DR group. In inserts are the image analyses by the software in which the red colour represents brown staining (immune complexes labelled with chromogen). For details, see the text. (A–C) Objective lens, 10; scale bars: 100 µm. These are the most representative images of articular cartilage from rats of each group (R, R-DS and R-DR).

Table 7. LUBRICIN Immunostaining—Articular cartilage

	R (Mean ± SD)	R-DS (Mean ± SD)	R-DR (Mean ± SD)	*P*-Value
Densitometric count (pixel^2)/µm^2	1.283 ± 0.34	2.427 ± 0.35	1.240 ± 0.50	R vs. R-DS: 0.001 R vs. R-DR: ns R-DS vs. R-DR: 0.0008

In VDR immunostaining, no significant differences were shown among experimental groups (R, R-DS and R-DR) (Figure 7A–C). In statistical analysis, the difference between R-DS (0.306 ± 0.05) compared to the R group (0.425 ± 0.08), R-DS compared to the R-DR group (0.347 ± 0.04) and R-DR compared to the R group was always not statistically significant (p = ns) (Table 8).

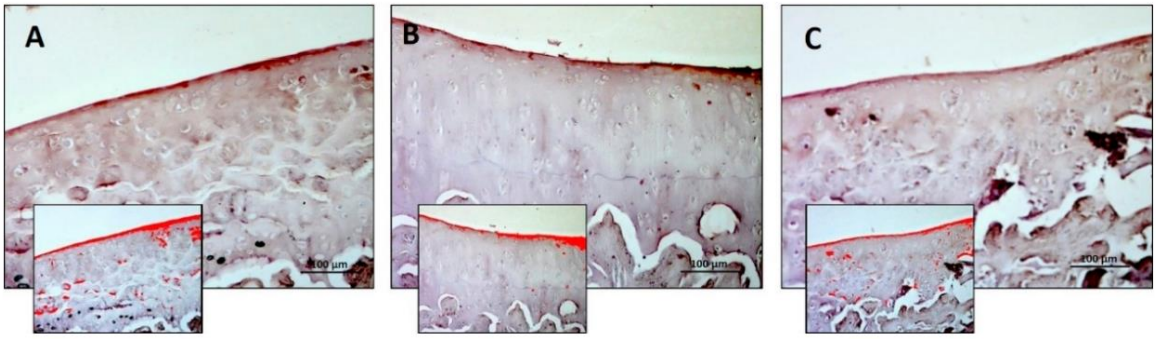

Figure 7. Vitamin D receptor (VDR) immunohistochemical evaluation in the articular cartilage through computerised densitometric measurements and image analysis. (A) R group; (B) R-DS group. (C) R-DR group. In inserts are the image analyses by the software in which the red colour represents brown staining (immune complexes labelled with chromogen). For details, see the text. (A–C) Objective lens, 10; scale bars: 100 μm. These are the most representative images of articular cartilage from rats of each group (R, R-DS and R-DR).

Table 8. VDR Immunostaining—Articular cartilage

	R (Mean ± SD)	R-DS (Mean ± SD)	R-DR (Mean ± SD)	*p*-Value
Densitometric count (pixel^2)/μm^2	0.425 ± 0.08	0.306 ± 0.05	0.347 ± 0.04	R vs. R-DS: ns R vs. R-DR: ns R-DS vs. R-DR: ns

4.4. Discussion

In the present study, the effects of exogenous Vit D supplementation on tibial articular cartilage, in a young healthy sedentary rat model, has been assessed. The results of this study demonstrate a favorable impact of exogenous Vit D supplementation (R-DS group) on the tibial articular cartilage thickness and structure. The impact of the Vit D supplementation has been further highlighted by the opposite results observed in a Vit D restricted diet group (R-DR), where the rats showed a much thinner tibial articular cartilage, supporting the data from literature [24]. An increased ECM and proteoglycan production in the R-DS group, supported both by histochemical and immunohistochemical analysis, determined a greater thickness development of the articular cartilage and a better definition of three cartilage characteristic zones (superficial, middle, and deep ones), which might suggest better mechanical properties of the latter. These findings are in accordance with the work by Pascual–Garrido and coauthors which analyzed femoral structure in rats subjected to a modified diet and UV light

restriction which provoked Vit D deficiency. Their results highlighted a significant loss of proteoglycan staining in the Vit D-deficient group but no other major histologic changes in cartilage and in the subchondral bone, concluding that low levels of Vit D have a deleterious effect on the articular cartilage [11]. Indeed, it is well known that the mechanical properties of the articular cartilage depend on the composition of the tissue, mainly collagen and proteoglycans, and their ultrastructural and molecular organization. Since proteoglycans are rich in fixed negative charges, the articular cartilage exhibits a significant osmotic pressure, which contributes to the total swelling pressure together with charge-to-charge repulsive forces exerted by the closely spaced negative charge groups along the proteoglycan molecules [25]. The more intense Alcian Blue staining in the R-DS group, when compared to the R-DR group, testifies that the amorphous substance of the ECM is particularly rich in GAGs, responsible for the physicochemical properties of the cartilage, responding better to the mechanical stress to which it is typically subjected. Mallory's trichrome staining was also evaluated to highlight the fibrous component (collagen fibers) of articular cartilage in the experimental groups. No significant differences in blue staining (which identifies the collagen fibers) were evidenced between the R-DS group and the control group (R), whereas in the R-DR group a weaker blue staining could be seen, suggesting a depletion in collagen fiber production resulting from an insufficient intake of Vit D with diet, as expected.

Furthermore, through immunohistochemical staining, the expression of some specific chondrocyte markers, such as Col II and lubricin, and a hypertrophic marker such as Col X, have been evaluated. The results of immunohistochemistry confirmed the results of Mallory's trichrome staining. Indeed, there was no higher expression of Col II in the R-DS group when compared to the control group R. Instead, the R-DR group had a lower Col II immunostaining both in comparison with the R group and the R-DS group. Moreover, the R-DS group showed increased immunostaining of lubricin, whose role is to enhance joint function, by greater tissue lubrication [26,27]. The R-DR group showed a decreased lubricin immunostaining, even if the difference was not significant when compared to the control group (R). It was also observed that lubricin, in the R-DS group, was localised in both ECM and cytoplasm of chondrocytes, while it was exclusively expressed in the chondrocyte cytoplasm of the R and R-DR groups. Concerning Col X, a higher immunoexpression was evidenced in the R-DR group compared to both R and R-DS groups, further confirming that

the Vit D restriction in the diet leads to cartilage hypertrophy and may trigger the OA onset [28].

Finally, the expression of VDR was evaluated by immunohistochemistry to assess if the increased expression of lubricin in the articular cartilage might be directly connected to the increased VDR expression and activation, following the link with Vit D to the latter. The results were not as expected. No significant differences in the VDR immunostaining were found among the groups (R, R-DS and R-DR). Although the results concerning VDR were not as expected, this does not exclude that there could be a more significant number of VDRs activated by the higher local presence of Vit D, which may exert its effect on the articular cartilage tissue, further highlighted by the higher expression of lubricin, Col II and ECM proteoglycans.

There are several studies suggesting that the Vit D deficiency is associated with the decreased articular cartilage thickness as well as with the increased risk of cartilage degeneration and, usually, with the OA onset. However, even if the symptoms of Vit D deficit are largely evidenced in literature referred to cartilage diseases, the novelty of this present study is that it has been assessed some new parameters/biomarkers (such as Col II and X, lubricin and VDR expression) not evidenced in literature in the same experimental conditions. As expected, the results strengthen the concept of the detrimental effect of Vit D deficiency on cartilage tissue, especially during the developmental period in young age. On the contrary, there is poor evidence in literature concerning the effects of the Vit D-enriched diet on the articular cartilage, particularly, in healthy young sedentary subjects. For example, the beneficial effects of Vit D have been recently demonstrated in an interesting study by Rai et al., where the Vit D supplementation attenuated the inflammation and fatty infiltration in joint tissues, in the microswine model subjected to high cholesterol diet, suggesting its importance in protecting the architecture of the articular cartilage [29]. In the present study, as described in the results, a novelty is that the Vit D-supplemented diet may support the healthy articular cartilage and its tribology in young age and in healthy animals.

Overall, in light of these findings, authors imply that rats fed with a diet supplemented with Vit D have thicker tibial cartilage when compared to the control and, especially, to those with Vit D restriction, which tibial cartilage appear much thinner and which molecular structure results altered. Moreover, the higher expression of the functional molecule as lubricin

induced by the Vit D-supplemented diet is a relevant scientific data supporting the beneficial effect on morphology/physiology of the articular cartilage. Although the results of the present study are encouraging in relation to the role of the Vit D supplementation in the diet, meta-analysis of randomized controlled trials showed moderate effect deriving from Vit D supplementation on pain, functionality and disease progression among patients with knee OA [30,31]. The results of these studies indicate that Vit D supplementation may not have a clinically significant effect on patients with a definite diagnosis of knee OA. The clinical relevance of the present study could be recognized considering the supplementation of Vit D as a non-pharmacological treatment in early osteoarthritic patients with a non-established diagnosis, since it has been shown that Vit D has different effects on cartilage morphology and molecular composition in healthy rats. Authors suggest that further studies are warranted to assess the clinical relevance of this change in cartilage thickness consequent to different exogenous Vit D provision, especially during the developmental period in young individuals and to further explore whether Vit D supplementation may allay clinical symptoms in the course of OA.

4.5. Conclusions

The results obtained in the present study show some preliminary data on the influence of introducing Vit D supplementation in the daily diet in standard health conditions. The results of this study support the idea of functional foods and their positive effects on tissue homeostasis, especially on the articular cartilage during its developmental period in young age. Today, a healthy diet is a fundamental topic for the physical well-being of people. Authors believe and hope, therefore, that this study may contribute to deepen this item and to constitute a preliminary data for further studies necessary to define the appropriate quantities of Vit D to be supplemented in the diet to be used as a preventive tool for the articular cartilage diseases. So, in the future, we would like to consider the effects of dietary Vit D supplementation on animals that have undergone a previous Vit D restriction, to verify whether the exogenous Vit D supplementation may reverse or attenuate the cartilage degeneration. Limitations of the Study: there are some limitations of the present study. One of them is represented by the lack of Vit D dosages in the biological fluids of animals, such as blood and/or synovial fluid, for a stronger proof of the presence of Vit D in its active form

(1,25(OH)2D3). Moreover, only male rats were used; therefore, the results cannot be extrapolated to females. Lastly, sample size is quite small according to the 3 Rs rule (Replacement, Reduction, Refinement) for more ethical use of experimental animals, surely recruiting more animals might sharpen the differences between the other groups as well. Furthermore, the effects on the number/density of the chondrocytes have not been evaluated. Further investigations will be required keeping in mind these limitations to better investigate the mechanism of action of Vit D in the articular cartilage in young age.

Author Contributions

All authors have made substantial intellectual contributions to the conception and design of the study as well as data acquisition, analysis and interpretation. Conceptualization, Methodology, Writing—original draft, M.A.S.; Data curation, Formal analysis, Investigation, Visualization, R.I. and P.C.; Investigation, Methodology, Writing—original draft, Investigation, C.G. and S.R.; Conceptualization, Methodology, Writing and Investigation, M.D.R.; Writing—review and editing, Project administration, G.M. All authors contributed to data interpretation and manuscript preparation. All authors approved the final submitted version.

Funding

This research gained the support of the University Research Project Grant (Triennial Research Plan 2016–2018), Department of Biomedical and Biotechnological Sciences (BIOMETEC), University of Catania, Italy.

Acknowledgments

The authors would like to express their gratitude to, Prof. Iain Halliday for his valuable work of correction of the paper.

Conflicts of Interest

The authors declare no conflict of interest.

4.6. References

1. Holick, M.F. High prevalence of vitamin D inadequacy and implications for health. *Mayo Clin. Proc.* **2006**, *81*, 353–373.
2. Wintermeyer, E.; Ihle, C.; Ehnert, S.; Stöckle, U.; Ochs, G.; de Zwart, P.; Flesch, I.; Bahrs, C.; Nussler, A.K. Crucial Role of Vitamin D in the Musculoskeletal System. *Nutrients* **2016**, *8*, 319.
3. Trovato, F.M.; Castrogiovanni, P.; Szychlinska, M.A.; Purrello, F.; Musumeci, G. Impact of Western and Mediterranean Diets and Vitamin D on Muscle Fibers of Sedentary Rats. *Nutrients* **2018**, *10*, 231.
4. Mueller, M.B.; Tuan, R.S. Anabolic/Catabolic balance in pathogenesis of osteoarthritis: Identifying molecular targets. *PM R* **2011**, *3*, S3–S11.
5. Musumeci, G.; Loreto, C.; Imbesi, R.; Trovato, F.M.; Di Giunta, A.; Lombardo, C.; Castorina, S.; Castrogiovanni, P. Advantages of exercise in rehabilitation, treatment and prevention of altered morphological features in knee osteoarthritis. A narrative review. *Histol. Histopathol.* **2014**, *29*, 707–719.
6. Felson, D.T.; Niu, J.; Clancy, M.; Aliabadi, P.; Sack, B.; Guermazi, A.; Hunter, D.J.; Amin, S.; Rogers, G.; Booth, S.L. Low levels of vitamin D and worsening of knee osteoarthritis: Results of two longitudinal studies. *Arthritis Rheumatol.* **2007**, *56*, 129–136.
7. Bergink, A.P.; Uitterlinden, A.G.; Van Leeuwen, J.P.; Buurman, C.J.; Hofman, A.; Verhaar, J.A.; Pols, H.A. Vitamin D status, bone mineral density, and thedevelopment of radiographic osteoarthritis of the knee: The Rotterdam Study. *J. Clin. Rheumatol.* **2009**, *15*, 230–237.
8. Corvol, M.T.; Dumontier, M.F.; Tsagris, L.; Lang, F.; Bourguignon, J. Cartilage and vitamin D in vitro. *Ann. Endocrinol.* **1981**, *42*, 482–487.
9. Schwartz, Z.; Bonewald, L.; Caulfield, F.; Brooks, B.; Boyan, B.D. Direct effects of transforming growth factors-B on chondrocytes are modulated by vitamin D metabolites in a cell maturation specific manner. *Endocrinology* **1993**, *132*, 1544–1552.
10. Dean, D.D.; Boyan, B.D.; Muniz, O.E.; Howell, D.S.; Schwartz, Z. Vitamin D metabolites regulate matrix vesicle metalloproteinase content in a cell maturation-dependent manner. *Calcif. Tissue Int.* **1995**, *59*, 109–116.
11. Pascual-Garrido, C.; Angeline, M.E.; Ma, R.; Chahla, J.; Voigt, C.; Deng, X.H.; Nguyen, J.; Warren, R.F.; Rodeo, S.A. Low Levels of Vitamin D have a Deleterious Effect on the Articular Cartilage in a Rat Model. *HSS J.* **2016**, *12*, 150–157.
12. Zhang, F.F.; Driban, J.B.; Lo, G.H.; Price, L.L.; Booth, S.; Eaton, C.B.; Lu, B.; Nevitt, M.; Jackson, B.; Garganta, C.; et al. Vitamin D deficiency is associated with progression of knee osteoarthritis. *J. Nutr.* **2014**, *144*, 2002–2008.
13. Konstari, S.; Paananen, M.; Heliovaara, M.; Knekt, P.; Marniemi, J.; Impivaara, O.; Arokoski, J.; Karppinen, J. Association of 25-hydroxyvitamin D with the incidence of knee and hip osteoarthritis: A 22-year follow-up study. *Scand. J. Rheumatol.* **2012**, *41*, 124–131.
14. Muraki, S.; Dennison, E.; Jameson, K.; Boucher, B.J.; Akune, T.; Yoshimura, N.; Judge, A.; Arden, N.K.; Javaid, K.; Cooper, C. Association of vitamin D status with knee pain and radiographic knee osteoarthritis. *Osteoarthr. Cartil.* **2011**, *19*, 1301–1306.
15. Wu, S.; Sun, J. Vitamin D, vitamin D receptor, and macroautophagy in inflammation and infection. *Discov. Med.* **2011**, *11*, 325–335.
16. Tetlow, L.C.; Woolley, D.E. Expression of vitamin D receptors and matrix metalloproteinases in osteoarthritic cartilage and human articular chondrocytes in vitro. *Osteoarthr. Cartil.* **2001**, *9*, 423–431.
17. Colombini, A.; Cauci, S.; Lombardi, G.; Lanteri, P.; Croiset, S.; Brayda-Bruno, M.; Banfi, G. Relationship between vitamin D receptor gene (VDR) polymorphisms, vitamin D status, osteoarthritis and intervertebral disc degeneration. *J. Steroid Biochem. Mol. Biol.* **2013**, *138*, 24–40.
18. Goula, T.; Kouskoukis, A.; Drosos, G.; Tselepis, A.S.; Ververidis, A.; Valkanis, C.; Zisimopoulos, A.; Kazakos, K. Vitamin D status in patients with knee or hip osteoarthritis in a Mediterranean country. *J. Orthop. Traumatol.* **2015**, *16*, 35–39.
19. Faul, F.; Erdfelder, E.; Lang, A.G.; Buchner, A. G*Power 3: A flexible statistical power analysis program for the social, behavioral, and biomedical sciences. *Behav. Res. Methods* **2007**, *39*, 175–191.
20. Pichler, K.; Loreto, C.; Leonardi, R.; Reuber, T.; Weinberg, A.M.; Musumeci, G. RANKL is downregulated in bone cells by physical activity (treadmill and vibration stimulation training) in rat with glucocorticoid-induced osteoporosis. *Histol. Histopathol.* **2013**, *28*, 1185–1196.

21. Gardner, O.F.W.; Musumeci, G.; Neumann, A.J.; Eglin, D.; Archer, C.W.; Alini, M.; Stoddart, M.J. Asymmetrical seeding of MSCs into fibrin-poly(ester-urethane) scaffolds and its effect on mechanically induced chondrogenesis. *J. Tissue Eng. Regen. Med.* **2017**, *11*, 2912–2921.
22. Castrogiovanni, P.; Di Rosa, M.; Ravalli, S.; Castorina, A.; Guglielmino, C.; Imbesi, R.; Vecchio, M.; Drago, F.; Szychlinska, M.A.; Musumeci, G. Moderate Physical Activity as a Prevention Method for Knee Osteoarthritis and the Role of Synoviocytes as Biological Key. *Int. J. Mol. Sci.* **2019**, *20*, 511.
23. Musumeci, G.; Castrogiovanni, P.; Coleman, R.; Szychlinska, M.A.; Salvatorelli, L.; Parenti, R.; Magro, G.; Imbesi, R. Somitogenesis: From somite to skeletal muscle. *Acta Histochem.* **2015**, *117*, 313–328.
24. Malas, F.U.; Kara, M.; Aktekin, L.; Ersöz, M.; Ozçakar, L. Does vitamin D affect femoral cartilage thickness? An ultrasonographic study. *Clin. Rheumatol.* **2014**, *33*, 1331–1334.
25. Mow, V.C.; Ratcliffe, A.; Poole, A.R. Cartilage and diarthrodial joints as paradigms for hierarchical materials and structures. *Biomaterials* **1992**, *13*, 67–97.
26. Szychlinska, M.A.; Castrogiovanni, P.; Trovato, F.M.; Nsir, H.; Zarrouk, M.; Lo Furno, D.; Di Rosa, M.; Imbesi, R.; Musumeci, G. Physical activity and Mediterranean diet based on olive tree phenolic compounds from two different geographical areas have protective effects on early osteoarthritis, muscle atrophy and hepatic steatosis. *Eur. J. Nutr.* **2019**, *58*, 565–581.
27. Szychlinska, M.A.; Trovato, F.M.; Di Rosa, M.; Malaguarnera, L.; Puzzo, L.; Leonardi, R.; Castrogiovanni, P.; Musumeci, G. Co-Expression and Co-Localization of Cartilage Glycoproteins CHI3L1 and Lubricin in Osteoarthritic Cartilage: Morphological, Immunohistochemical and Gene Expression Profiles. *Int. J. Mol. Sci.* **2016**, *17*, 359.
28. Masuyama, R.; Stockmans, I.; Torrekens, S.; Van Looveren, R.; Maes, C.; Carmeliet, P.; Bouillon, R.; Carmeliet, G. Vitamin D receptor in chondrocytes promotes osteoclastogenesis and regulates FGF23 production in osteoblasts. *J. Clin. Investig.* **2006**, *116*, 3150–3159.
29. Rai, V.; Dietz, N.E.; Dilisio, M.F.; Radwan, M.M.; Agrawal, D.K. Vitamin D attenuates inflammation, fatty infiltration, and cartilage loss in the knee of hyperlipidemic microswine. *Arthritis Res. Ther.* **2016**, *18*, 203.
30. Diao, N.; Yang, B.; Yu, F. Effect of vitamin D supplementation on knee osteoarthritis: A systematic review and meta-analysis of randomized clinical trials. *Clin. Biochem.* **2017**, *50*, 1312–1316.
31. Gao, X.R.; Chen, Y.S.; Deng, W. The effect of vitamin D supplementation on knee osteoarthritis: A meta-analysis of randomized controlled trials. *Int. J. Surg.* **2017**, *46*, 14–20.

5. MODERATE PHYSICAL ACTIVITY AS A PREVENTION METHOD FOR KNEE OSTEOARTHRITIS AND THE ROLE OF SYNOVIOCYTES AS BIOLOGICAL KEY

Paola Castrogiovanni[1,†], Michelino Di Rosa[1,†], Silvia Ravalli[1], Alessandro Castorina[2,3], Claudia Guglielmino[1], Rosa Imbesi[1], Michele Vecchio[4], Filippo Drago[4], Marta Anna Szychlinska[1] and Giuseppe Musumeci[1,5,]*

[1]Department of Biomedical and Biotechnological Sciences, Anatomy, Histology and Movement Sciences Section, School of Medicine, University of Catania, 95123 Catania, Italy;

[2]School of Life Science, Faculty of Science, University of Technology Sydney, Sydney, NSW 123, Australia;

[3]Discipline of Anatomy & Histology, School of Medical Sciences, The University of Sydney, Sydney, NSW 123, Australia;

[4]Department of Biomedical and Biotechnological Sciences, Section of Pharmacology, University of Catania, via S. Sofia 67, 95123 Catania, Italy;

[5]School of the Sport of the Italian National Olympic Committee "CONI" Sicily, Via Emanuele Notarbartolo, 90141 Palermo, Italy;

[*]Correspondence: g.musumeci@unict.it; Tel.: +095-378-2036

[†]These authors have contributed equally to this work.

Int. J. Mol. Sci. 2019, 20(3), 511; DOI:10.3390/ijms20030511

5.1. Introduction

Physical inactivity represents the fourth leading cause of morbidity and mortality globally. Regular exercise is highly beneficial for the management of many common chronic diseases [1]. There is substantial evidence for the benefits arising from physical activity in cardiovascular diseases, diabetes, obesity, and musculoskeletal conditions, including knee osteoarthritis (OA) [2]. Walking and running provide repeated loading to the knee, which is thought to be essential for joint's health within a physiological window. Physical activity, as a fast track rehab, also becomes an important treatment in patients after arthroplasty, reducing hospitalization and recovery times [3]. However, exercising outside the physiological window, e.g. excessive cyclical loading, may produce mechanical stress that could be detrimental to joint health and lead to injury and, ultimately, to OA onset [1-4].

It is well known that movement requires positioning of the body weight in horizontal (running and walking) and vertical (jumping) directions, being managed by the knee joint, one of the major and most complex joints in our body [5]. The knee consists of a modified hinge joint, a type of synovial one, bathed in synovial fluid, which is contained inside the articular capsule that is coated by the synovial membrane. The synovium is a specialized connective tissue that envelops diarthrodial joints and maintains the fluid-filled cavity to provide a lubricating environment for the articulating surfaces [6,7]. Since the articular cartilage is avascular, chondrocytes extract the oxygen and nourishing factors that are needed for cell survival from the synovial fluid by simple diffusion. The synovium produces specific substances that lubricate the joint and paracrine factors, having an important impact on articular cartilage metabolism [6,7]. The synovium displays a superficial cellular lining that is composed of two types of synoviocytes: Type A cells containing vacuoles that are related to phagocytic function (macrophages) and Type B cells with secretory fibroblast-like functions producing hyaluronan and lubricin. The latter are the lubricating molecules embedded within an extracellular matrix, rich in collagen and proteoglycans that act as a semi-permeable membrane to mediate solute transport. The Type B cells are capable of transforming into fibrocytes, depending on the inflammatory response to coexistent cytokines [8-10]. Synovium has various purposes, including lubrication, phagocytosis, and immune function. Synovial lubrication diminishes the joint frictional coefficient in healthy joints, thus reducing heating and wearing of the cartilage [11]. The loss of synovial

lubricating ability is implicated in the pathogenesis of degenerative joint diseases, including OA [12,13]. Alterations in the normal function of synoviocytes type B are related to OA, since pro-inflammatory cytokines released by the inflamed synovium shift chondrocyte activity to produce degradative enzymes, breaking down the cartilage and inhibiting tissue repair and regeneration [14].

Current evidence suggests that exercise is effective in enhancing musculoskeletal strength and power capacity, balance, range of motion, body coordination, functional joint stability, improves physical and psychological conditions, and decreases morbidity and pain in patients with OA [15,16]. In this way, muscles around the affected joints become stronger, bone loss and joint swelling decrease, and stiffness and pain improve thanks to a better lubrication of the joint cartilage [17]. However, the mechanisms mediating these effects are still not well understood. Since synoviocyte dysfunction is related to OA pathogenesis, due to the production by these cells of a number of enzymes and cytokines/chemokines that mediate tissue damage and inflammation, we hypothesized that moderate physical activity (MPA) might rescue type B synoviocyte function, as already reported for cartilage and muscle tissues [18], opening new perspectives for the prevention or treatment of OA.

Up-to-date scientific research on the biology of cartilages has been focused on finding a possible solution to treat advanced OA, either through cellular therapy, tissue engineering and other clinical methods, but few studies have dedicated their attention to OA prevention. When considering all of these aspects, and the multifactorial nature of OA in relation to hypomobility (aging, obesity, joint traumas, discordant joints, meniscal injuries, joint dislocation, ligamentous lesions, and so on) and our previous scientific evidence [3,15,17], the purpose of this morphological study is to assess the influence of synovium alterations in the OA onset and to evaluate the effects of MPA on this tissue, suggesting MPA as a biological key for OA prevention, based on its effects as a natural anti-inflammatory remedy that also enhances joint lubrication.

For this purpose, we investigated synthesis and secretory activity of the synovium, specifically in relationship to the expression of OA biomarkers, such as IL-1β, IL-6, TNF-α, and MMP-13, and anti-inflammatory and chondroprotective markers, such as IL-4, IL-10, and lubricin, in OA-induced rats that were subjected to MPA.

5.2. Materials and Methods

5.2.1. Breeding, Housing of Animals and Experimental Design

For the purpose of these studies, we used thirty-two adult male Wistar rats (Charles River Laboratories, Milan, Italy), with an average body weight of 250 ± 20 g. Rats were housed in polycarbonate cages (cage dimensions: 10.25″W × 18.75″D × 8″H) at controlled temperature (24 °C) and humidity during the whole period of the research (14 weeks) with access to water and food ad libitum and 12 h light/dark cycle. Animals were divided into four groups: Group 1, control health rats (n = 8); Group 2: rats performing MPA (treadmill training exercise) (n = 8); Group 3: ACLT-rats with early OA (n = 8); and, Group 4: ACLT-rats with early OA performing MPA (treadmill training exercise) (n = 8).

Surgical procedures for anterior cruciate ligament transection (ACLT) were performed in accordance with the method that was previously described [19,20]. The ACLT surgery (Figure 1) procedure was made under total anesthesia to induce the OA model, 30 mg/kg Zoletil 100 + altadol 5 mg/kg + maintenance mixture of O2 and isoflurane 2–2.5%, (Vibrac, Milan, Italy). The anterior portion of the left hind limb was shaved with an electric clipper and cleaned with ethanol. The skin around the kneecap was vertically incised along the medial border of the knee cap. The patella was displaced laterally to expose the anterior cruciate ligament. Subsequently, the anterior cruciate ligament was cut with surgical scissors without injury to the cartilage of the tibia. The patella was then replaced back and the fascia and skin were closed with a 3-0 polydioxanone suture. A single dose of antibiotic Convenia® 0.1 mL/kg, (Vibrac) cream was applied to avoid postoperative infection. After surgery, free cage movement without joint immobilization was permitted to all animals. The pre-operative examinations included physical and photographical examination.

Figure 1. Surgical procedures for anterior cruciate ligament transection (ACLT) step by step. (A) Pre-operative examinations and weighing of the rat; (B) Anesthesia of the rat; (C) Shearing of the rat; (D) Cutting the skin of the rat; (E) Cutting the capsule of the rat; (F) The patella was displaced laterally to expose the anterior cruciate ligament, then, the anterior cruciate ligament was cut with surgical scissors; (G) The skin around the knee cap was vertically incised along the medial border of the knee cap; (H) The patella was then replaced back, and the fascia and skin were closed with a 3–0 polydioxanone suture; (I) The rat after the suture under anesthesia before awakening; (J) The rat in the heated bed before awakening from anesthesia; (K) After surgery, free cage movement without joint immobilization was permitted to the rat; (L) Rats from Group 3 during exercise on Treadmill; (M) Knee joint covered to capsule; (N) Capsule removal; and, (O) Knee joint without capsule.

At the end of the experiment, after the physical activity protocol, animals were humanely sacrificed by an intravenous lethal injection of anesthetic overdose using a mixture of Zoletil 100 (Virbac) at a dose of 80 mg/kg and DEXDOMITOR (Virbac) at a dose of 50 mg/kg. After euthanasia, the synovial membrane from knee joint and the articular cartilage were explanted, and the samples were used to perform histological and immunohistochemical evaluation in synovium and histomorphometric analysis in articular cartilage. All of the experiments were designed to minimize animal suffering and to use the minimum number of animals required to achieve a valid statistical evaluation according the principles of the 3R's (replacement, reduction and

refinement of animal use). All of the procedures conformed to the guidelines of the Institutional Animal Care and Use Committee (I.A.C.U.C.) at the Center for Advanced Preclinical In Vivo Research (CAPIR), University of Catania, and approved by Italian Ministry of Health, Protocol n. 2112015-PR of the 14.01.2015 (14 January 2015). The experiments were conducted in accordance with the European Community Council Directive (86/609/EEC) and the Italian Animal Protection Law (116/1992).

5.2.2. Treadmill Training Exercise

Following two weeks of acclimatization to the housing environment after ACLT, rats from Groups 2 and 4 were exposed to their respective exercise program on the treadmill (2Biological instrument, Varese, Italy), for 12 weeks [1,17]. The exercise (from mild to moderate) progressively built up to 25 min of treadmill training each day, three times per week at 20 meters/min (see Table 1 for details of the exercise program). The treadmill was inclined at 2° (between two and six degrees). A mild electric shock (0.2 mA) forced the rat to walk on the treadmill at a speed and inclination adapted to it. The shock serves to stimulate the rat to walk and to instruct it. The rat usually learns this activity in the first two minutes of exercise. This type of exercise is used to stimulate the muscles, joints, and bones in the work of flexion-extension of the limbs and to release more synovial fluid into the articular capsula. All electric shock data were acquired by Data acquisition software (2Biological instrument, Varese, Italy). Before and after exercise, rats were left free without immobilization in their cages. During the exercise, the possible suffering of the animal was evaluated. Potential rats discarded from the experiment: rats that exhibited difficulties in walking; and rats that exceeded the number of 10 electric shocks (0.2 mA) without learning the work to be done on the treadmill. None of the rats presented any of these characteristics and thus no animals were excluded from the study.

Table 1. Twelve-week treadmill training program (mild to moderate physical activity)

Week	Speed (m/min)	Session/Week	Session/Day	Duration (min)
1	5	3	1	5
2	10	3	1	10
3–6	15	3	1	15
7–12	20	3	1	25

8.2.3. Histology Analysis

Synovium and articular cartilage samples were fixed in 10% neutral buffered-formalin (Bio-Optica, Milan, Italy), following overnight washing and routinely embedded in paraffin, as previously described [21]. Samples were positioned in the cassettes after wax infiltration. A rotary manual microtome (Leica RM2235, Milan, Italy) was used to cut 4–5 μm thick sections from paraffin blocks that were mounted on silane-coated slides (Menzel-

Gläser, Braunschweig, Germany) and stored at room temperature. After dewaxing in xylene, the slides were hydrated using graded ethanol and were stained by Hematoxylin & Eosin (H&E) staining for histological and histomorphometric evaluation, detecting possible structural alterations in tissues. The samples were examined with a Zeiss Axioplan light microscope (Carl Zeiss, Oberkochen, Germany) and a digital camera (AxioCam MRc5, Carl Zeiss) was used to take the pictures.

5.2.4. Histomorphometric Analysis

The femur explantation procedure and the subsequent cleaning of soft tissues were performed as previously described [22]. Samples from all rats (both medial and lateral femoral condyles of untreated and surgically treated animals) were used for the histomorphometric analysis. Histomorphometry was performed with image analysis, Kontron KS 300 software (Kontron Electronics, Eching bei Munchen, Germany) by three blinded investigators (two anatomical morphologists and one histologist). Evaluations were assumed to be correct if there were no statistically significant differences between the investigators. Seven fields randomly selected from each section were analysed. Multiple measurements of cartilage thickness in different points of cartilage were detected in all groups and the semi-quantitative grading criteria of macroscopic Kraus' modified Mankin score [23] and microscopic histopathology OARSI system [24] were used.

The Kraus' modified Mankin score provides grades from 0 to 4: Grade 0, normal cartilage; Grade 1, minimal articular damage; Grade 2, articular cartilage damage affecting up to 30% of the articular surface; Grade 3, loss of up to 50% of the articular cartilage; Grade 4, severe loss of cartilage affecting more than 50% of the articular surface.

The Histopathology OARSI system provides grades from 0 to 6: Grade 0, normal articular cartilage; Grade 1, intact surface; Grade 2, surface discontinuity; Grade 3, vertical fissures extending into mid zone; Grade 4, erosion; Grade 5, denudation; Grade 6, deformation.

5.2.5. Immunohistochemistry (IHC) Analysis

Synovium samples were processed for immunohistochemical analysis, as previously described [25]. Briefly, after dewaxing in xylene, the slides were hydrated through graded ethanol and incubated for 30 min in 0.3% H_2O_2/methanol to quench endogenous peroxidase activity and then rinsed for 20 min with phosphate-buffered saline (PBS; Bio-Optica). The sections were then heated (5 min × 3) in capped polypropylene slide-holders with citrate buffer (10 mM citric acid, 0.05% Tween 20, pH 6.0; Bio-Optica), using a microwave oven (750 W) to unmask antigenic sites. The blocking step to prevent non-specific binding of the antibody was performed before application of the primary antibody with 5% bovine serum albumin (BSA, Sigma, Milan, Italy) in PBS for 1 h in a moist chamber. After blocking, the sections were incubated overnight at 4°C with rabbit polyclonal anti-IL-1β (ab9787; Abcam), diluted 1:100 in PBS (Bio-Optica); rabbit polyclonal anti-IL-4 (ab9622; Abcam), diluted 1:100 in PBS (Bio-Optica); goat polyclonal anti-IL-6 antibody (sc-1265; Santa Cruz Biotechnology Inc., Dallas, TX, USA) diluted 1:100 in PBS (Bio-Optica); rabbit polyclonal anti-IL-10 (ab34843; Abcam), diluted 1:100 in PBS (Bio-Optica); mouse monoclonal anti-TNF-α antibody (ab199013; Abcam) diluted 1:100

in PBS (Bio-Optica); mouse monoclonal anti-MMP-13 antibody (sc-81547; Santa Cruz Biotechnology Inc.) diluted 1:100 in PBS (Bio-Optica); rabbit polyclonal anti-lubricin antibody (ab28484; Abcam), diluted 1:100 in PBS (Bio-Optica). Immune complexes were then treated with a biotinylated link antibody (HRP-conjugated were used as secondary antibodies) and were then detected with peroxidase labeled streptavin, both incubated for 10 min at room temperature (LSAB+ System-HRP, K0690, Dako, Glostrup, Denmark). The immunoreaction was visualized by incubating the sections for 2 min in a 0.1% 3,3′-diaminobenzidine and 0.02% hydrogen peroxide solution (DAB substrate Chromogen System; Dako). The samples were lightly counterstained with Mayer's Hematoxylin (Histolab Products AB, Goteborg, Sweden) mounted in GVA mount (Zymed, Laboratories Inc., San Francisco, CA, USA) and observed with an Axioplan Zeiss light microscope (Carl Zeiss) and photographed with a digital camera (AxioCam MRc5, Carl Zeiss).

5.2.6. Evaluation of Immunohistochemistry

The IL-1β-, IL-4-, IL-6-, IL-10-, TNF-α-, MMP-13-, and lubricin-staining status was identified as either negative or positive. As previously described, immunohistochemical staining was defined positive if brown chromogens were detected on the edge of the hematoxylin-stained cell nucleus, within the cytoplasm or in the membrane [26]. Light microscopy was used to evaluate stain intensity and the percentage of immunopositive cells. Intensity of staining (IS) was evaluated on a four grades scale (0–4), as following: no detectable staining = 0, weak staining = 1, moderate staining = 2, strong staining = 3, and very strong staining = 4. Three investigators (2 anatomical morphologists and one histologist) independently evaluated the percentage of antibodies immunopositive cells through the five categories of Extent Score (ES): <5% (0); 5–30% (+); 31–50% (++); 51–75% (+++); and, >75% (++++). Counting was performed under Zeiss Axioplan light microscope at 200× magnification. If disputes concerning the interpretation occurred, the case was revised to reach a unanimous agreement, as previously described [27]. A digital camera (Canon, Tokyo Japan) at 20×, 40× and 60× magnifications was used to take digital pictures. In this study, positive controls, consisting of rat cartilage tissue, and negative control sections, which were treated with PBS without the primary antibody, were performed to test the specific reaction of primary antibodies used at a protein level. Positive immunolabeling for antibodies were nuclear/cytoplasmic.

5.2.7. Computerized Densitometric Measurements and Image Analysis

Image analysis software (AxioVision Release 4.8.2-SP2 Software, Carl Zeiss Microscopy GmbH, Jena, Germany), which quantifies the level of staining of positive anti-IL-1β, anti-IL-4, anti-IL-6, anti-IL-10, anti-TNF-α, anti-MMP-13, and anti-lubricin antibodies immunolabelling, was used to calculate the densitometric count (pixel^2) in seven fields, area of which was about 150.000 μm^2, randomly selected from each section. Digital micrographs were taken using the Zeiss Axioplan light microscope (Carl Zeiss, using objective lens of magnification 20× i.e., total magnification 200×) fitted with a digital camera (AxioCam MRc5, Carl Zeiss). Three blinded investigators (two anatomical morphologists and one histologist) made the evaluations that were assumed to be correct if values have not statistically significant difference [28]. If disputes concerning interpretation occurred, unanimous agreement was reached after sample re-evaluation.

5.2.8. Statistical Analysis

Statistical analysis was performed using GraphPad Instat® Biostatistics version 3.0 software (GraphPad Software, Inc. La Jolla, CA, USA). Analysis of variance (one-way ANOVA—Tukey's multiple comparisons test) was used for comparison between more than two groups; Unpaired t test with Welch's correction was used for comparison between two groups. p-values of less than 0.05 were considered to be statistically significant (* $p < 0.05$; ** $p < 0.01$; *** $p < 0.001$; **** $p < 0.0001$ and ns: not significant). Data are presented as the mean ± SD.

5.3. Results

5.3.1. Histology

Hematoxylin & Eosin (H&E) staining in articular cartilage samples was used to verify the onset of experimentally induced early OA through histomorphometric analyses detailed below. In Group 1 and 2, articular cartilage showed normal cytoarchitecture. Cells appeared flat and small in the superficial zone; chondrocytes displayed a columnar organization in the middle and deep zone; the tidemark was evident; cartilage thickness measured, respectively, 383.0 ± 76.76 and 396.5 ± 61.68 µm, with no statistical difference between them ($p \geq 0.05$, ns = not significant) (Figure 2A,B,E). Group 3 showed signs of moderate OA. In fact, articular cartilage presented with structural alterations in the superficial and middle zones and chondrocytes were poorly organized in columns in the intermediate and deep zones; moreover, a reduction of thickness was observed (260.7 ± 62.34 µm) and the difference was statistically significant when compared with both Group 1 and 2 ($p < 0.0001$) (Figure 2C,E). In Group 4, better general tissue preservation was observed in comparison with Group 3, where the articular cartilage showed a slight but not statistically significant reduction in thickness (357.9 ± 61.88 µm) when compared with Group 1 ($p \geq 0.05$, ns). The cartilage also showed a reduced number of cells (Figure 2D,E). From the histochemical analyses (H&E stainings) of synovium samples, synovium from neither group manifested any alteration, as expected (Figure 2F–I).

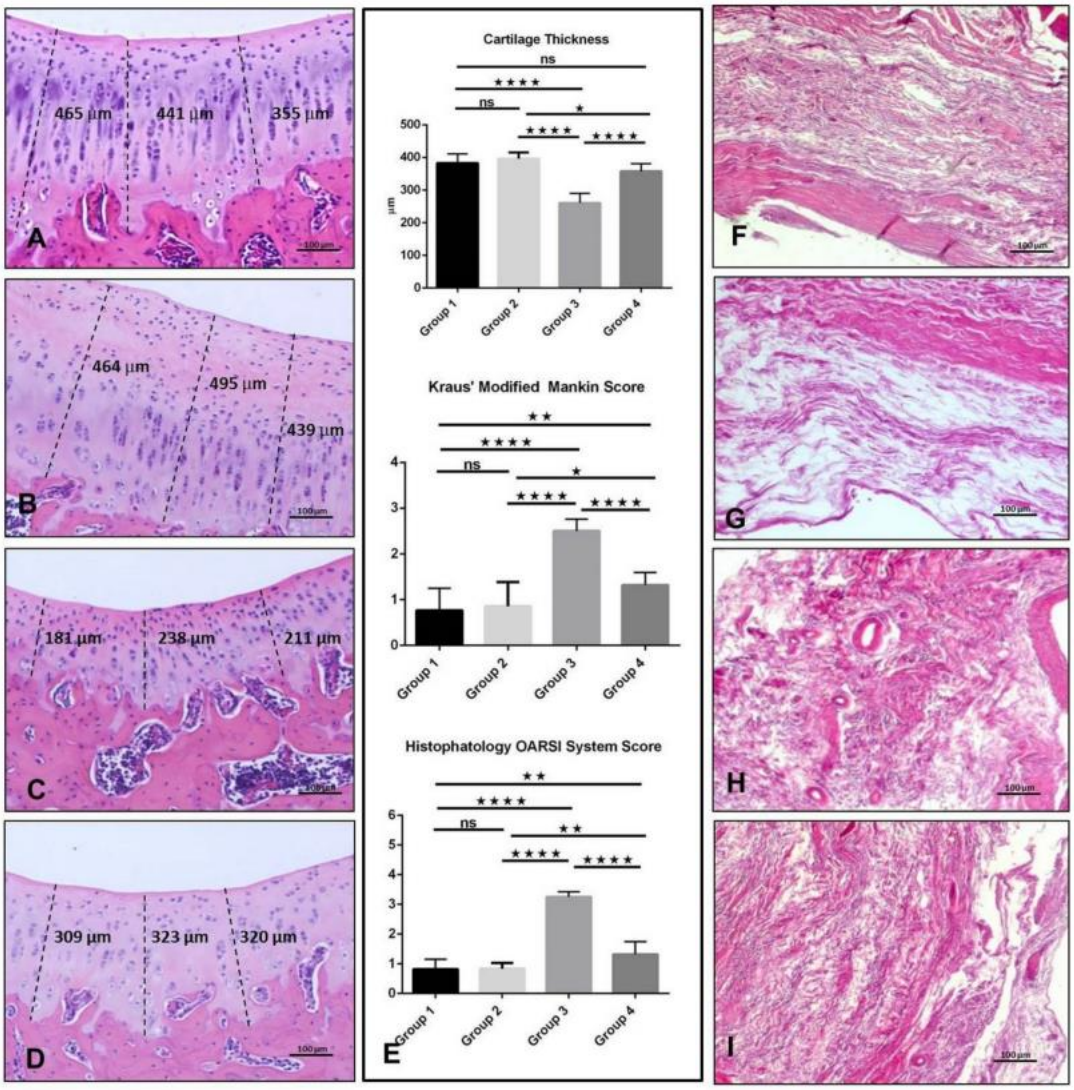

Figure 2. Histological evaluation and histomorphometric analysis of articular cartilage and synovium by Hematoxylin & Eosin (H&E) staining. (A) Group 1. Cells flat and small in the superficial zone; chondrocytes in columns in the middle and deep zone; tidemark evident; cartilage thickness 383.0 ± 76.76 µm. (B) Group 2. Numerous and small cells in the superficial zone; chondrocytes in columns in the middle and deep zone; tidemark evident; cartilage thickness 396.5 ± 61.68 µm. (C) Group 3. Articular cartilage showing structural alterations in the superficial and the middle zones and chondrocytes poorly organized in columns in the intermediate and deep zone; cartilage thickness 260.7 ± 62.34 µm. (D) Group 4. Articular cartilage showing only a slight reduction of the total thickness 357.9 ± 61.88 µm and a better general tissue preservation. (E) Graphs representing measures of the cartilage thickness, the Kraus' Modified Mankin Score and the Histopathology OARSI System identified among groups. Results were presented as the mean ± SD. ANOVA was used to evaluate the significance of the results. * $p < 0.05$; ** $p < 0.01$; **** $p < 0.0001$; ns, not significant. For details, see the text. (F) H&E staining of synovium of Group 1. G H&E staining of synovium of Group 2. H H&E staining of synovium of Group 3. I H&E staining of synovium of Group 4. No histological alterations were evidenced in the synovium area of all groups. (A–D,F–I): Objective lens, 10×; scale bars: 100 µm.

5.3.2. Histomorphometric Analyses

The histomorphometric analyses on articular cartilage samples were conducted to verify the onset of induced early OA. Histomorphometric parameters that were performed in Group 1 confirmed that there were no obvious signs of cartilage degeneration, with animals showing an intact and normal cartilage structure. Moreover, the Kraus' Modified Mankin Score was 0.76 ± 0.87 and Histopathology OARSI System Score was 0.82 ± 0.76. Group 2 also showed no signs of cartilage degeneration, with a Kraus' Modified Mankin Score of 0.85 ± 0.90 and a Histopathology OARSI System Score of 0.83 ± 0.73. Conversely, animals from Group 3 demonstrated pathological changes in the cartilage, with Kraus' Modified Mankin Score of 2.5 ± 0.83, and Histopathology OARSI System Score of 3.25 ± 0.71. Group 4 showed a better cartilage preservation as compared to Group 3, with a Kraus' Modified Mankin Score of 1.32 ± 0.76, and a Histopathology OARSI System Score of 1.32 ± 0.78 (Figure 2E). Statistical analyses highlighted that, for both scores, there was a significant difference among groups. In particular: Group 1 vs. Group 2, ($p \geq 0.05$, ns) both in Kraus' Modified Mankin Score and Histopathology OARSI System Score; Group 1 vs. Group 3, $p < 0.0001$ both in Kraus' Modified Mankin Score and Histopathology OARSI System Score; Group 1 vs. Group 4 had a $p = 0.0018$ in Kraus' Modified Mankin Score and a $p = 0.0025$ in Histopathology OARSI System Score; Group 2 vs. Group 3, had a $p < 0.0001$ both in Kraus' Modified Mankin Score and in Histopathology OARSI System Score; Group 2 vs. Group 4, had a $p = 0.0130$ in Kraus' Modified Mankin Score and a $p = 0.0038$ in Histopathology OARSI System Score; Group 3 vs. Group 4, $p < 0.0001$ in Kraus' Modified Mankin Score and also in Histopathology OARSI System Score (Figure 1E). Inter-observer reliability among the five observers for the Mankin system showed a similar good intra-class correlation coefficient (ICC > 0.92) as for the OARSI system (ICC > 0.90). Repeated scoring by three of the five investigators resulted in a very good agreement (ICC > 0.94). Data are presented as the mean ± SD.

5.3.3. Immunohistochemistry (IHC) and Statistical Analysis

Different patterns of immunopositive cells in the sets of specimens were observed (Table 2).

Table 2. Evaluation of IL-1β-, IL-4-, IL-6-, IL-10-, TNF-α-, MMP-13-, and lubricin-immunostaining. Intensity of staining (IS) was graded on a scale of 0–4, based on the following criteria: No detectable staining (0), weak staining (1), moderate staining (2), strong staining (3), and very strong staining (4). The percentage of immunopositive cells (Extent Score = ES) was independently evaluated by three investigators (two anatomical morphologists and one histologist) and ranked according to the following criterium: <5% (0); 5–30% (+); 31–50% (++); 51–75% (+++), and >75% (++++).

Group	IL-1β	IL-4	IL-6	IL-10	TNF-α	MMP-13	Lubricin
1	ES = 0 IS = 1	ES = + IS = 2	ES = + IS = 2	ES = ++ IS = 2	ES = 0 IS = 1	ES = 0 IS = 1	ES = +++ IS = 3
2	ES = 0 IS = 1	ES = ++ IS = 3	ES = + IS = 3	ES = +++ IS = 3	ES = 0 IS = 1	ES = 0 IS = 1	ES = ++++ IS = 4
3	ES = ++ IS = 2	ES = + IS = 1	ES = +++ IS = 4	ES = + IS = 1	ES = +++ IS = 3	ES = ++ IS = 3	ES = ++ IS = 2
4	ES = + IS = 1	ES = ++ IS = 3	ES = +++ IS = 4	ES = +++ IS = 3	ES = + IS = 1	ES = + IS = 1	ES = +++ IS = 3

• IL-1β immunolabeling was very weak in the synovium of both Group 1 and 2 (ES = 0; IS = 1) (Figure 3A,B). IL-1β immunolabeling was moderate (ES = ++; IS = 2) in the synovium of Group 3 (Figure 3C). IL-1β immunolabeling was weak (ES = +; IS = 1) in the synovial membrane of Group 4 (Figure 3D).

• IL-4 immunolabeling was moderate in the synovium of Group 1 (ES = +; IS = 2) (Figure 3F). IL-4-immunostaining was weak (ES = +; IS = 1) in the synovium of Group 3 (Figure 3H) and it was strong in the synovial membrane of both Group 2 (ES = ++; IS = 3) (Figure 3G) and Group 4 (ES = ++; IS = 3) (Figure 3I).

• IL-6 immunolabeling was moderate in the synovium of Group 1 (ES = +; IS = 2) (Figure 3K). IL-6-immunostaining was strong (ES = +; IS = 3) in the synovium of Group 2 (Figure 3L). IL-6-immunostaining was very strong (ES = +++; IS = 4) in the synovium of both Group 3 (Figure 3M) and Group 4 (Figure 3N).

• IL-10 immunolabeling was moderate in the synovium of Group 1 (ES = ++; IS = 2) (Figure 3P). IL-10-immunostaining was weak (ES = +; IS = 1) in the synovium of Group 3 (Figure 3R) and it was strong (ES = +++; IS = 3) in the synovial membrane of both Group 2 and 4 (Figure 3Q,S).

• TNF-α immunolabeling was very weak in the synovium of both Group 1 and 2 (ES = 0; IS = 1) (Figure 4A,B). On the contrary, TNF-α-immunostaining was strong (ES = +++; IS = 3) in the synovium of Group 3 (Figure 4C) and weak (ES = +; IS = 1) in Group 4 (Figure 4D).

• MMP-13 immunolabeling was very weak in the synovium of both Group 1 and 2 (ES = 0; IS = 1) (Figure 4F,G). MMP-13-immunostaining was strong (ES = ++; IS = 3) in the synovium of Group 3 (Figure 4H) and it was weak (ES = +; IS = 1) in Group 4 (Figure 4I).

• Lubricin immunolabeling was strong in the synovium of both in Group 1 and 4 (ES = +++; IS = 3) (Figure 4K,N). It was very strong (ES = ++++; IS = 4) in the synovium of Group 2 (Figure 4L) and moderate (ES = ++; IS = 2) in the synovium of Group 3 (Figure 4M).

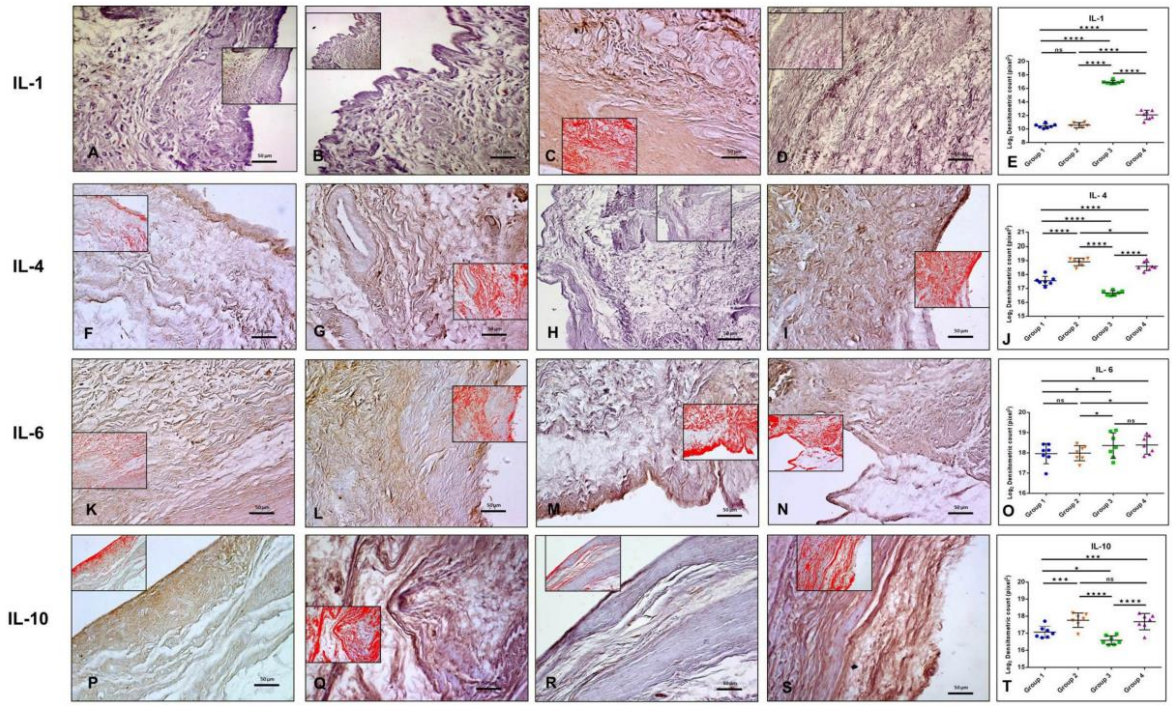

Figure 3. (A–E): IL-1β immunohistochemistry. (A) IL-1β immunolabeling was very weak in the synovium of Group 1; (B) IL-1β immunolabeling was very weak in the synovium of Group 2; (C) IL-1β immunolabeling was moderate in the synovium of Group 3; (D) IL-1β immunolabeling was weak in the synovial membrane of Group 4; (E) Graph representing the densitometric count (Log2 densitometric count − pixel^2) of IL-1-immunolabeling identified among groups. For details, see the text. (F–J): IL-4 immunohistochemistry. (F) IL-4 immunolabeling was moderate in the synovium of Group 1; (G) IL-4 immunolabeling was strong in the synovium of Group 2; (H) IL-4 immunolabeling was weak in the synovium of Group 3; (I) IL-4 immunolabeling was strong in the synovial membrane of Group 4; (J) Graph representing the densitometric count (Log2 densitometric count − pixel^2) of IL-4-immunolabeling identified among groups. For details, see the text. (K–O): IL-6 immunohistochemistry. (K) IL-6 immunolabeling was moderate in the synovium of Group 1; (L) IL-6 immunolabeling was strong in the synovium of Group 2; (M) IL-6 immunolabeling was very strong in the synovium of Group 3; (N) IL-6 immunolabeling was very strong in the synovial membrane of Group 4; (O) Graph representing the densitometric count (Log2 densitometric count − pixel^2) of IL-6-immunolabeling identified among groups. For details, see the text. (P–T): IL-10 immunohistochemistry. (P) IL-10 immunolabeling was moderate in the synovium of Group 1; (Q) IL-10 immunolabeling was strong in the synovium of Group 2; (R) IL-10 immunolabeling was weak in the synovium of Group 3; (S) IL-10 immunolabeling was strong in the synovial membrane of Group 4; and, (T) Graph representing the densitometric count (Log2 densitometric count − pixel^2) of IL-10-immunolabeling identified among groups. For details, see the text. In inserts are the image analyses by the software in which red color represents immunolabeling. (A–D,F–I,K–N,P–S): Objective lens, 20×; scale bars: 50 µm. Results were presented as the mean ± SD. ANOVA was used to evaluate the significance of the results. * $p < 0.05$; ** $p < 0.01$; *** $p < 0.001$; **** $p < 0.0001$; ns, not significant.

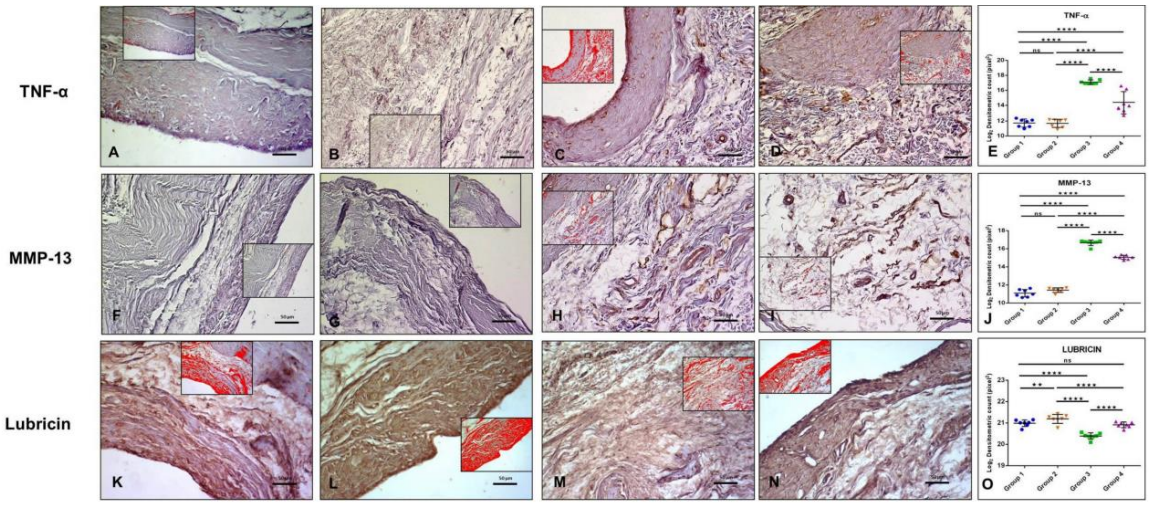

Figure 4. (A–E): TNF-α immunohistochemistry. (A) TNF-α immunolabeling was weak in Group 1; (B) TNF-α immunolabeling was weak in Group 2; (C) TNF-α-immunostaining was strong in Group 3; (D) TNF-α-immunostaining was weak in Group 4; (E) Graph representing the densitometric count (Log2 densitometric count − pixel^2) of TNF-α-immunolabeling identified among groups. For details, see the text. (F–J): MMP-13 immunohistochemistry. (F) In Group 1, MMP-13 was very weak; (G) In Group 2, MMP-13 was very weak; (H) MMP-13-immunostaining was strong in Group 3; (I) MMP-13-immunostaining was weak in Group 4; (J) Graph representing the densitometric count (Log2 densitometric count − pixel^2) of MMP-13-immunolabeling identified among groups. For details, see the text. (K–O): Lubricin immunohistochemistry. (K) Lubricin immunolabeling was strong in the synovium of Group 1; (L) Lubricin immunolabeling was very strong in the synovium of Group 2; (M) Lubricin immunolabeling was moderate in Group 3; (N) Lubricin immunolabeling was strong in the synovial membrane of Group 4; and, (O) Graph representing the densitometric count (Log2 densitometric count − pixel^2) of Lubricin-immunolabeling identified among groups. For details, see the text. In inserts are the image analyses by the software in which red color represents immunolabeling. (A–D,F–I,K–N): Objective lens, 20×; scale bars: 50 µm. Results were presented as the mean ± SD. ANOVA was used to evaluate the significance of the results. ** $p < 0.01$; **** $p < 0.0001$; ns, not significant.

The above-mentioned results were confirmed by densitometric count (pixel), as obtained through image analysis by AxioVision software and statistical analysis, in which a statistically significant difference among groups was highlighted and in particular:

• IL-1β immunolabeling was much higher in Group 3 (16.92 ± 1.077) with respect to Group 1 (10.43 ± 1.139), Group 2 (10.56 ± 0.97), and Group 4 (12.08 ± 1.225). Group 1 and 2 had similar values ($p \geq 0.05$, ns), whereas there was a statistically significant difference among groups (Groups 1 and 2 vs. 3, $p < 0.0001$; Groups 1 and 2 vs. 4, $p < 0.0001$; Group 3 vs. Group 4, $p < 0.0001$ (Figure 3E).

• IL-4 immunolabeling was higher both in Group 2 and 4 (respectively, 18.91 ± 0.768 and 18.59 ± 0.632) when compared to both Group 1 (17.55 ± 0.562) and Group 3 (16.67 ± 0.375). There was a statistically significant difference between Group 1 vs. Group 2, $p < 0.0001$; Group 1 vs. Group 3, $p < 0.0001$; Group 1 vs. Group 4, $p < 0.0001$; Group 2 vs. Group 3, $p < 0.0001$; Group 2 vs. Group 4, $p = 0.0196$; Group 3 vs. Group 4, $p < 0.0001$, (Figure 3J).

• IL-6 immunolabeling manifested a statistically significant difference between Group 1 (17.96 ± 0.786) vs. Group 3 (18.36 ± 1.106) ($p = 0.0321$) and Group 1 vs. Group 4 (18.39 ± 0.829) ($p = 0.0188$) with a higher IL-6 expression in both Group 3 and 4. Also, the differences between Group 2 (17.99 ± 0.638) vs. Group 3 and Group 2 vs. Group 4 were statistically significant, respectively $p = 0.0468$ and 0.0281. Conversely, the difference between Group 1 vs. Group 2 and between Group 3 vs. Group 4 was not statistically significant ($p \geq 0.05$, ns) (Figure 3O).

• IL-10 immunolabeling was evident and similar in both Group 2 (17.76 ± 0.953) and Group 4 (17.68 ± 0.979) (p = ns). A statistically significant difference was evident among all groups and in particular: Group 1 (17.07 ± 0.817) vs. Group 2 had a $p = 0.0001$; Group 1 vs. Group 3 (16.59 ± 0.686) had a $p = 0.0145$; Group 1 vs. Group 4 had a $p = 0.0009$; Group 2 vs. Group 3 had a $p < 0.0001$; Group 3 vs. Group 4 had a $p < 0.0001$ (Figure 3T).

• TNF-α immunolabeling was higher in Group 3 (17.10 ± 0.608) when compared to all other groups, Group 1 (11.73 ± 0.968), Group 2 (11.69 ± 0.956) and Group 4 (14.39 ± 1.726) (Group 1 vs. Group 3, $p < 0.0001$; Group 2 vs. Group 3, $p < 0.0001$; Group 3 vs. Group 4, $p < 0.0001$). There was a statistically significant difference also between Group 1 vs. Group 4 ($p < 0.0001$); no statistical significance was found between Group 1 vs. Group 2 ($p \geq 0.05$, ns), (Figure 4E).

• MMP-13-immunostaining was much higher in Group 3 (16.65 ± 0.664) when compared to Group 1 (11.09 ± 0.869) ($p < 0.0001$), Group 2 (11.42 ± 0.963) ($p < 0.0001$) and Group 4 (15.05 ± 0.646) ($p < 0.0001$). Furthermore, a statistically significant difference was shown also between Group 1 vs. Group 4 ($p < 0.0001$) and Group 2 vs. Group 4 ($p < 0.0001$). No statistically significant difference was found between Group 1 vs. Group 2 ($p \geq 0.05$, ns) (Figure 4J).

• Lubricin immunolabeling in Group 3 (20.39 ± 0.275) was lower than in other groups. In particular: Group 1 (20.99 ± 0.226) vs. Group 3, $p < 0.0001$; Group 2 (21.19 ± 0.529) vs. Group 3, $p < 0.0001$; Group 3 vs. Group 4 (20.91 ± 0.267), $p < 0.0001$). Moreover, Group 1 vs. Group 2 had a statistically significant difference ($p = 0.0066$), whereas lubricin-immunostaining was similar in Group 1 and Group 4, hence showing no statistical difference ($p \geq 0.05$, ns) (Figure 4O).

5.4. Discussion

The purpose of this study was to investigate the possible influence of MPA on the expression of OA-related biomarkers as well as anti-inflammatory and chondroprotective markers by synoviocytes type B in OA rat model. As recommended by World Health Organization, MPA refers to the activity that requires energy of 3.0 to 5.9 times higher than that of the resting state [19]. The MPA-based approach may support joint tribology and synovial lubrication, leading to improved joint function and pain relief. Our hypothesis is that the adapted MPA/movement may counteract synoviocyte Type B dysfunction at the early stages of OA, impeding overt onset of OA. Potential physical non-pharmacologic treatment strategies at the initial stages of OA may reduce the pathological burden of the condition at its early stages and possibly postpone the need for joint replacement (Figure 5).

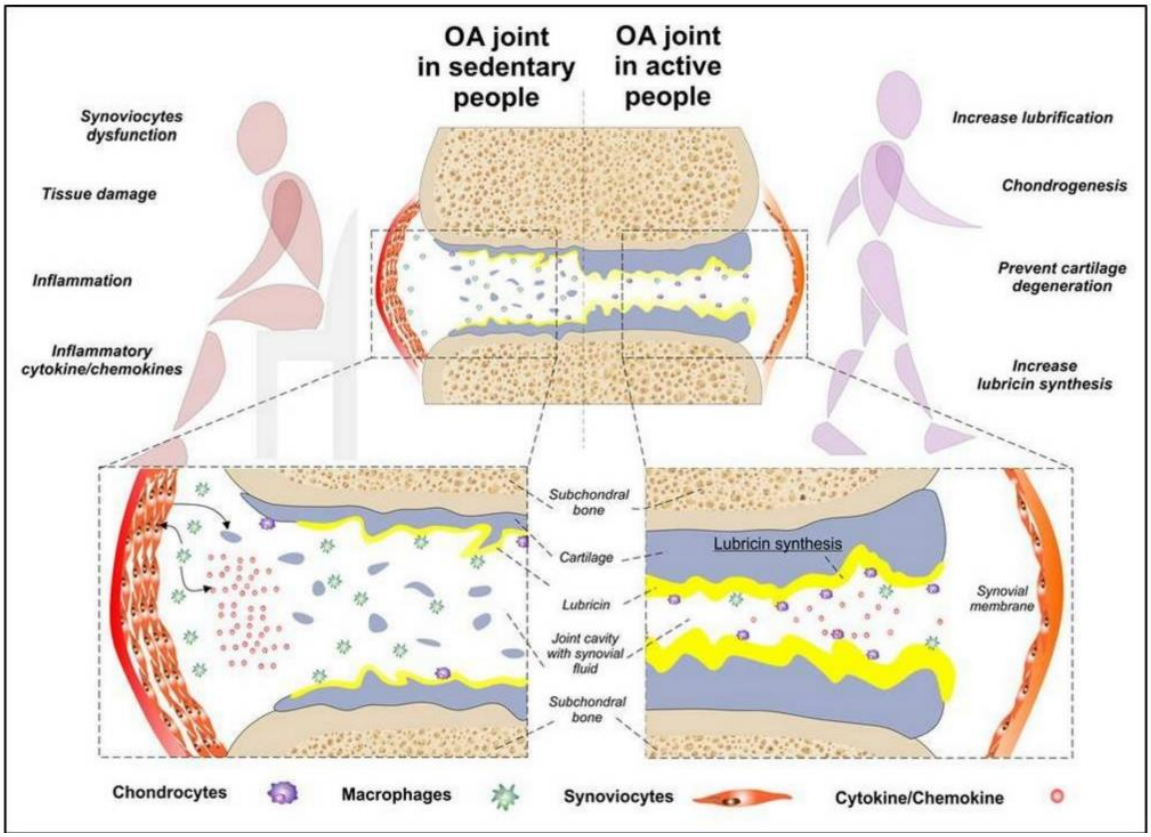

Figure 5. Graphical representation of a joint affected by moderate osteoarthritis (OA) in sedentary people and in active people with relative benefits and disadvantages. Pro-inflammatory cytokines play a key role in the pathogenesis of OA, by mediating the progressive degeneration of the articular cartilage within the joint. The deteriorating processes involve different types of cells including macrophages, chondrocytes and synoviocytes.

In the present work, we used a well-established model to induce an early OA through the anterior cruciate ligament transection (ACLT) technique [20,22,29]. The ACLT model is a short-term surgically induced OA model that in this study has surely benefited from exercise. This model of early OA is different from chronic OA based on the long-term inflammation, where the disease develops over decades and it is often combined with other systemic conditions and comorbidities, such as sarcopenia [13,16]. However, as well known, if OA is not adequately treated at its prodromal stages by lifestyle interventions, such as MPA and/or surgery or pharmacological therapy, then OA would become chronic due to the ongoing joint instability and consequent joint degeneration [20,22,29].

The results that were obtained in the present study on synovium, are in line with both our previous data and those of other authors on several joint tissues [15-17,20,22,29-35]. In this morphological study, we investigated the expression of some pro-inflammatory molecules (IL-1β, IL-6, TNF-α), OA-related enzymes (MMP-13), anti-inflammatory cytokines (IL-4, IL-10), and chondroprotective markers (lubricin) in synovium of OA-induced rats that were subjected to MPA.

Firstly, in the ACLT-rat group (Group 3), the above-mentioned OA-related markers were significantly increased, while IL-4, IL-10, and lubricin expression were drastically decreased when compared with Groups 1 and 2, as expected. Lubricin is one of the major joint lubricants. It is a glycoprotein, as expressed by the chondrocytes from the superficial layer and by synoviocytes B and it has received considerable attention as a chondroprotective molecule [36-39]. The relationships between articular cartilage, boundary lubrication, and alterations in cartilage tissue after injury have not yet been clearly understood, but it emerges from literature that poor lubrication could predispose the articular cartilage to degeneration, thereby promoting the development of OA [38,40]. Joint immobilization, in OA patients, facilitates future damage and chondrocyte apoptosis, since it inhibits the release within the joint cavity of synovial fluid that represents the main source of nourishment for the cartilage, which is rich in glycosaminoglycans, such as hyaluronan, and proteoglycans, such as lubricin [15,41]. On the other hand, MPA with normal joint loading generates, through mechanical stimulation, a greater synovial fluid perfusion of the superficial layer of the cartilage, improving lubrication, chondrocyte homeostasis, and proliferation, whilst preventing

cartilage degeneration [20]. In the present study, lubricin expression was significantly decreased in ACLT-rats group (Group 3) as compared with Groups 1 and 2, which agrees with previous results from studies on OA articular cartilage chondrocytes [29,42], thus suggesting its important role as a chondroprotective agent.

The results from our MPA experimental group (Group 4: ACLT-rats and MPA) highlighted the decreased expression of OA-related biomarkers (IL-1β, TNF-α, MMP-13) and the increased expression of chondroprotective ones (IL-4, IL-10, and lubricin) following physical activity, prompting on the beneficial effect of MPA on the synovium and, consequently, on cartilage preservation. In pathologic conditions, synoviocytes type A produce and secrete cathepsins, MMPs, and pro-inflammatory cytokines/chemokines into the extracellular matrix, triggering tissue damage and, in turn, resulting in OA onset [11,29]. Exercise therapy may decrease cytokines and related genes expression and inhibit inflammatory factors-mediated cartilage degradation, through the synthesis of IL-10 by synoviocytes type A, thus, effectively blocking cartilage damage [43,44]. Our results on MMP-13 expression in the synovium are in accordance with the above-mentioned literature, as Group 4 (ACLT-rats and MPA) displayed significantly reduced MMP-13 levels, whilst the IL-10 levels were significantly increased.

Concerning the pro-inflammatory cytokine IL-6, we observed that its expression in Group 4 did not decrease, as we would expect, but it remained similar to Group 3 (ACLT osteoarthritic rats). During the initial phase of the inflammatory process, the production of IL-6 is likely to be due to the activity of type A synoviocytes. Subsequently, heightened IL-6 production might persist due to the action of type B synoviocytes, which are transformed into fibroblasts [45]. Our explanation is that moderate exercise cannot revert the cellular transformation of type B synoviocytes, but at most it can reduce/impede further transformations.

The role of IL-6 has been widely treated in the literature and there are no doubts regarding its pro-inflammatory function. It has been shown that it is promptly produced in response to tissue injuries and that its dysregulated synthesis has pathological consequences featured during chronic inflammatory states [46]. However, IL-6, in some cases, exerts protective effects [47,48]. Furthermore, during exercise, IL-6 is produced and released by contracting skeletal muscle fibers, exerting its effects in other organs of the body, as reported in literature

[49], and for this reason, IL-6 is considered often referred to as a "myokine". As a myokine, IL-6 stimulates the secretion into the circulation of anti-inflammatory cytokines, such as IL-1RA and IL-10, and inhibits the production of additional pro-inflammatory cytokines, including TNF-α by synoviocytes type A cells [41]. These other roles of IL-6 might, probably, explain the similar expression of this cytokine that we have seen in Group 4. Nevertheless, the role of IL-6 should be certainly further studied and clarified. The weakness of the present study was to evaluate only the morphological evidence based on the immunohistochemistry methods, to investigate the expression of OA-related biomarkers as well as anti-inflammatory and chondroprotective markers. Further studies are needed to confirm our morphological data with other relevant and sensitive techniques, such as quantitative RT-PCR, ELISA (or similar), and/or western blot.

In conclusion, the taboo that joints that are affected by OA should not be subjected to physical activity and must be absolutely disproved, as many international medical societies have recently recommended. The benefits arising from physical activity for the prophylaxis and treatment of a number of chronic conditions are renowned. For some chronic pathologies, well-planned exercise interventions and a healthy diet are at least as effective as drug therapy [50-52]. MPA in OA knee patients (walking, moderate running, swimming, riding a bike, and using elliptical machines) may protect joints against the damaging effects of excessively repetitive joint use and replace glycoproteins lost during periods of immobility, improving clinical benefits [53]. Moreover, as a non-surgical and non-pharmacological approach, MPA could re-establish normal synoviocyte function at the initial phases of OA, hence delaying the onset of overt OA and finally postponing the need for joint replacement. It needs, however, to report recent scientific data showing that moderate physical activity, in some cases and specific experimental conditions, does not protect against the development of OA [54]. Indeed, further studies are warranted to further validate our findings. Preservation of the joint health is critical for retaining independent living, a good health status, and quality of life. We hope that this contribution and theory may help readers and the scientific community to gain a better understanding of the importance of MPA in OA treatment. Exercise is an effective evidence-based medicine, and our findings have, at least in part, provided a proof-of-concept consisting of morphological, molecular, and biochemical

evidence to support the statement that there is less risk in activity than in continuous inactivity.

Author Contributions

All authors have made substantial intellectual contributions to the conception and design of the study as well as data acquisition, analysis and interpretation. P.C. participating in the conception, in the design and in manuscript writing of the study. M.D.R. contributed to data collection, literature research and drawn Figure 4 and Figure 5. S.R. and C.G. carried out the experimental work and study execution. A.C. and M.V. contributed to data collection and manuscript editing. R.I. and F.D. provided technical assistance. M.A.S., participating in the design, literature research and in manuscript writing. G.M. conceived the study design, planning and editing, coordinated the execution of all the experimental procedures, the analysis and discussion of results and wrote the manuscript. All authors contributed to data interpretation and manuscript preparation. All authors approved the final submitted version.

Funding

This study was supported by the University Research Project Grant (Triennial Research Plan 2016–2018), Department of Biomedical and Biotechnological Sciences (BIOMETEC), University of Catania, Italy.

Acknowledgments

The authors would like to thank Iain Halliday for commenting and making corrections to the paper.

Conflicts of Interest

The authors declare no conflict of interest.

5.5. References

1. Rios, J.L.; Boldt, K.R.; Mather, J.W.; Seerattan, R.A.; Hart, D.A.; Herzog, W. Quantifying the Effects of Different Treadmill Training Speeds and Durations on the Health of Rat Knee Joints. *Sport. Med. Open* **2018**, *4*, 15.
2. Green, A.; Engstrom, C.; Friis, P. Exercise: An essential evidence-based medicine. *Med. J. Aust.* **2018**, *208*, 242–243.
3. Castorina, S.; Guglielmino, C.; Castrogiovanni, P.; Szychlinska, M.A.; Ioppolo, F.; Massimino, P.; Leonardi, P.; Maci, C.; Iannuzzi, M.; Di Giunta, A.; et al. Clinical evidence of traditional vs fast track recovery methodologies after total arthroplasty for osteoarthritic knee treatment. A retrospective observational study. *Muscles Ligaments Tendons J.* **2018**, *7*, 504–513.
4. Musumeci, G. The Effect of Mechanical Loading on Articular Cartilage. *J. Funct. Morphol. Kinesiol.* **2016**, *1*, 154–161.
5. Blackburn, T.A.; Craig, E. Knee anatomy. A brief review. *Phys. Ther.* **1980**, *60*, 1556–1560.
6. Iwanaga, T.; Shikichi, M.; Kitamura, H.; Yanase, H.; Nozawa-Inoue, K. Morphology and functional roles of synoviocytes in the joint. *Arch. Histol. Cytol.* **2000**, *63*, 17–31.
7. Shikichi, M.; Kitamura, H.P.; Yanase, H.; Konno, A.; Takahashi-Iwanaga, H.; Iwanaga, T. Three-dimensional Ultrastructure of Synoviocytes in the Horse Joint as Revealed by the Scanning Electron Microscope. *Arch. Histol. Cytol.* **1999**, *62*, 219–229.
8. Nio, J.; Yokoyama, A.; Okumura, M.; Iwanaga, T. Three-dimensional ultrastructure of synoviocytes in the knee joint of rabbits and morphological changes in osteoarthritis model. *Arch. Histol. Cytol.* **2002**, *65*, 189–200.
9. Blewis, M.E.; Lao, B.J.; Jadin, K.D.; McCarty, W.J.; Bugbee, W.D.; Firestein, G.S.; Sah, R.L. Semi-permeable membrane retention of synovial fluid lubricants hyaluronan and proteoglycan 4 for a biomimetic bioreactor. *Biotechnol. Bioeng.* **2010**, *106*, 149–160.
10. Hui, A.Y.; McCarty, W.J.; Masuda, K.; Firestein, G.S.; Sah, R.L. A systems biology approach to synovial joint lubrication in health, injury, and disease. *Wiley Interdiscip. Rev. Syst. Biol. Med.* **2012**, *4*, 15–37.
11. Ingram, K.R.; Wann, A.K.T.; Angel, C.K.; Coleman, P.J.; Levick, J.R. Cyclic movement stimulates hyaluronan secretion into the synovial cavity of rabbit joints. *J. Physiol.* **2008**, *586*, 1715–1729.
12. Estell, E.G.; Murphy, L.A.; Silverstein, A.M.; Tan, A.R.; Shah, R.P.; Ateshian, G.A.; Hung, C.T. Fibroblast-like synoviocyte mechanosensitivity to fluid shear is modulated by interleukin-1α. *J. Biomech.* **2017**, *60*, 91–99.
13. Szychlinska, M.A.; Leonardi, R.; Al-Qahtani, M.; Mobasheri, A.; Musumeci, G. Altered joint tribology in osteoarthritis: Reduced lubricin synthesis due to the inflammatory process. New horizons for therapeutic approaches. *Ann. Phys. Rehabil. Med.* **2016**, *59*, 149–156.
14. Abramson, S.B.; Attur, M. Developments in the scientific understanding of osteoarthritis. *Arthritis Res. Ther.* **2009**, *11*, 227.
15. Musumeci, G.; Loreto, C.; Leonardi, R.; Castorina, S.; Giunta, S.; Carnazza, M.L.; Trovato, F.M.; Pichler, K.; Weinberg, A.M. The effects of physical activity on apoptosis and lubricin expression in articular cartilage in rats with glucocorticoid-induced osteoporosis. *J. Bone Miner. Metab.* **2013**, *31*, 274–284.
16. Musumeci, G. Effects of exercise on physical limitations and fatigue in rheumatic diseases. *World J. Orthop.* **2015**, *6*, 762.
17. Musumeci, G.; Castrogiovanni, P.; Trovato, F.M.; Imbesi, R.; Giunta, S.; Szychlinska, M.A.; Loreto, C.; Castorina, S.; Mobasheri, A. Physical activity ameliorates cartilage degeneration in a rat model of aging: A study on lubricin expression. *Scand. J. Med. Sci. Sport.* **2015**, *25*, e222–e230.
18. Musumeci, G.; Maria Trovato, F.; Imbesi, R.; Castrogiovanni, P. Effects of dietary extra-virgin olive oil on oxidative stress resulting from exhaustive exercise in rat skeletal muscle: A morphological study. *Acta Histochem.* **2014**, *116*, 61–69.
19. World Health Organization (WHO). *Global Recommendations on Physical Activity for Health*; World Health Organization: Geneva, Switzerland, 2010.
20. Musumeci, G.; Trovato, F.M.; Pichler, K.; Weinberg, A.M.; Loreto, C.; Castrogiovanni, P. Extra-virgin olive oil diet and mild physical activity prevent cartilage degeneration in an osteoarthritis model: An in vivo and in vitro study on lubricin expression. *J. Nutr. Biochem.* **2013**, *24*, 2064–2075.

21. Szychlinska, M.A.; Trovato, F.M.; Di Rosa, M.; Malaguarnera, L.; Puzzo, L.; Leonardi, R.; Castrogiovanni, P.; Musumeci, G. Co-expression and co-localization of cartilage glycoproteins CHI3L1 and lubricin in osteoarthritic cartilage: Morphological, immunohistochemical and gene expression profiles. *Int. J. Mol. Sci.* **2016**, *17*, 359.
22. Di Rosa, M.; Szychlinska, M.A.; Tibullo, D.; Malaguarnera, L.; Musumeci, G. Expression of CHI3L1 and CHIT1 in osteoarthritic rat cartilage model. A morphological study. *Eur. J. Histochem.* **2014**, *58*, 2423.
23. Zhang, S.L.; Liu, H.Q.; Xu, X.Z.; Zhi, J.; Geng, J.J.; Chen, J. Effects of exercise therapy on knee joint function and synovial fluid cytokine levels in patients with knee osteoarthritis. *Mol. Med. Rep.* **2013**, *7*, 183–186.
24. Szychlinska, M.A.; Castrogiovanni, P.; Trovato, F.M.; Nsir, H.; Zarrouk, M.; Lo Furno, D.; Di Rosa, M.; Imbesi, R.; Musumeci, G. Physical activity and Mediterranean diet based on olive tree phenolic compounds from two different geographical areas have protective effects on early osteoarthritis, muscle atrophy and hepatic steatosis. *Eur. J. Nutr.* **2018**.
25. Lapaj, L.; Markuszewski, J.; Wierusz-Kozlowska, M. Current views on the pathogenesis of osteoarthritis. *Chir. Narzadow Ruchu Ortop. Pol.* **2010**, *75*, 248–260.
26. Xie, X.W.; Wan, R.Z.; Liu, Z.P. Recent Research Advances in Selective Matrix Metalloproteinase-13 Inhibitors as Anti-Osteoarthritis Agents. *ChemMedChem.* **2017**, *12*, 1157–1168.
27. Roos, H.; Dahlberg, L.; Hoerrner, L.A.; Lark, M.W.; Thonar, E.J.M.A.; Shinmei, M.; Lindqvist, U.; Stefan Lohmander, L. Markers of cartilage matrix metabolism in human joint fluid and serum: The effect of exercise. *Osteoarthr. Cartil.* **1995**, *3*, 7–14.
28. Assis, L.; Milares, L.P.; Almeida, T.; Tim, C.; Magri, A.; Fernandes, K.R.; Medalha, C.; Muniz Renno, A.C. Aerobic exercise training and low-level laser therapy modulate inflammatory response and degenerative process in an experimental model of knee osteoarthritis in rats. *Osteoarthr. Cartil.* **2016**, *24*, 169–177.
29. Jay, G.D.; Fleming, B.C.; Watkins, B.A.; McHugh, K.A.; Anderson, S.C.; Zhang, L.X.; Teeple, E.; Waller, K.A.; Elsaid, K.A. Prevention of cartilage degeneration and restoration of chondroprotection by lubricin tribosupplementation in the rat following anterior cruciate ligament transection. *Arthritis Rheum.* **2010**, *62*, 2382–2391.
30. Elsaid, K.A.; Zhang, L.; Waller, K.; Tofte, J.; Teeple, E.; Fleming, B.C.; Jay, G.D. The impact of forced joint exercise on lubricin biosynthesis from articular cartilage following ACL transection and intra-articular lubricin's effect in exercised joints following ACL transection. *Osteoarthr. Cartil.* **2012**, *20*, 940–948.
31. Leonardi, R.; Musumeci, G.; Sicurezza, E.; Loreto, C. Lubricin in human temporomandibular joint disc: An immunohistochemical study. *Arch. Oral Biol.* **2012**, *57*, 614–619.
32. Musumeci, G.; Loreto, C.; Carnazza, M.L.; Strehin, I.; Elisseeff, J. Oa cartilage derived chondrocytes encapsulated in poly(ethylene glycol) diacrylate (PEGDA) for the evaluation of cartilage restoration and apoptosis in an in vitro model. *Histol. Histopathol.* **2011**, *26*, 1265–1278.
33. Loeser, R.F. Osteoarthritis year in review 2013: Biology. *Osteoarthr. Cartil.* **2013**, *21*, 1436–1442.
34. Musumeci, G.; Castrogiovanni, P.; Trovato, F.M.; Weinberg, A.M.; Al-Wasiyah, M.K.; Alqahtani, M.H.; Mobasheri, A. Biomarkers of chondrocyte apoptosis and autophagy in osteoarthritis. *Int. J. Mol. Sci.* **2015**, *16*, 20560–20575.
35. Musumeci, G.; Trovato, F.M.; Loreto, C.; Leonardi, R.; Szychlinska, M.A.; Castorina, S.; Mobasheri, A. Lubricin expression in human osteoarthritic knee meniscus and synovial fluid: A morphological, immunohistochemical and biochemical study. *Acta Histochem.* **2014**, *116*, 965–972.
36. Mathiessen, A.; Conaghan, P.G. Synovitis in osteoarthritis: Current understanding with therapeutic implications. *Arthritis Res. Ther.* **2017**, *19*, 18.
37. Fernandes, J.C.; Martel-Pelletier, J.; Pelletier, J.P. The role of cytokines in osteoarthritis pathophysiology. *Biorheology* **2002**, *39*, 237–246.
38. Pearson, M.J.; Herndler-Brandstetter, D.; Tariq, M.A.; Nicholson, T.A.; Philp, A.M.; Smith, H.L.; Davis, E.T.; Jones, S.W.; Lord, J.M. IL-6 secretion in osteoarthritis patients is mediated by chondrocyte-synovial fibroblast cross-talk and is enhanced by obesity. *Sci. Rep.* **2017**, *7*, 3451.
39. Tanaka, T.; Narazaki, M.; Kishimoto, T. Il-6 in inflammation, Immunity, And disease. *Cold Spring Harb. Perspect. Biol.* **2014**, *6*.

40. Voiriot, G.; Razazi, K.; Amsellem, V.; Tran Van Nhieu, J.; Abid, S.; Adnot, S.; Mekontso Dessap, A.; Maitre, B. Interleukin-6 displays lung anti-inflammatory properties and exerts protective hemodynamic effects in a double-hit murine acute lung injury. *Respir. Res.* **2017**, *18*, 64.
41. Nandi, D.; Mishra, M.K.; Basu, A.; Bishayi, B. Protective effects of interleukin-6 in lipopolysaccharide (LPS)-induced experimental endotoxemia are linked to alteration in hepatic anti-oxidant enzymes and endogenous cytokines. *Immunobiology* **2010**, *215*, 443–451.
42. Petersen, A.M.W.; Pedersen, B.K. The anti-inflammatory effect of exercise. *J. Appl. Physiol.* **2005**, *98*, 1154–1162.
43. Tohidnezhad, M.; Bayer, A.; Rasuo, B.; Hock, J.V.P.; Kweider, N.; Fragoulis, A.; Sönmez, T.T.; Jahr, H.; Pufe, T.; Lippross, S. Platelet-Released Growth Factors Modulate the Secretion of Cytokines in Synoviocytes under Inflammatory Joint Disease. *Mediat. Inflamm.* **2017**, *2017*, 1–9.
44. Thornton, J.S.; Frémont, P.; Khan, K.; Poirier, P.; Fowles, J.; Wells, G.D.; Frankovich, R.J. Physical activity prescription: A critical opportunity to address a modifiable risk factor for the prevention and management of chronic disease: A position statement by the Canadian Academy of Sport and Exercise Medicine. *Br. J. Sports Med.* **2016**, *50*, 1109–1114.
45. Marosi, K.; Moehl, K.; Navas-Enamorado, I.; Mitchell, S.J.; Zhang, Y.; Lehrmann, E.; Aon, M.A.; Cortassa, S.; Becker, K.G.; Mattson, M.P. Metabolic and molecular framework for the enhancement of endurance by intermittent food deprivation. *FASEB J.* **2018**, *32*, 3844–3858.
46. Castrogiovanni, P.; Musumeci, G. Which is the Best Physical Treatment for Osteoarthritis? *J. Funct. Morphol. Kinesiol.* **2016**, *1*, 54–68.
47. Siebelt, M.; Groen, H.C.; Koelewijn, S.J.; de Blois, E.; Sandker, M.; Waarsing, J.H.; Müller, C.; van Osch, G.; de Jong, M.; Weinans, H. Increased physical activity severely induces osteoarthritic changes in knee joints with papain induced sulfate-glycosaminoglycan depleted cartilage. *Arthritis Res. Ther.* **2014**, *16*, R32.
48. Bonyadi Rad, E.; Musumeci, G.; Pichler, K.; Heidary, M.; Szychlinska, M.A.; Castrogiovanni, P.; Marth, E.; Böhm, C.; Srinivasaiah, S.; Krönke, G.; et al. Runx2 mediated Induction of Novel Targets ST2 and Runx3 Leads to Cooperative Regulation of Hypertrophic Differentiation in ATDC5 Chondrocytes. *Sci. Rep.* **2017**, *7*, 17947.
49. Ostergaard, K.; Petersen, J.; Andersen, C.B.; Benutzen, K.; Salter, D.M. Histologic/histochemical grading system for osteoarthritic articular cartilage: Reproducibility and validity. *Arthritis Rheum.* **1997**, *40*, 1766–1771.
50. Gerwin, N.; Bendele, A.M.; Glasson, S.; Carlson, C.S. The OARSI histopathology initiative—Recommendations for histological assessments of osteoarthritis in the rat. *Osteoarthr. Cartil.* **2010**, *18*, S24–S34.
51. Giunta, S.; Castorina, A.; Marzagalli, R.; Szychlinska, M.A.; Pichler, K.; Mobasheri, A.; Musumeci, G. Ameliorative effects of PACAP against cartilage degeneration. Morphological, immunohistochemical and biochemical evidence from in vivo and in vitro models of rat osteoarthritis. *Int. J. Mol. Sci.* **2015**, *16*, 5922–5944.
52. Leonardi, R.; Rusu, M.C.; Loreto, F.; Loreto, C.; Musumeci, G. Immunolocalization and expression of lubricin in the bilaminar zone of the human temporomandibular joint disc. *Acta Histochem.* **2012**, *114*, 1–5.
53. Gardner, O.F.W.; Musumeci, G.; Neumann, A.J.; Eglin, D.; Archer, C.W.; Alini, M.; Stoddart, M.J. Asymmetrical seeding of MSCs into fibrin–poly(ester-urethane) scaffolds and its effect on mechanically induced chondrogenesis. *J. Tissue Eng. Regen. Med.* **2017**, *11*, 2912–2921.
54. Musumeci, G.; Mobasheri, A.; Trovato, F.M.; Szychlinska, M.A.; Graziano, A.C.E.; Lo Furno, D.; Avola, R.; Mangano, S.; Giuffrida, R.; Cardile, V. Biosynthesis of collagen I, II, RUNX2 and lubricin at different time points of chondrogenic differentiation in a 3D in vitro model of human mesenchymal stem cells derived from adipose tissue. *Acta Histochem.* **2014**, *116*, 1407–1417.

6. MORPHOLOGICAL EVIDENCE OF TELOCYTES IN SKELETAL MUSCLE INTERSTITIUM OF EXERCISED AND SEDENTARY RODENTS

Silvia Ravalli[1], Concetta Federico[2], Giovanni Lauretta[1], Salvatore Saccone[2], Elisabetta Pricoco[1], Federico Roggio[1,3], Michelino Di Rosa[1], Grazia Maugeri[1] and Giuseppe Musumeci[1,4,5,]*

[1]Department of Biomedical and Biotechnological Sciences, Human, Histology and Movement Science Section, University of Catania, Via S. Sofia 87, 95123 Catania, Italy

[2]Department of Biological, Geological and Environmental Sciences, Section of Animal Biology, University of Catania, Via Androne 81, 95124 Catania, Italy

[3]Department of Psychology, Educational Science and Human Movement, University of Palermo, Via Giovanni Pascoli 6, 90144 Palermo, Italy

[4]Research Center on Motor Activities (CRAM), University of Catania, Via S. Sofia 97, 95123 Catania, Italy

[5]Department of Biology, College of Science and Technology, Temple University, Philadelphia, PA 19122, USA

[*]Correspondence: g.musumeci@unict.it; Tel.: +095-378-2036

Biomedicines 2021, 9(7), 807; DOI:10.3390/biomedicines9070807

6.1. Introduction

The skeletal muscle is a highly dynamic and plastic tissue that promptly responds to physical activity and sedentary behavior [1]. Skeletal muscle disuse atrophy (SMDA) refers to biochemical, morphological, and functional changes in skeletal muscle that may result from states of hypokinesis or immobilization, e.g., following fractures or elective orthopedic surgery, and represents a major topic in the fields of regenerative and rehabilitation medicine [2,3]. On the contrary, both resistance and aerobic training induce metabolic changes within the muscle by altering protein synthesis, muscle proteolysis, therefore inducing molecular and cellular adaptations that regulate homeostasis and hypertrophy [4-6]. A large variety of stromal cells are involved during physiological processes following physical exercise, in order to sustain remodeling and regeneration [7,8]. More specifically, the involvement of Pax+ cells, side population cells (SP cells), pericytes, fibro/adipogenic progenitor cells (FAPs), and PW1+/Pax7– interstitial progenitor cells (PICs), has received attention to investigate exercise-based interventions preventing sarcopenia or in response to injury [8-13].

Alexander Mauro described, for the first time, in 1961, a population of mononucleated cells which had been called “satellite cells” (SCs) by virtue of their localization: underneath the surrounding basal lamina and outside the plasma membrane of the muscle fiber they are associated with [14]. These cells have been immunophenotypically identified by Pax7 [15], M-cadherin [16], CD34 [17], and α7-integrin [18] and originate from Pax3+ progenitors in the somites of the embryo that migrate to the limb bud [19-21]. In his dissertation, Mauro speculated about the role of these cells to be involved in muscle regeneration as dormant myoblasts, able to initiate the development of skeletal muscle fibers in the event of damage or exogenous triggers [14,22,23]. Besides SCs, other cells concur to the maintenance of skeletal muscle homeostasis and contribute to stem cell niche [24]. Fibroblasts proliferate in close proximity to satellite cells [25], providing structural reliability through assembly of collagen, elastic fibers, and other matrix substances [12,26-28]. FAPs are mesenchymal resident cells able to sustain SCs differentiation during tissue regeneration [29-31]. Furthermore, muscle-associated vessels accommodate pericytes and mesoangioblasts, participating in endothelial cell communication, angiogenesis, mechanisms of survivals, and cross-talk [32].

Lastly, another type of cell, recently identified in the muscle interstitium, is represented by the so-called “Telocytes” (TCs), which appear to physically reside near satellite cells, nerve, and microvascular network [13]. The discovery of this population is referred to as a case of serendipity by the Romanian research group led by Professor Laurentiu M. Popescu, just ten years ago [33]. To understand the road that leads to the definition of these new type of cells, it needs to be reminded the work of Santiago Ramón y Cajal, who described, at the beginning of 1900, the presence of unknown cells in the loose connective tissue of the tunica muscularis of the gut, considering them as primitive interstitial neurons [34]. Although their existence was not fully recognized by the scientific community for half a century, M.S. Faussone-Pellegrini [35] and, independently, L. Thuneberg [36] acknowledged that these cells were not neurons and called them “Interstitial Cells of Cajal (ICCs)”. Extended studies, following the annotation of Cajal, lead to the identification of Interstitial Cajal-like Cells (ICLCs), named “Telocytes” in 2010, in many organs [33], testifying the ubiquity of the novel cell type [37]. Since they were identified, the number of scientific works on TCs is growing exponentially [38] (Figure 1).

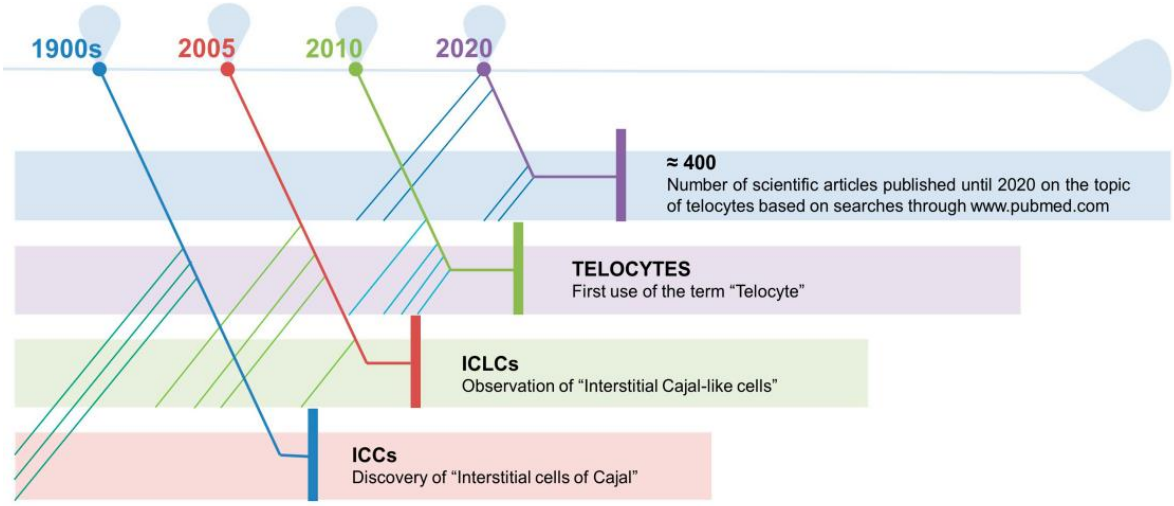

Figure 1. At the beginning of 1900, Santiago Ramón y Cajal described the presence of what he considered primitive interstitial neurons in the loose connective tissue of the tunica muscularis of the gut. Half a century later, M.S. Faussone-Pellegrini and L. Thuneberg observed that these cells were not neurons and called them “Interstitial Cells of Cajal (ICCs)”. These type of cells were then found in many other organs. Finally, Faussone-Pellegrini together with L. M. Popescu, proposed, in 2010, to use the term “Telocyte” to indicate an ICLC. Since their identification, TCs have received attention and the number of scientific articles on the topic is growing considerably.

It is noteworthy to mention that this discovery raised skepticism and controversy, since ICLCs were also described merely as CD34-positive stromal cells acting as stem cells during regeneration processes [39,40], or the term was used interchangeably to describe fibroblasts [41]. Therefore, there is a need for new evidence that can discriminate the different populations hosted in the stem cell niche of the tissues, not only for their morphology but also for their function. TCs are typically described as cells with small bodies, reported as pear-, spindle-, triangular-shaped, and very long cytoplasmic processes, up to hundreds of micrometers but only approximately 0.2 μm thick [42,43]. The identification of TCs, via transmission electron microscopy, showed characteristic features [33,44] (Table 1).

Table 1. Characteristic features of TCs and of their telopodes

Cell Structure	Characteristic Features of Telocytes	
Body	small, oval- pear- spindle- triangular-shaped; average dimensions: 9.39 μm ± 3.26 μm; the nucleus occupies about 25% of the cell volume and contains clusters of heterochromatin attached to the nuclear envelope	
Cytoplasm	mitochondria: approximately 5%–10% of the cytoplasmic volume; small Golgi complex; endoplasmic reticulum: 1%–2% of the cyto-plasmic volume	
Plasmalemma	thin or absent basal lamina; caveolae occupy about 2–3% of cytoplasmic volume;	
Telopodes	Number	on average from 1 to 5;
	Length	up to hundreds of μm;
	Thickness	uneven calibre, mostly below 0.2 μm;
	Aspect	moniliform with dilations and branches;
	Organization	three-dimensional network communicating through gap junctions;

Although it is still unclear, the role of TCs seems to participate in sustaining cross-talk communication between stromal cells through signaling transmission via exosomes [13,45], secreting vascular endothelial growth factor (VEGF) and, broadly, promoting myofibers regenerative mechanisms by supporting local stem cell niche differentiation, vasculogenesis, and preventing fibrosis [46]. The presence of this population has been observed, under physiological conditions, in numerous organs and tissues [47,48], and also following pathologic situations, such as musculoskeletal injuries [49], suggesting their role in healing processes and their function for regenerative medicine strategies [50-53]. As already

mentioned, physical inactivity and activity have been extensively studied in relation to stem cell niche and, more recently, are also attracting attention with regard to TCs [49,54,55]. Finally, the aim of this morphologic study was to investigate the presence/absence of TCs in tibialis anterior muscle of healthy rats who underwent a protocol of endurance training for either 4 weeks or 16 weeks in comparison to sedentary rats who were inactive, i.e., not engaging in any physical exercise, throughout the duration of the experiment.

6.2. Materials and Methods

6.2.1. Ethical Approval

All the procedures involving alive animals were performed at the Center for Advanced Preclinical In Vivo Research (CAPIR), University of Catania. The guidelines of the Institutional Animal Care and Use Committee (I.A.C.U.C.) of the University of Catania (Approved protocol n. 2112015-PR of the 14.01.2015, Italian Ministry of Health) have been complied with. Animal care and handling were carried out in accordance with the EU Directive 2010/63/EU, as well as the Italian law (D.Lgs. 26/2014).

6.2.2. Animals: Housing and Breeding

Two-month-old healthy female Wistar outbred rats, with a bodyweight of 200 ± 20 g, were purchased from Charles River Laboratories, Milan, Italy and bred in the animal facilities at the University of Catania. Rats were maintained and kept in polycarbonate cages (10.25″ W × 18.75″ D × 8″ H) in stable hygrometric and thermic conditions (20–23 °C) on 12 h light/dark cycle with ad libitum access to water and food, throughout the whole period of the experiment. It was used a standard rat chow: carbohydrates (40%), proteins containing all essential amino acids (30%), and lipids (30%). Lipids were a mixture of neutral fatty acids, saturated fatty acids, and unsaturated fatty acids. Diets were provided by Laboratorio Dottori Piccioni, Gessate (Milan), Italy. Twenty rats were used in this study equally divided into two groups, sedentary and undergoing physical exercise, respectively CTRL and PA, sacrificed at two different time points, 4 and 16 weeks: CTRL4W, control sedentary rats sacrificed at 4 weeks; PA4W, rats performing physical exercise sacrificed at 4 weeks; CTRL16W, control sedentary rats sacrificed at 16 weeks; PA16W, rats performing physical exercise sacrificed at 4 weeks. All animals were randomly distributed to groups. All efforts were made to minimize the number of mice, according to the principles of the 3Rs and the resource equation approach, and reduce their suffering [56]. Throughout the whole period of the experiment, the animals were free to move in the cages and their wellness was monitored through objective observation and daily checks (weight, claudication, fur and eyes appearance, consumption of food and water, lethargy) [57]. The animals were sacrificed by carbon dioxide (CO_2) overdose, at the established time points. After euthanasia, tibialis anterior muscles were explanted and processed for the planned experiments since the high responsivity of this muscle to exercise [58].

6.2.3. Treadmill Training

Two groups of rats (PA4W and PA16W) performed physical activity in the form of running on a treadmill (2Biological instrument, Varese, Italy) (Figure 2 and Supplementary Video S1). Rats were made familiar with the instrument for 1 week prior to surgery, at a speed of 10 m/min (type of exercise: interval training, between mild and moderate) for 5 min daily. This type of exercise is used to stimulate the muscles, joints, and bones in the work of flexion-extension of the limbs. The rats exercised 3 days a week and, in order to adapt the settings to the time-dependent ability of the rats to perform the exercise, the speeds and the durations were gradually incremented from 10–15 m/min for 5 min to 20–30 m/min for 15 min (from week 1 to week 4), from 10–15 m/min for 5 min to 30–40 m/min for 20 min (from week 1 to week 8), from 10–15 m/min for 5 min to 40–50 m/min for 25 min (from week 1 to week 16). The treadmill was gradually inclined between 2° and 6° degrees. A minimal electric shock (0.2 mA) was used to avoid the rat to stop running, if distracted, to stimulate the walking and to instruct the rats in the first place. All-electric shock bouts were closely monitored in real-time and acquired by the embedded data acquisition software (2Biological instrument, Varese, Italy). Rats that exceeded the number of five electric shocks, in one session, were suspended from the exercise.

Figure 2. Rats exercising on the treadmill. Speeds and the durations were gradually incremented, respectively, from 10–15 m/min for 5 min to 40–50 m/min for 25 min (from week 1 to week 16).

6.2.4. Histology Analysis

Tibialis anterior muscle samples were washed in phosphate-buffered saline (PBS, Bio-Optica, Milano, Italy), fixed in 10% buffered-formalin (Bio-Optica, Milan, Italy) for 24 h at room temperature. Afterwards, the samples were dehydrated in graded ethanol (Bio-Optica, Milan, Italy), cleaned in xylene (Bio-Optica, Milan, Italy) and paraffin-embedded (Bio-Optica, Milan, Italy), being careful to preserve the desired anatomical orientation. Slides of 5 μm thickness were cut from the obtained paraffin blocks and hematoxylin and eosin-stained (H&E, Bio-Optica, Milan, Italy) following a protocol described elsewhere [59]. The samples were then examined in triplicate for morphological evaluation with a Zeiss Axioplan light microscope (Carl Zeiss, Oberkochen, Germany) and by a digital camera (AxioCam MRc5, Carl Zeiss, Oberkochen, Germany), used to take images.

6.2.5. Histomorphometric Analysis

Each H&E stained muscle cross section was subjected in triplicate to morphometric analysis by calculating the area of twenty muscle fibers of five randomly selected fields with a total area of about 35.000 μm2, using a software for image acquisition (AxioVision Release 4.8.2—SP2 Software, Carl Zeiss Microscopy GmbH, Jena, Germany) [60]. Data were then expressed as diameter mean ± standard deviation (SD). Statistical significance of results was thus accomplished. Three investigators (two anatomical morphologists and one histologist) made the morphological assessment. If disputes occurred, a unanimous agreement was reached after section re-evaluation and before proceeding with data interpretation.

6.2.6. Double Immunofluorescence Analysis

Paraffin-embedded muscle tissue sections of 5 μm thickness were subjected in triplicate to double immunofluorescence (IF) combining anti-mouse and anti-rabbit goat secondary antibodies with either mouse or rabbit primary antibodies. Muscle sections were deparaffinized with xylene and rehydrated in graded ethanol scale. Afterwards, the slides were cleaned for 20 min with phosphate-buffered saline (PBS; Bio-Optica, Milan, Italy) and unmasked in citrate buffer (pH 6.0; Bio-Optica, Milan, Italy), or in ethylenediaminetetraacetic acid-Tris buffer (Tris-EDTA pH 8.0, Bio-Optica, Milan, Italy) for the antigenic retrieval and incubated in 0.3% H2O2/PBS, for 30 min, to block endogenous peroxidase activity. Non-specific antibody binding sites were blocked by applying a solution of 1% bovine serum albumin (BSA; Sigma-Aldrich, Saint Louis, MO, USA) in PBS 1X for 1 h at room temperature. Tissue slides were washed in PBS and, then, incubated overnight at +4 °C with a mixture of mouse and rabbit primary antibodies at appropriate dilution in antibody dilution buffer: mouse monoclonal anti-CD34 (1:100; Dako, Agilent, Santa Clara, CA, USA), rabbit monoclonal anti-CD34 (1:100; Invitrogen, Thermo Fisher Scientific, Waltham, MA, USA), rabbit polyclonal anti-CD117 (1:500; Dako, Agilent, Santa Clara, CA, USA), mouse monoclonal anti-Vimentin (VIM, 1:200; Dako, Agilent, Santa Clara, CA, USA). Primary antibodies were revealed using specific fluorescent-dye Goat anti-Mouse Alexa Fluor 488-conjugated IgG (1 μg/mL; Invitrogen, Thermo Fischer Scientific, Waltham, MA, USA) and Goat anti-Rabbit 594-conjugated IgG (2 μg/mL; Invitrogen, Thermo Fisher Scientific, Waltham, MA, USA) for 1 h at room temperature. Details on primary and secondary antibody sources and dilutions are shown in Table 2. Negative controls were performed by replacing primary antibodies with non-immune serum, while cross reactivity of secondary antibodies was verified by omitting primary antibodies. Immunolabeled samples were

rinsed in PBS and mounted using an anti-fade mounting medium containing 4′,6-diamidino-2-phenylindole (DAPI) for nuclear counterstaining (Vectashield, Vector Laboratories, Burlingame, CA, USA) and sealed with nail polish.

Table 2. Primary and secondary antibody used in IF and their dilutions

Primary Antibody	Host Species	Producer	Dilution	Secondary Antibody	Producer	Dilution
Anti-CD34	MOUSE	Dako	1:100	AF488	Invitrogen	1 μg/mL
Anti-CD117	RABBIT	Dako	1:500	AF594	Invitrogen	2 μg/mL
Anti-CD34	RABBIT	Invitrogen	1:100	AF594	Invitrogen	2 μg/mL
Anti-VIM	MOUSE	Dako	1:200	AF488	Invitrogen	1 μg/mL

6.2.7. Computerized Densitometric Measurements and Image Analysis

Digital micrographs of double immunofluorescence sections were taken using a confocal laser scanning microscopy (CLSM, Zeiss LSM700, Carl Zeiss, Oberkochen, Germany) with ZEN-2010 software. In order to detect the fluorophore signal, three lasers with 405, 488, and 555 nm wavelengths were used for the analysis of blue, green, and red signals, respectively. Image analysis software (AxioVision Release 4.8.2-SP2 Software, Carl Zeiss Microscopy GmbH, Jena, Germany), which quantifies the level of double positive staining of anti-CD34/anti-CD117 and anti-CD34/anti-Vimentin immunolabeling, was used to calculate the densitometric count in five fields, 10× magnification, randomly selected from each section. Statistical results are expressed as densitometric count (pixel^2)/(pixel^2) of double immunostaining on muscle tissue. Three blinded investigators (two anatomical morphologists and one histologist) made the evaluations that were assumed to be correct if values have not statistically significant difference. If disputes concerning interpretation occurred, unanimous agreement was reached after sample re-evaluation.

6.2.8. Immunohistochemistry

Skeletal muscle samples, 5 μm-thick, were processed for immunohistochemical analysis. Briefly, the slides were dewaxed in xylene, hydrated using graded ethanols, and therefore heated (5 min × 3) in capped polypropylene slide-holders with citrate buffer—pH 6 (Bio-Optica, Milan, Italy), using a microwave oven (750 W, LG Electronics Italia S.p.A., Milan, Italy) to unmask antigenic sites. The slides were incubated for 30 min in 0.3% H2O2/PBS to quench endogenous peroxidase activity before being rinsed for 20 min with PBS (Bio-Optica, Milan, Italy). After blocking, the sections were incubated overnight at 4 °C with rabbit monoclonal anti-CD34 (1:100; Invitrogen, Thermo Fisher Scientific, Waltham, MA USA). Immune complexes were then treated with biotinylated link antibodies (horseradish peroxidase polymer (HRP)-conjugated anti-rabbit and anti-mouse were used as secondary antibodies) and then detected with peroxidase-labelled streptavidin, both incubated for 10 min at room temperature (LSAB + System-HRP, K0690, Dako, Glostrup, Denmark). Immunoreactivity was visualized by incubating the sections for 2 min in 0.1% 3,3′-diaminobenzidine (DAB) (DAB substrate Chromogen System, Dako, Glostrup, Denmark). The sections were lightly counterstained with Mayer's hematoxylin (Histolab Products AB, Göteborg, Sweden), mounted in Glycerol Vinyl Alcohol (GVA) (Zymed Laboratories, San Francisco, CA, USA), observed with an Axioplan Zeiss light microscope (Carl Zeiss,

Oberkochen, Germany), and photographed with a digital camera (AxioCam MRc5, Carl Zeiss, Oberkochen, Germany).

6.2.9. Statistical Analysis

Statistical analysis was performed using GraphPad Instat® Biostatistics version 8.0 software (GraphPad Software, Inc., La Jolla, CA, USA). The sample size calculation for this study was established using the resource equation approach, including minimum and maximum sample sizes, because it was not possible to assume standard deviation and effect size [56]. Data were tested for normality with the Kolmogorov–Smirnov and Shapiro–Wilk test. All variables were normally distributed. Differences between experimental groups were evaluated by using one-way ANOVA (histomorphometric and immunofluorescence analysis) and two-way ANOVA (weights) followed by Tukey's multiple comparison post hoc test. For all experiments, p-values of less than 0.05 ($p < 0.05$) were considered statistically significant; p values of less than 0.01 ($p < 0.01$) were considered to be highly statistically significant. The data are presented as the mean value ± SD. Cohen's κ was applied to measure the agreement between the three blinded observers and averaged to evaluate overall agreement.

6.3. Results

6.3.1. Body Weight

Body weights and food and drink consumption were monitored throughout the experiment, 3 days per week, for a total of 48 time points. A physiological increase in body weight during the weeks in all groups was observed since the differences between groups, for each time point, are never significant ($p > 0.05$), as expected (Figure 3). At the start of the experiment, the mean ± SD body weight of all rats was 209.4 ± 13.52 g, at the end of the fourth week, it was 240.95 ± 10.95 g, reaching 290.7 ± 15.97 g, at the end of the sixteenth week, for the remaining animals.

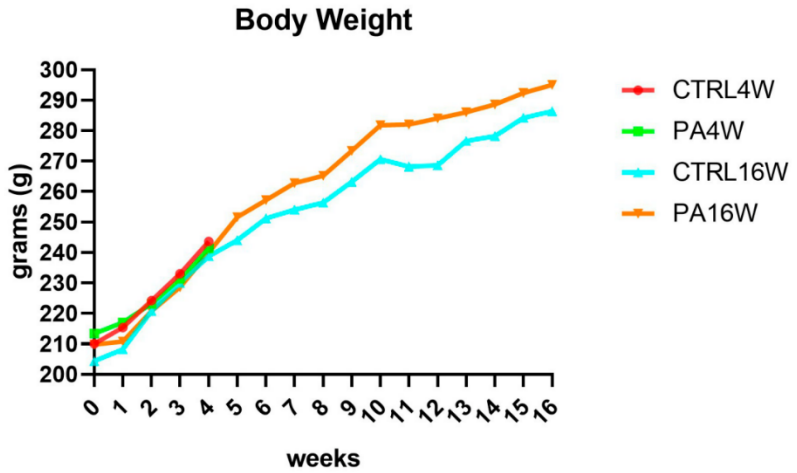

Figure 3. Body weight variations over 16 weeks, showing a physiological increase in all groups. The differences between groups, analyzed by two-way ANOVA followed by Tukey's multiple comparison post hoc test, are not significant, as expected ($p > 0.05$). CTRL4W, control sedentary rats sacrificed at 4 weeks; PA4W, rats performing physical exercise sacrificed at 4 weeks; CTRL16W, control sedentary rats sacrificed at 16 weeks; PA16W, rats performing physical exercise sacrificed at 4 weeks.

6.3.2. Histology and Histomorphometry

Histological analysis with H&E were examined to highlight the possible structural alterations in muscle tissue of all experimental groups. No cytological alteration is detected in the muscle fibers of all groups. The morphometric analysis of the diameter (μm) (mean ± SD) of the muscle fibers highlights a significant hypertrophy of the groups PA16W (30.46 ± 1.43 μm) (** $p < 0.0001$) and PA4W (27.47 ± 1.61 μm) (* $p < 0.001$) vs. CTRL16W (21.39 ± 2.19 μm). PA16W (27.47 ± 1.61 μm) also shows a predictable hypertrophy when compared to CTRL4W (24.01 ± 1.57 μm), (* $p < 0.001$). On the contrary, PA16W (30.46 ± 1.43 μm) does not show a statistically significant hypertrophy when compared with group PA4W (27.47 ± 1.61 μm), (ns) (Figure 4). No significant differences are revealed when compared CTRL4W vs. CTRL16W and PA4W vs. CTRL4W.

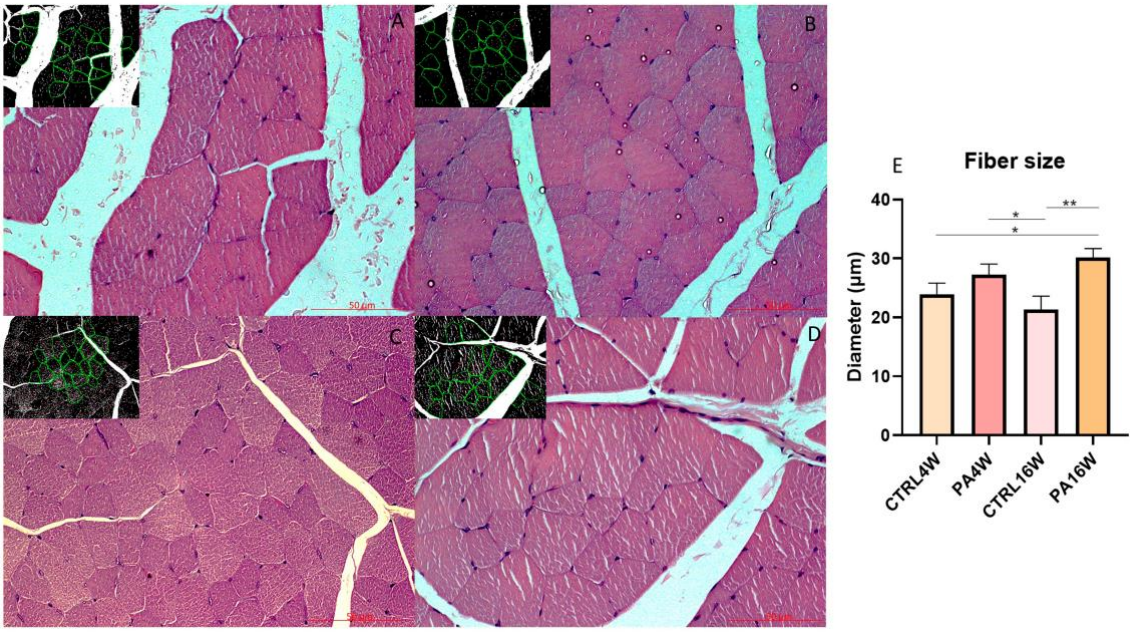

Figure 4. Hematoxylin and eosin staining (A–D) and morphometric analysis of the diameter (µm) (mean ± SD) of the muscle fibers (E). (A–D) (A) group CTRL4W and in the inset morphometric analysis by the software; (B) group PA4W and in the inset morphometric analysis by the software; (C) group CTRL16W and in the inset morphometric analysis by the software; (D) group PA16W and in the inset morphometric analysis by the software. (E) The morphometric analysis highlights a significant hypertrophy of the groups PA16W (30.46 ± 1.43 µm) (** $p < 0.0001$), and to PA4W (* $p < 0.001$) when compared to CTRL16W (21.39 ± 2.19 µm). Comparison between CTRL4W and PA16W highlights a significant hypertrophy of the latter group (* $p < 0.001$). No other comparisons show to be significant. Data were tested for normality with the Kolmogorov–Smirnov and Shapiro–Wilk test, and differences between experimental groups were evaluated by using one-way ANOVA, followed by Tukey's multiple comparison post hoc test. Lens magnification: ×20. Scale bars: 50 µm. ** $p < 0.0001$, * $p < 0.001$. CTRL4W, control sedentary rats sacrificed at 4 weeks; PA4W, rats performing physical exercise sacrificed at 4 weeks; CTRL16W, control sedentary rats sacrificed at 16 weeks; PA16W, rats performing physical exercise sacrificed at 4 weeks.

6.3.3. Double Immunofluorescence and Densitometric Analysis

Although transmission electron microscopy (TEM) examination is the golden standard for TCs identification [33,61], double-immunostaining is currently the most common tool for semi-quantitative analysis of TCs [62,63,64], since it can help in discriminate this population from other interstitial cells. In this work, double positive immunofluorescences for CD34/CD177 and CD34/VIM were used to identify TCs in sedentary and exercised muscle rat tissue at 4 and 16 weeks (Figure 5A and Figure 6A). Statistical results are expressed as

mean ± SD of the densitometric count (pixel^2)/(pixel^2) of double immunostaining on muscle tissue. CD34 and CD117 double labeling analysis indicates a statistically significant increase in the expression of TCs in PA16W ($7.7 \times 10^{-4} \pm 1.3 \times 10^{-4}$ (pixel^2)/(pixel^2)) vs. CTRL16W ($3.9 \times 10^{-4} \pm 2 \times 10^{-4}$ (pixel^2)/(pixel^2)) (* $p < 0.05$) (Figure 5B). Densitometric values for CTRL4W and PA4W groups are, respectively, $4.9 \times 10^{-4} \pm 1.4 \times 10^{-4}$ (pixel^2)/(pixel^2) and $6.1 \times 10^{-4} \pm 2.5 \times 10^{-4}$ (pixel^2)/(pixel^2). Similarly, the number of interstitial TCs is highly significant higher in PA16W ($1.3 \times 10^{-3} \pm 3.1 \times 10^{-4}$ (pixel^2)/(pixel^2)), vs. CTRL16W ($6.9 \times 10^{-4} \pm 1 \times 10^{-4}$ (pixel^2)/(pixel^2)) (** $p < 0.01$) as determined by CD34/VIM double-immunostaining (Figure 6B). Densitometric values for CTRL4W and PA4W groups are, respectively, $1 \times 10^{-3} \pm 2.6 \times 10^{-4}$ (pixel^2)/(pixel^2) and $9.3 \times 10^{-4} \pm 2.5 \times 10^{-4}$ (pixel^2)/(pixel^2). No other statistically significant differences are highlighted between groups, in both experiments.

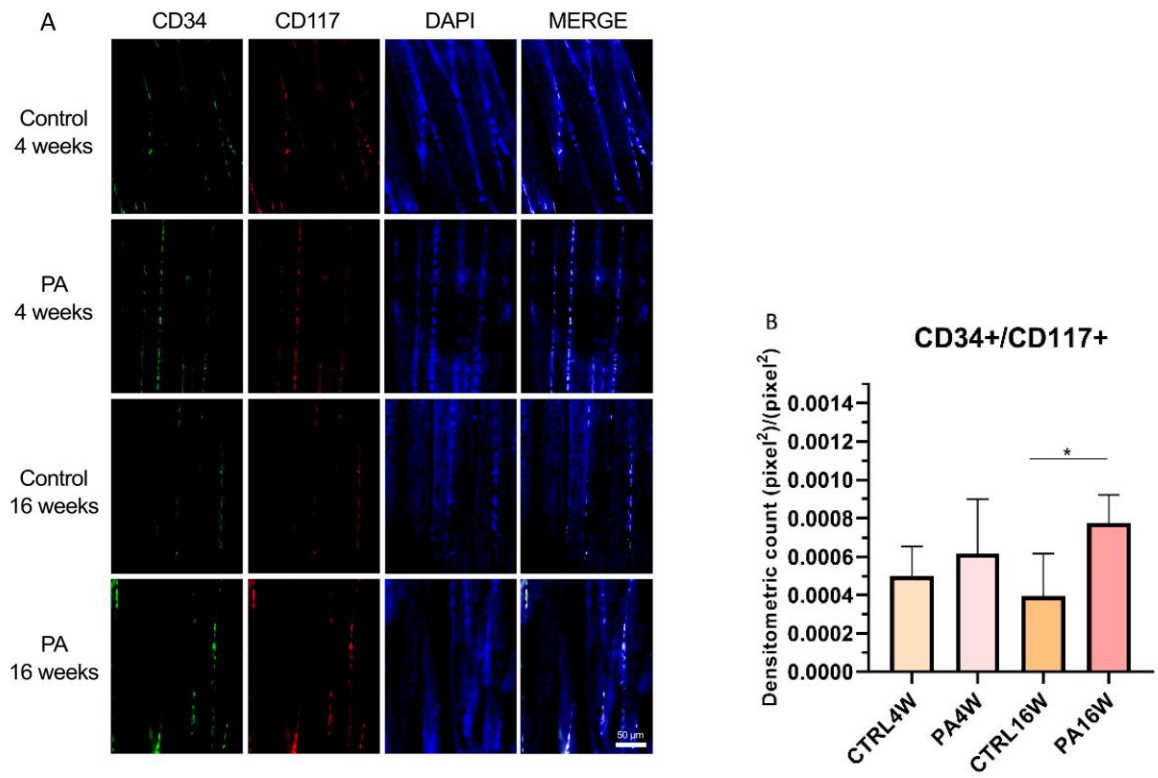

Figure 5. (A) Representative images of double immunofluorescence staining for muscle tissue TCs as determined by CD34+/CD117+. CD34 (green) and CD117 (red) immunostaining with 4′,6-diamidino-2-phenylindole (DAPI; blue) counterstain for nuclei. (B) Comparison between PA16W and CTRL16W highlights a significant higher expression of TCs in exercised rats at 16 weeks (* $p < 0.05$). No other comparisons show to be significant. Data were tested for normality with the Kolmogorov–Smirnov and Shapiro–Wilk test, and

differences between experimental groups were evaluated by using one-way ANOVA, followed by Tukey's multiple comparison post hoc test. The slides are scanned by confocal laser scanning microscopy (CLSM; Zeiss LSM700, Oberkochen, Germany) at 200× magnification. Scale bars: 50 μm. CTRL4W, control sedentary rats sacrificed at 4 weeks; PA4W, rats performing physical exercise sacrificed at 4 weeks; CTRL16W, control sedentary rats sacrificed at 16 weeks; PA16W, rats performing physical exercise sacrificed at 4 weeks.

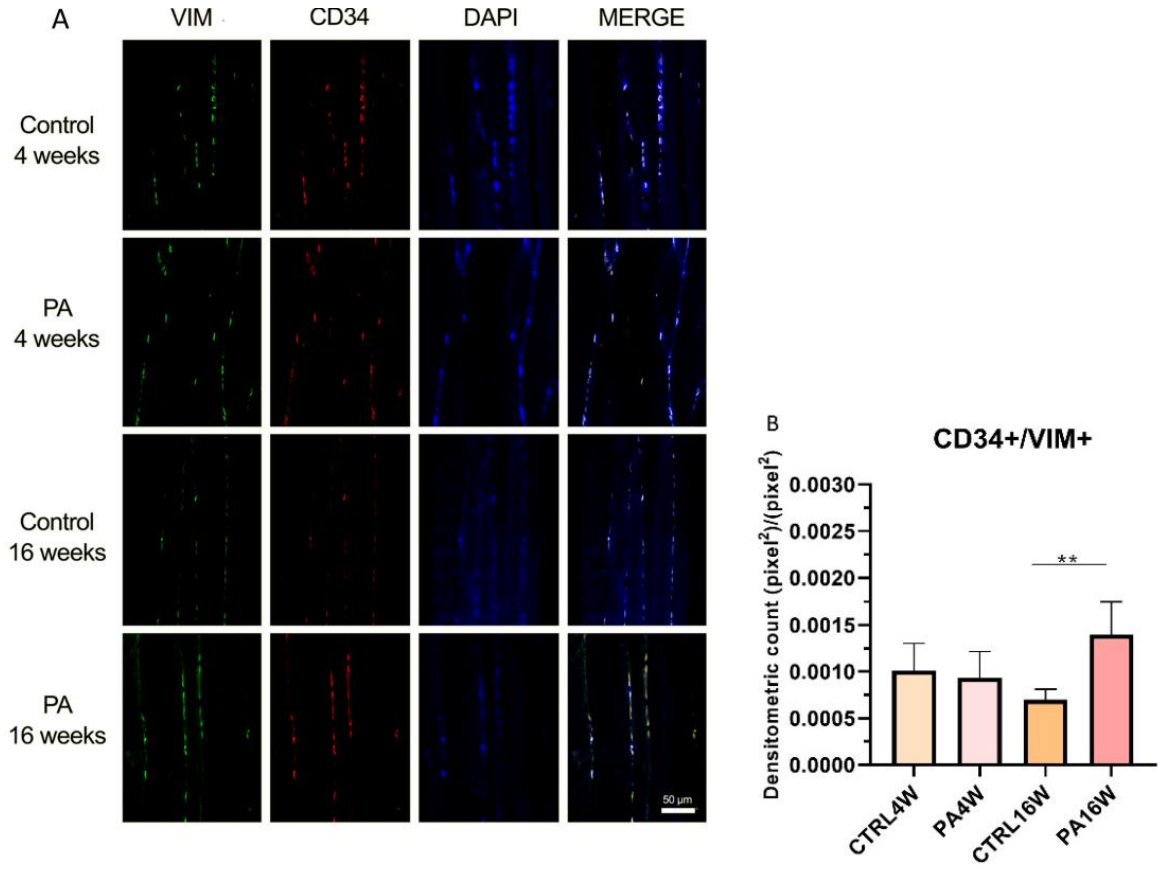

Figure 6. (A) Representative images of double immunofluorescence staining for muscle tissue TCs as determined by CD34+/VIM+. CD34 (red) and VIM (green) immunostaining with 4′,6-diamidino-2-phenylindole (DAPI; blue) counterstain for nuclei. (B) Comparison between PA16W and CTRL16W highlights a highly significant higher expression of TCs in exercised rats at 16 weeks (** $p < 0.01$). No other comparisons show to be significant. Data were tested for normality with the Kolmogorov–Smirnov and Shapiro–Wilk test, and differences between experimental groups were evaluated by using one-way ANOVA, followed by Tukey's multiple comparison post hoc test. The slides are scanned by confocal laser scanning microscopy (CLSM; Zeiss LSM700, Oberkochen, Germany) at 200× magnification. Scale bars: 50 μm. CTRL4W, control sedentary rats sacrificed at 4 weeks; PA4W, rats performing physical exercise sacrificed at 4 weeks; CTRL16W, control sedentary rats sacrificed at 16 weeks; PA16W, rats performing physical exercise sacrificed at 4 weeks.

6.3.4. Immunohistochemistry

Skeletal muscle sections showed CD34+ cells at the periphery of the fibers, within the interstitium between muscle fibers (Figure 7). These cells appear to exhibit morphological features of TCs, i.e., spindle nuclei, approximately 5–10 μm in diameter, and multiple long cytoplasmic processes, approximately 10–25 μm in length and 0.1–0.2 μm in thickness, identifiable with telopodes.

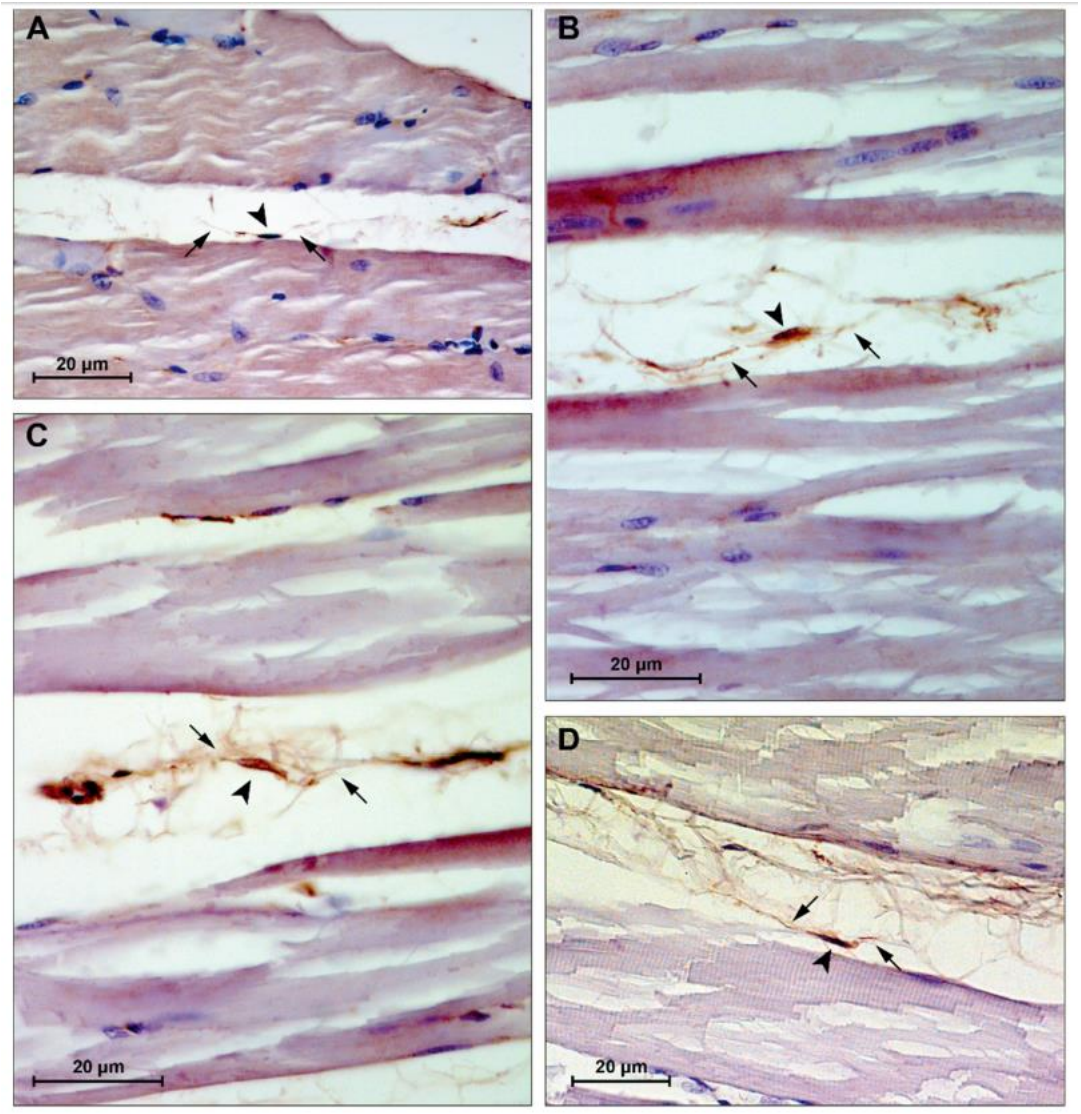

Figure 7. Representative images of immunohistochemistry staining for muscle tissue CD34+ cells. (A) group CTRL4W, estimated size body (arrowhead): 5.23 μm, estimated cytoplasmic processes length (arrows): 13.28 and 24.28 μm; (B) group PA4W, estimated size body (arrowhead): 5.04 μm, estimated cytoplasmic processes length (arrows): 26.68 and 11.94 μm; (C) group CTRL16W, estimated size body (arrowhead): 8.69 μm, estimated cytoplasmic processes length (arrows): 13.07 and 20.56 μm; (D) group PA16W, estimated size body

(arrowhead): 9.56 μm, estimated cytoplasmic processes length (arrows): 22.03 and 13.36 μm. Lens magnification: ×40. Scale bars: 20 μm. CD34+ cells nuclei and cytoplasmic processes were measured using a caliper tool of the software for image acquisition (AxioVision Release 4.8.2—SP2 Software, Carl Zeiss Microscopy GmbH, Jena, Germany). CTRL4W, control sedentary rats sacrificed at 4 weeks; PA4W, rats performing physical exercise sacrificed at 4 weeks; CTRL16W, control sedentary rats sacrificed at 16 weeks; PA16W, rats performing physical exercise sacrificed at 4 weeks.

6.4. Discussion

TCs have been largely identified, over the last ten years, as populating the stromal compartments of a variety of organs, belonging to the tissue stem cell niche [33,49,65]. Within the skeletal muscle tissue, TCs are distributed throughout the perimysium and endomysium and could reach long-distances through their telopodes which allow these cells to make contact with myofibers, nerve terminals, blood vessels, and other stromal populations, including SCs, sited beneath the surrounding basal lamina of the myofiber.

In the present morphological study, the presence of TCs in tibialis anterior muscle of healthy rats who underwent a protocol of endurance training for either 4 weeks or 16 weeks was investigate in relation to sedentary rats who were inactive, i.e., not engaging in any physical exercise, throughout the duration of the experiment.

H&E staining shows no cytological alteration in the muscle tissue of all groups, although the morphometric analysis of the size of the muscle fibers highlights a significant atrophy, defined as a decrease in the size of myofibers, of the sedentary control group at 16 weeks (CTRL16W) when compared to physically active rats undergoing treadmill training for both 16 weeks (** $p < 0.0001$) and 4 weeks (* $p < 0.001$) (Figure 4). Muscle morphological adaptations to active/inactive styles were not, however, accompanied by statistically significant differences ($p > 0.05$) in body weights in all groups, indicating a physiological growth of the rats during the weeks, as expected (Figure 3).

Whether atrophy may affect muscle stem cells numbers or behavior is still controversial and should be further elucidated to assess the role of daily mechanical stress administered through exercise [66]. Mitchell et al. [67] reported that the number of stem cells in hindlimb muscles of mice was reduced after 2 weeks of hind limb suspension, and Verdijk et al. [68] observed similar decline in human vastus lateralis muscle following sarcopenia, reversed by resistance training which increased satellite cell content and type II muscle fiber size. Conversely,

aerobic and resistance training have been reported to be a stimulus for the formation of new muscle fibers and maintain their homeostasis [4,5].

Although SCs are the main characters of renewal programme in skeletal muscle, other tissue residents and recruited stromal cells, e.g., fibroblasts, fibro-adipogenic progenitors, endothelial cells, perycites, and macrophages, are paramount supporting players [16,22,69]. Among these cell-cell interactions, TCs and SCs seem to interact by juxtacrine and paracrine intercellular signaling, in order to support in a concerted manner [13] the network mediating new tissue organization [70]. However, the interplay between these two cell types, especially in skeletal muscle injury [49], has yet to be elucidated in depth since cue-based investigations rely mainly on knowledge of the close proximity of TCs to SCs and their ability to communicate.

This study provides a novel finding that interstitial TCs are decreased in the muscles of sedentary rats compared to exercised rats, supporting the recent reports that TCs are, otherwise, increased in exercise-induced cardiac growth [55], participate in early moderate exercise-induced remodeling after acute myocardial infarct [71] and in eccentric contraction-induced skeletal muscle injury, in rodents. Since their discovery is relatively recent, TCs are not yet defined by specific antigenic markers, although CD34 is the most commonly used antigen to characterize their presence [48,72]. Vimentin, CD117/c-kit, PDGFR-β (platelet-derived growth factor receptor β), and SMA (smooth muscle actin) are the antigens most frequently associated with TCs [47,62,73,74]. Bei et al. analyzed immunofluorescence double staining for cardiac TCs and fibroblasts in vitro. CD34/CD117, CD34/vimentin, and CD34/PDGFR-β were positive for TCs, whereas fibroblasts showed positivity only for vimentin and PDGFR-β [75].

In this work, double positivity for CD34+/CD117+ and CD34+/vimentin+ were used to individuate TCs and to discriminate this population from fibroblasts which are CD34-/CD117-/vimentin+. CD34 is a sialomucin mainly expressed in hematopoietic stem cells (HSCs) surface but it has also been found in other tissue-specific stem cells [76]. Vimentin is cytoskeletal type III intermediate filament protein found in mesenchymal-derived cells that provides an architectural network for organelles anchoring to cytoplasm [73]. CD117 is a transmembrane receptor tyrosine kinase widely used for TCs identification which is active in proliferation and differentiation [77]. Based on two distinct double-immunostainings for

CD34/CD117 and CD34/Vimentin, skeletal muscle TCs were identified in all groups. CD34/CD177 statistical analysis indicates a significant difference in the higher level of TCs in exercised rats at 16 weeks in relation to their control group (* $p < 0.05$) (Figure 5). This result is also more significantly supported by CD34/VIM double-immunostaining (** $p < 0.01$) (Figure 6). These results indicate a potential targeting of TCs, as belonging to muscle stem cell niche, in cell dysfunction associated with atrophic condition [67]. This latter negatively affects stem cells via presence of catabolic factors such as myostatin [78] and tumor necrosis factor α [79] as well as decreases in trophic factors [80]. In contrast, in this work, rats subjected to regular physical training for 16 weeks maintained a stable TCs population, although not statistically increased compared to rats who performed exercise for only 4 weeks.

Finally, immunohistochemistry showed CD34+ cells, within the interstitium between muscle fibers (Figure 7), with characteristic features of TCs and telopodes, i.e., spindle nuclei and multiple long cytoplasmic processes. These observations are in support with current evidence suggesting TCs' role in intercellular signaling through their strategic position and organized network of telopodes with local cellular neighborhood, nerves, and capillaries [33,81,82]. Homo- and heterocellular communication seems to be carried out via small molecules and shedding microvesicles carrying various molecules like proteins, RNAs, and microRNA [49,83,84]. These mechanisms of transmission allow rapid cell engagement in the tissue milieu, in order to approach adaptations to biochemical and physical changes. The use of TEM would have been useful to determine the ultrastructural features of TCs in exercised rats and this should be noticed as a limitation of this study.

6.5. Conclusions

These findings herein are intended to encourage knowledge about TCs population and their role in the stem cells niche of skeletal muscles. Further studies investigating TCs in response to different types of exercise (resistance, aerobic, isotonic, flexibility), sedentary behavior, ageing, and pathophysiological conditions, as well as studies on the possibility of triggering TCs through exercise to reverse atrophic conditions, would be scientifically valuable.

This study may be framed in a field still in its infancy, although it is rapidly attracting the attention of the scientific community. The understanding of the above-mentioned

mechanisms between the cells involved in the tissue remodeling process could offer new chances in regenerative tissue strategies and insights about finding possible triggers for TCs in sarcopenia and other musculoskeletal disorders, in clinical medicine.

Finally, since exercise training has been shown to exert protective effects against sedentary-induced atrophy, rather by sustaining muscle remodeling and maintenance of TCs, this finding might promote further skeletal muscle adapted physical activity and rehabilitation programmes for humans.

Author Contributions

Conceptualization, S.R. and G.M. (Giuseppe Musumeci); methodology, S.R., C.F. and G.M. (Grazia Maugeri); software, S.R., C.F. and M.D.R.; validation, S.S. and M.D.R.; formal analysis, S.R., C.F. and G.M. (Grazia Maugeri); investigation, S.R., G.L., E.P.; resources, C.F. and S.S.; data curation, S.R. and G.M. (Giuseppe Musumeci); writing—original draft preparation, S.R.; writing—review and editing, S.R. and G.M. (Giuseppe Musumeci); visualization, S.R. and F.R.; supervision G.M. (Giuseppe Musumeci); project administration, G.M. (Giuseppe Musumeci); funding acquisition, G.M. (Giuseppe Musumeci). All authors have read and agreed to the published version of the manuscript.

Funding

This work was funded by the University Research Project Grant (PIACERI Found—NATURE-OA—2020–2022), Department of Biomedical and Biotechnological Sciences (BIOMETEC), University of Catania, 95123 Catania, Italy.

Institutional Review Board Statement

The study was conducted according to the guidelines of the Institutional Animal Care and Use Committee (I.A.C.U.C.) of the University of Catania (Approved protocol n. 2112015-PR of the 14.01.2015, Italian Ministry of Health). The procedures were carried out in accordance with the Italian Animal Protection Law (D.Lgs. 26/2014) and the European Community Council Directive (2010/63/EU).

Data Availability Statement

The data presented in this study are available on request from the corresponding author.

Acknowledgments

In loving memory of R. Forrest.

Conflicts of Interest

The authors declare no conflict of interest.

6.6. References

1. Marini, M.; Veicsteinas, A. The exercised skeletal muscle: A review. *Eur. J. Transl. Myol.* **2010**, *20*, 105.
2. Zhang, S.F.; Zhang, Y.; Li, B.; Chen, N. Physical inactivity induces the atrophy of skeletal muscle of rats through activating AMPK/FoxO3 signal pathway. *Eur. Rev. Med. Pharmacol. Sci.* **2018**, *22*, 199–209.
3. Rudrappa, S.S.; Wilkinson, D.J.; Greenhaff, P.L.; Smith, K.; Idris, I.; Atherton, P.J. Human skeletal muscle disuse atrophy: Effects on muscle protein synthesis, breakdown, and insulin resistance-A qualitative review. *Front. Physiol.* **2016**, *7*, 361.
4. Konopka, A.R.; Harber, M.P. Skeletal muscle hypertrophy after aerobic exercise training. *Exerc. Sport Sci. Rev.* **2014**, *42*, 53–61.
5. Minetto, M.A.; Giannini, A.; McConnell, R.; Busso, C.; Massazza, G. Effects of exercise on skeletal muscles and tendons. *Curr. Opin. Endocr. Metab. Res.* **2019**, *9*, 90–95.
6. Musumeci, G.; Maria Trovato, F.; Imbesi, R.; Castrogiovanni, P. Effects of dietary extra-virgin olive oil on oxidative stress resulting from exhaustive exercise in rat skeletal muscle: A morphological study. *Acta Histochem.* **2014**, *116*, 61–69.
7. Bani, D.; Nistri, S. New insights into the morphogenic role of stromal cells and their relevance for regenerative medicine. lessons from the heart. *J. Cell. Mol. Med.* **2014**, *18*, 363–370.
8. Ceccarelli, G.; Benedetti, L.; Arcari, M.L.; Carubbi, C.; Galli, D. Muscle stem cell and physical activity: What point is the debate at? *Open Med.* **2017**, *12*, 144–156.
9. Brett, J.O.; Arjona, M.; Ikeda, M.; Quarta, M.; de Morrée, A.; Egner, I.M.; Perandini, L.A.; Ishak, H.D.; Goshayeshi, A.; Benjamin, D.I.; et al. Exercise rejuvenates quiescent skeletal muscle stem cells in old mice through restoration of Cyclin D1. *Nat. Metab.* **2020**, *2*, 307–317.
10. Boppart, M.D.; De Lisio, M.; Witkowski, S. Exercise and Stem Cells. *Prog. Mol. Biol. Transl. Sci.* **2015**, *135*, 423–456.
11. Kadi, F.; Charifi, N.; Denis, C.; Lexell, J.; Andersen, J.L.; Schjerling, P.; Olsen, S.; Kjaer, M. The behaviour of satellite cells in response to exercise: What have we learned from human studies? *Pflugers Arch. Eur. J. Physiol.* **2005**, *451*, 319–327.
12. Marini, M.; Rosa, I.; Ibba-Manneschi, L.; Manetti, M. Telocytes in skeletal, cardiac and smooth muscle interstitium: Morphological and functional aspects. *Histol. Histopathol.* **2019**, *33*, 1151–1165.
13. Popescu, L.M.; Manole, E.; Şerboiu, C.S.; Manole, C.G.; Suciu, L.C.; Gherghiceanu, M.; Popescu, B.O. Identification of telocytes in skeletal muscle interstitium: Implication for muscle regeneration. *J. Cell. Mol. Med.* **2011**, *15*, 1379–1392.
14. Mauro, A. Satellite cell of skeletal muscle fibers. *J. Biophys. Biochem. Cytol.* **1961**, *9*, 493–495.
15. Sambasivan, R.; Yao, R.; Kissenpfennig, A.; van Wittenberghe, L.; Paldi, A.; Gayraud-Morel, B.; Guenou, H.; Malissen, B.; Tajbakhsh, S.; Galy, A. Pax7-expressing satellite cells are indispensable for adult skeletal muscle regeneration. *Development* **2011**, *138*, 3647–3656.
16. Kyryachenko, S.; Formicola, L.; Ollitrault, D.; Correra, R.; Denizot, A.L.; Kyrylkova, K.; Marazzi, G.; Sassoon, D.A. The Adult Stem Cell Niche: Multiple Cellular Players in Tissue Homeostasis and Regeneration. In *Encyclopedia of Cell Biology*; Bradshaw, R.A., Stahl, P.D., Eds.; Academic Press: Waltham, MA, USA, 2016; Volume 3, pp. 794–806.
17. Beauchamp, J.R.; Heslop, L.; Yu, D.S.W.; Tajbakhsh, S.; Kelly, R.G.; Wernig, A.; Buckingham, M.E.; Partridge, T.A.; Zammit, P.S. Expression of CD34 and Myf5 defines the majority of quiescent adult skeletal muscle satellite cells. *J. Cell Biol.* **2000**, *151*, 1221–1233.
18. LaBarge, M.A.; Blau, H.M. Biological progression from adult bone marrow to mononucleate muscle stem cell to multinucleate muscle fiber in response to injury. *Cell* **2002**, *111*, 589–601.
19. Kassar-Duchossoy, L.; Giacone, E.; Gayraud-Morel, B.; Jory, A.; Gomès, D.; Tajbakhsh, S. Pax3/Pax7 mark a novel population of primitive myogenic cells during development. *Genes Dev.* **2005**, *19*, 1426–1431.
20. Gros, J.; Manceau, M.; Thomé, V.; Marcelle, C. A common somitic origin for embryonic muscle progenitors and satellite cells. *Nature* **2005**, *435*, 954–958.
21. Musumeci, G.; Castrogiovanni, P.; Coleman, R.; Szychlinska, M.A.; Salvatorelli, L.; Parenti, R.; Magro, G.; Imbesi, R. Somitogenesis: From somite to skeletal muscle. *Acta Histochem.* **2015**, *117*, 313–328.

22. Pannérec, A.; Marazzi, G.; Sassoon, D. Stem cells in the hood: The skeletal muscle niche. *Trends Mol. Med.* **2012**, *18*, 599–606.
23. Montarras, D.; Morgan, J.; Colins, C.; Relaix, F.; Zaffran, S.; Cumano, A.; Partridge, T.; Buckingham, M. Developmental biology: Direct isolation of satellite cells for skeletal muscle regeneration. *Science* **2005**, *309*, 2064–2067.
24. Zickri, M.B. Possible local stem cells activation by microcurrent application in experimentally injured soleus muscle. *Int. J. Stem Cells* **2014**, *7*, 79–86.
25. Murphy, M.M.; Lawson, J.A.; Mathew, S.J.; Hutcheson, D.A.; Kardon, G. Satellite cells, connective tissue fibroblasts and their interactions are crucial for muscle regeneration. *Development* **2011**, *138*, 3625–3637.
26. Balduino, A.; Leite Duarte, M.E.; Taichman, R.S. Skeletal Resident Stem Cells. In *Resident Stem Cells Regenerative Therapy*; Dos Santos Goldenberg, R.C., Campos, A.C., Eds.; Academic Press: Cambridge, MA, USA, 2013; pp. 123–140.
27. Kang, Y.; Zhu, Z.; Zheng, Y.; Wan, W.; Manole, C.G.; Zhang, Q. Skin telocytes versus fibroblasts: Two distinct dermal cell populations. *J. Cell. Mol. Med.* **2015**, *19*, 2530–2539.
28. Gatchalian, C.L.; Schachner, M.; Sanes, J.R. Fibroblasts that proliferate near denervated synaptic sites in skeletal muscle synthesize the adhesive molecules tenascin(J1), N-CAM, fibronectin, and a heparan sulfate proteoglycan. *J. Cell Biol.* **1989**, *108*, 1873–1890.
29. Biferali, B.; Proietti, D.; Mozzetta, C.; Madaro, L. Fibro–Adipogenic Progenitors Cross-Talk in Skeletal Muscle: The Social Network. *Front. Physiol.* **2019**, *10*, 1074.
30. Joe, A.W.B.; Yi, L.; Natarajan, A.; Le Grand, F.; So, L.; Wang, J.; Rudnicki, M.A.; Rossi, F.M.V. Muscle injury activates resident fibro/adipogenic progenitors that facilitate myogenesis. *Nat. Cell Biol.* **2010**, *12*, 153–163.
31. Uezumi, A.; Fukada, S.I.; Yamamoto, N.; Takeda, S.; Tsuchida, K. Mesenchymal progenitors distinct from satellite cells contribute to ectopic fat cell formation in skeletal muscle. *Nat. Cell Biol.* **2010**, *12*, 143–152.
32. Gautam, J.; Yao, Y. Pericytes in skeletal muscle. *Adv. Exp. Med. Biol.* **2019**, *1122*, 59–72.
33. Popescu, L.M.; Faussone-Pellegrini, M.S. TELOCYTES—A case of serendipity: The winding way from Interstitial Cells of Cajal (ICC), via Interstitial Cajal-Like Cells (ICLC) to TELOCYTES. *J. Cell. Mol. Med.* **2010**, *14*, 729–740.
34. Ramón y Cajal, S. *Histologie du Systeme Nerveux de l'Homme & des Vertébrés*; Tome II.; Maloine: Paris, France, 1911.
35. Faussone Pellegrini, M.S.; Cortesini, C.; Romagnoli, P. Sull'Ultrastruttura Della Tunica Muscolare Della Porzione Cardiale Dell'Esofago E Dello Stomaco Umano Con Particolare Riferimento Alle Cosiddette Cellule Interstiziali Di Cajal. *Arch. Ital. Anat. Embriol.* **1977**, *82*, 157–177.
36. Thuneberg, L. Interstitial cells of Cajal: Intestinal pacemaker cells? *Adv. Anat. Embryol. Cell Biol.* **1982**, *71*, 1–130.
37. Pieri, L.; Vannucchi, M.G.; Faussone-Pellegrini, M.S. Histochemical and ultrastructural characteristics of an interstitial cell type different from ICC and resident in the muscle coat of human gut. *J. Cell. Mol. Med.* **2008**, *12*, 1944–1955.
38. Aleksandrovych, V.; Pasternak, A.; Basta, P.; Sajewicz, M.; Walocha, J.A.; Gil, K. Telocytes: Facts, speculations and myths. *Folia Med. Cracov.* **2017**, *57*, 5–22.
39. Díaz-Flores, L.; Gutiérrez, R.; García, M.P.; González, M.; Sáez, F.J.; Aparicio, F.; Díaz-Flores, L.; Madrid, J.F. Human resident CD34+ stromal cells/telocytes have progenitor capacity and are a source of αSMA+ cells during repair. *Histol. Histopathol.* **2015**, *30*, 615–627.
40. Díaz-Flores, L.; Gutiérrez, R.; Goméz, M.G.; Sáez, F.J.; Madrid, J.F. Behaviour of telocytes during physiopathological activation. *Semin. Cell Dev. Biol.* **2016**, *55*, 50–61.
41. Ivey, M.J.; Tallquist, M.D. Defining the cardiac fibroblast. *Circ. J.* **2016**, *80*, 2269–2276.
42. Kucybala, I.; Janas, P.; Ciuk, S.; Cholopiak, W.; Klimek-Piotrowska, W.; Holda, M.K. A comprehensive guide to telocytes and their great potential in cardiovascular system. *Bratislava Med. J.* **2017**, *118*, 302–309.
43. Cretoiu, M.S.; Cretoiu Anca Simionescu, D.; Popescu, L.M. Telocytes in Human Fallopian Tube and Uterus Express Estrogen and Progesterone Receptors. In *Sex Steroids*; Kahn, S.M., Ed.; IntechOpen, 2012; pp. 91–114. Available online: https://www.intechopen.com/books/sex-steroids/telocytes-in-human-fallopian-tube-and-uterus-express-estrogen-and-progesterone-receptors (accessed on 7 June 2021).

44. Gherghiceanu, M.; Popescu, L.M. Interstitial Cajal-like cells (ICLC) in human resting mammary gland stroma. Transmission electron microscope (TEM) identification. *J. Cell. Mol. Med.* **2005**, *9*, 893–910.
45. Valadi, H.; Ekström, K.; Bossios, A.; Sjöstrand, M.; Lee, J.J.; Lötvall, J.O. Exosome-mediated transfer of mRNAs and microRNAs is a novel mechanism of genetic exchange between cells. *Nat. Cell Biol.* **2007**, *9*, 654–659.
46. Deasy, B.M.; Feduska, J.M.; Payne, T.R.; Li, Y.; Ambrosio, F.; Huard, J. Effect of VEGF on the regenerative capacity of muscle stem cells in dystrophic skeletal muscle. *Mol. Ther.* **2009**, *17*, 1788–1798.
47. Cretoiu, D.; Radu, B.M.; Banciu, A.; Banciu, D.D.; Cretoiu, S.M. Telocytes heterogeneity: From cellular morphology to functional evidence. *Semin. Cell Dev. Biol.* **2017**, *64*, 26–39.
48. Díaz-Flores, L.; Gutiérrez, R.; García, M.P.; Sáez, F.J.; Díaz-Flores, L.; Valladares, F.; Madrid, J.F. CD34+ stromal cells/fibroblasts/fibrocytes/telocytes as a tissue reserve and a principal source of mesenchymal cells. Location, morphology, function and role in pathology. *Histol. Histopathol.* **2014**, *29*, 831–870.
49. Manetti, M.; Tani, A.; Rosa, I.; Chellini, F.; Squecco, R.; Idrizaj, E.; Zecchi-Orlandini, S.; Ibba-Manneschi, L.; Sassoli, C. Morphological evidence for telocytes as stromal cells supporting satellite cell activation in eccentric contraction-induced skeletal muscle injury. *Sci. Rep.* **2019**, *9*, 14515.
50. Ibba-Manneschi, L.; Rosa, I.; Manetti, M. Telocyte implications in human pathology: An overview. *Semin. Cell Dev. Biol.* **2016**, *55*, 62–69.
51. Boos, A.M.; Weigand, A.; Brodbeck, R.; Beier, J.P.; Arkudas, A.; Horch, R.E. The potential role of telocytes in Tissue Engineering and Regenerative Medicine. *Semin. Cell Dev. Biol.* **2016**, *55*, 70–78.
52. Richter, M.; Kostin, S. The failing human heart is characterized by decreased numbers of telocytes as result of apoptosis and altered extracellular matrix composition. *J. Cell. Mol. Med.* **2015**, *19*, 2597–2606.
53. Manetti, M.; Guiducci, S.; Ruffo, M.; Rosa, I.; Faussone-Pellegrini, M.S.; Matucci-Cerinic, M.; Ibba-Manneschi, L. Evidence for progressive reduction and loss of telocytes in the dermal cellular network of systemic sclerosis. *J. Cell. Mol. Med.* **2013**, *17*, 482–496.
54. Pimentel Neto, J.; Rocha, L.C.; Barbosa, G.K.; dos Santos Jacob, C.; Krause Neto, W.; Watanabe, I.S.; Ciena, A.P. Myotendinous junction adaptations to ladder-based resistance training: Identification of a new telocyte niche. *Sci. Rep.* **2020**, *10*, 14124.
55. Xiao, J.; Chen, P.; Qu, Y.; Yu, P.; Yao, J.; Wang, H.; Fu, S.; Bei, Y.; Chen, Y.; Che, L.; et al. Telocytes in exercise-induced cardiac growth. *J. Cell. Mol. Med.* **2016**, *20*, 973–979.
56. Arifin, W.N.; Zahiruddin, W.M. Sample size calculation in animal studies using resource equation approach. *Malaysian J. Med. Sci.* **2017**, *24*, 101–105.
57. Castrogiovanni, P.; Di Rosa, M.; Ravalli, S.; Castorina, A.; Guglielmino, C.; Imbesi, R.; Vecchio, M.; Drago, F.; Szychlinska, M.A.; Musumeci, G. Moderate physical activity as a prevention method for knee osteoarthritis and the role of synoviocytes as biological key. *Int. J. Mol. Sci.* **2019**, *20*, 511.
58. Ishihara, A.; Hirofuji, C.; Nakatani, T.; Itoh, K.; Itoh, M.; Katsuta, S. Effects of running exercise with increasing loads on tibialis anterior muscle fibres in mice. *Exp. Physiol.* **2002**, *87*, 113–116.
59. Fischer, A.H.; Jacobson, K.A.; Rose, J.; Zeller, R. Hematoxylin and eosin staining of tissue and cell sections. *Cold Spring Harb. Protoc.* **2008**, *3*.
60. Trovato, F.M.; Castrogiovanni, P.; Szychlinska, M.A.; Purrello, F.; Musumeci, G. Impact of western and mediterranean diets and vitamin D on muscle fibers of sedentary rats. *Nutrients* **2018**, *10*, 231.
61. Bei, Y.; Wang, F.; Yang, C.; Xiao, J. Telocytes in regenerative medicine. *J. Cell. Mol. Med.* **2015**, *19*, 1441–1454.
62. Cretoiu, S.M.; Popescu, L.M. Telocytes revisited. *Biomol. Concepts* **2014**, *5*, 353–369.
63. Fu, S.; Wang, F.; Cao, Y.; Huang, Q.; Xiao, J.; Yang, C.; Popescu, L.M. Telocytes in human liver fibrosis. *J. Cell. Mol. Med.* **2015**, *19*, 676–683.
64. Wang, F.; Bei, Y.; Zhao, Y.; Song, Y.; Xiao, J.; Yang, C. Telocytes in pregnancy-induced physiological liver growth. *Cell. Physiol. Biochem.* **2015**, *36*, 250–258.
65. Díaz-Flores, L.; Gutiérrez, R.; García, M.P.; González-Gómez, M.; Carrasco, J.L.; Alvarez-Argüelles, H.; Díaz-Flores, L. Telocytes/cd34+ stromal cells in pathologically affected white adipose tissue. *Int. J. Mol. Sci.* **2020**, *21*, 9694.
66. Fukada, S.I. The roles of muscle stem cells in muscle injury, atrophy and hypertrophy. *J. Biochem.* **2018**, *163*, 353–358.

67. Mitchell, P.O.; Pavlath, G.K. Skeletal muscle atrophy leads to loss and dysfunction of muscle precursor cells. *Am. J. Physiol. Cell Physiol.* **2004**, *287*, C1753–C1762.
68. Verdijk, L.B.; Snijders, T.; Drost, M.; Delhaas, T.; Kadi, F.; Van Loon, L.J.C. Satellite cells in human skeletal muscle; From birth to old age. *Age* **2014**, *36*, 545–557.
69. Scharner, J.; Zammit, P.S. The muscle satellite cell at 50: The formative years. *Skelet. Muscle* **2011**, *1*, 28.
70. Albulescu, R.; Tanase, C.; Codrici, E.; Popescu, D.I.; Cretoiu, S.M.; Popescu, L.M. The secretome of myocardial telocytes modulates the activity of cardiac stem cells. *J. Cell. Mol. Med.* **2015**, *19*, 1783–1794.
71. Liao, Z.; Li, D.; Chen, Y.; Li, Y.; Huang, R.; Zhu, K.; Chen, H.; Yuan, Z.; Zheng, X.; Zhao, H.; et al. Early moderate exercise benefits myocardial infarction healing via improvement of inflammation and ventricular remodelling in rats. *J. Cell. Mol. Med.* **2019**, *23*, 8328–8342.
72. Romano, E.; Rosa, I.; Fioretto, B.S.; Lucattelli, E.; Innocenti, M.; Ibba-Manneschi, L.; Matucci-Cerinic, M.; Manetti, M. A two-step immunomagnetic microbead-based method for the isolation of human primary skin telocytes/cd34+ stromal cells. *Int. J. Mol. Sci.* **2020**, *21*, 5877.
73. Varga, I.; Kyselovič, J.; Danišovič, Ľ.; Gálfiová, P.; Kachlík, D.; Polák, Š.; Klein, M. Recently discovered interstitial cells termed telocytes: Distinguishing cell-biological and histological facts from fictions. *Biologia* **2019**, *74*, 195–203.
74. Lis, G.J.; Dubrowski, A.; Lis, M.; Solewski, B.; Witkowska, K.; Aleksandrovych, V.; Jasek-Gajda, E.; Hołda, M.K.; Gil, K.; Litwin, J.A. Identification of cd34+/pgdfrα+ valve interstitial cells (Vics) in human aortic valves: Association of their abundance, morphology and spatial organization with early calcific remodeling. *Int. J. Mol. Sci.* **2020**, *21*, 6330.
75. Bei, Y.; Zhou, Q.; Fu, S.; Lv, D.; Chen, P.; Chen, Y.; Wang, F.; Xiao, J. Cardiac telocytes and fibroblasts in primary culture: Different morphologies and immunophenotypes. *PLoS ONE* **2015**, *10*, e0115991.
76. Nielsen, J.S.; McNagny, K.M. Erratum: Novel functions of the CD34 family. *J. Cell Sci.* **2008**, *121*, 3683–3692.
77. Klein, M.; Urban, L.; Deckov, I.; Danisovic, L.; Polak, S.; Danihel, L.; Varga, I. Distribution of telocytes in the corpus and cervix of human uterus: An immunohistochemical study. *Biologia* **2017**, *72*, 1217–1223.
78. Reardon, K.A.; Davis, J.; Kapsa, R.M.I.; Choong, P.; Byrne, E. Myostatin, insulin-like growth factor-1, and leukemia inhibitory factor mRNAs are upregulated in chronic human disuse muscle atrophy. *Muscle Nerve* **2001**, *24*, 893–899.
79. Reid, M.B.; Li, Y.P. Tumor necrosis factor-α and muscle wasting: A cellular perspective. *Respir. Res.* **2001**, *2*, 269–272.
80. Stevenson, E.J.; Giresi, P.G.; Koncarevic, A.; Kandarian, S.C. Global analysis of gene expression patterns during disuse atrophy in rat skeletal muscle. *J. Physiol.* **2003**, *551*, 33–48.
81. Cretoiu, D.; Roatesi, S.; Bica, I.; Plesca, C.; Stefan, A.; Bajenaru, O.; Condrat, C.E.; Cretoiu, S.M. Simulation and modeling of telocytes behavior in signaling and intercellular communication processes. *Int. J. Mol. Sci.* **2020**, *21*, 2615.
82. Vannucchi, M.G. The telocytes: Ten years after their introduction in the scientific literature. An update on their morphology, distribution, and potential roles in the gut. *Int. J. Mol. Sci.* **2020**, *21*, 4478.
83. Cocucci, E.; Racchetti, G.; Meldolesi, J. Shedding microvesicles: Artefacts no more. *Trends Cell Biol.* **2009**, *19*, 43–51.
84. Gandahi, N.S.; Ding, B.; Shi, Y.; Bai, X.; Gandahi, J.A.; Vistro, W.A.; Chen, Q.; Yang, P. Identification of telocytes in the pancreas of Turtles—A role in cellular communication. *Int. J. Mol. Sci.* **2020**, *21*, 2057.

7. LIST OF PUBBLICATIONS

1. Ravalli S, Szychlinska MA, Leonardi RM, Musumeci G. Recently highlighted nutraceuticals for preventive management of osteoarthritis. World J Orthop. 2018.
2. Castrogiovanni P, Di Rosa M, Ravalli S, Castorina A, Guglielmino C, Imbesi R, Vecchio M, Drago F, Szychlinska MA, Musumeci G. Moderate Physical Activity as a Prevention Method for Knee Osteoarthritis and the Role of Synoviocytes as Biological Key. Int J Mol Sci. 2019.
3. Szychlinska MA, D'Amora U, Ravalli S, Ambrosio L, Di Rosa M, Musumeci G. Functional Biomolecule Delivery Systems and Bioengineering in Cartilage Regeneration. Curr Pharm Biotechnol. 2019.
4. Szychlinska MA, Imbesi R, Castrogiovanni P, Guglielmino C, Ravalli S, Di Rosa M, Musumeci G. Assessment of Vitamin D Supplementation on Articular Cartilage Morphology in a Young Healthy Sedentary Rat Model. Nutrients. 2019
5. Szychlinska MA, Ravalli S, Musumeci G. Pleiotropic effect of fibrates on senescence and autophagy in osteoarthritis. EBioMedicine. 2019.
6. Ravalli S, Pulici C, Binetti S, Aglieco A, Vecchio M, Musumeci G. An Overview of the Pathogenesis and Treatment of Elbow Osteoarthritis. J. Funct. Morphol. Kinesiol. 2019.
7. Di Rosa, M, Castrogiovanni P, Trovato FM, Malatino L, Ravalli S, Imbesi R, Szychlinska MA, Musumeci G. Adapted Moderate Training Exercise Decreases the Expression of Ngal in the Rat Kidney: An Immunohistochemical Study. Appl. Sci. 2019.
8. Musumeci G, Ravalli S, Amorini AM, Lazzarino G. Concussion in Sports. J. Funct. Morphol. Kinesiol. 2019.
9. Ravalli S, Castrogiovanni P, Musumeci G. Exercise as medicine to be prescribed in osteoarthritis. World J Orthop. 2019.
10. Bianco A, Ravalli S, Maugeri G, D'Agata V, Vecchio M, D'Amico AG, Pavone V, Lucenti L, Amato A, Gentile A, Giustino V, Feka K, Thomas E, Musumeci G. The "Journal of Functional Morphology and Kinesiology" Journal Club Series: Highlights

on Recent Papers in Overtraining and Exercise Addiction. J. Funct. Morphol. Kinesiol. 2019.

11. Caltabiano R, Castrogiovanni P, Barbagallo I, Ravalli S, Szychlinska MA, Favilla V, Schiavo L, Imbesi R, Musumeci G, Di Rosa M. Identification of Novel Markers of Prostate Cancer Progression, Potentially Modulated by Vitamin D. Appl. Sci. 2019.
12. Bianco A, Ravalli S, Maugeri G, D'Agata V, Vecchio M, D'Amico AG, Pavone V, Lucenti L, Amato A, Gentile A, Giustino V, Feka K, Thomas E, Musumeci G. The "Journal of Functional Morphology and Kinesiology" Journal Club Series: Highlights on Recent Papers in Overtraining and Exercise Addiction. J Funct Morphol Kinesiol. 2019.
13. Szychlinska MA, Calabrese G, Ravalli S, Parrinello NL, Forte S, Castrogiovanni P, Pricoco E, Imbesi R, Castorina S, Leonardi R, Di Rosa M, Musumeci G. Cycloastragenol as an Exogenous Enhancer of Chondrogenic Differentiation of Human Adipose-Derived Mesenchymal Stem Cells. A Morphological Study. Cells. 2020.
14. Ravalli S, Musumeci G. New Horizons of Knowledge in Intervertebral Disc Disease. Journal of Investigative Surgery. 2020.
15. Szychlinska MA, Calabrese G, Ravalli S, Dolcimascolo A, Castrogiovanni P, Fabbi C, Puglisi C, Lauretta G, Di Rosa M, Castorina A, Parenti R, Musumeci G. Evaluation of a Cell-Free Collagen Type I-Based Scaffold for Articular Cartilage Regeneration in an Orthotopic Rat Model. Materials. 2020.
16. Ravalli S, Musumeci G. Coronavirus Outbreak in Italy: Physiological Benefits of Home-Based Exercise During Pandemic. J. Funct. Morphol. Kinesiol. 2020.
17. Lauretta G, Ravalli S, Szychlinska MA, Castorina A, Maugeri G, D'Amico AG, D'Agata V, Musumeci G. Current knowledge of Pituitary adenylate cyclase activating polypeptide (PACAP) in articular cartilage. Histol. Histopathol. 2020.
18. Fisher JP, Ravalli S, Carlson L, Bridgeman LA, Roggio F, Scuderi S, Maniaci M, Cortis C, Fusco A, Musumeci G. The "Journal of Functional Morphology and Kinesiology" Journal Club Series: Utility and Advantages of the Eccentric Training through the Isoinertial System. J Funct Morphol Kinesiol. 2020.

19. Sanfilippo C, Musumeci G, Castrogiovanni P, Fazio F, Li Volti G, Barbagallo I, Maugeri G, Ravalli S, Imbesi R, Di Rosa M. Hippocampal transcriptome deconvolution reveals differences in cell architecture of not demented elderly subjects underwent late-life physical activity. J Chem Neuroanat. 2021.
20. Roggio F, Ravalli S, Maugeri G, Bianco A, Palma A, Di Rosa M, Musumeci G. Technological advancements in the analysis of human motion and posture management through digital devices. World J Orthop. 2021.
21. Maugeri G, D'Agata V, Magrì B, Roggio F, Castorina A, Ravalli S, Di Rosa M, Musumeci G. Neuroprotective Effects of Physical Activity via the Adaptation of Astrocytes. Cells. 2021.
22. Roggio F, Trovato B, Ravalli S, Di Rosa M, Maugeri G, Bianco A, Palma A, Musumeci G. One Year of COVID-19 Pandemic in Italy: Effect of Sedentary Behavior on Physical Activity Levels and Musculoskeletal Pain among University Students. Int. J. Environ. Res. Public Health. 2021.
23. Ravalli S, Federico C, Lauretta G, Saccone S, Pricoco E, Roggio F, Di Rosa M, Maugeri G, Musumeci G. Morphological Evidence of Telocytes in Skeletal Muscle Interstitium of Exercised and Sedentary Rodents. Biomedicines. 2021.
24. Ravalli S, Roggio F, Lauretta G, Di Rosa M, D'amico AG, D'Agata V, Maugeri G, Musumeci G. Exploiting real-world data to Monitor physical activity in patients with osteoarthritis: the opportunity of Digital epidemiology. Heliyon. 2022.
25. Ravalli S, Roggio F, Magrì B, Lauretta G, Broggi G, Caltabiano R, Vecchio GM, Magro G, Loreto C, Musumeci G. Immunohistochemical evaluation of Autotaxin and Lubricin in mild osteoarthritic rat model performing moderate physical activity. Under revision.

8. ORAL COMMUNICATIONS AND POSTERS

• Annual Retreat of the Department of Biomedical and Biotechnological Sciences (Biometec), University of Catania - 22-24/11/2018 – Castiglione di Silcilia, Italy – *Oral communication* Title: “Exercise and nutrition protective effects on cartilage disorders and muscle wasting”.

• Conference on “Mind in Movement, physical activity and neuroscience” – 12/06/2019 – University of Catania, Italy – *Oral communication* Title: “Sport addiction: overtraining and extreme risk”.

• 73rd National Congress of Italian Society of Human Anatomy and Histology (SIAI) - 22-24/09/2019 – Naples, Italy – *Oral Communication* Title: "Computational modelling of hMSCs/scaffold construct adaptations in response to mechanically induced chondrogenesis".

• 93rd National Congress of the Italian Society of Experimental Biology (SIBS) - 22-25/04/2021 – Palermo, Italy – *Videoposter* Title: “Computational modelling of hMSCs/scaffold construct adaptations in response to mechanically induced chondrogenesis”.

• 74th National Congress of Italian Society of Human Anatomy and Histology (SIAI) - 24-25/09/2021 – Bologna, Italy – *Videoposter* Title: “Effect of physical exercise on Telocyte population in the Skeletal muscle tissue of rats”.

• XII National Congress of the Italian Society of Motor and Sports Sciences (SISMES) – 8-10/10/2021 – Padua, Italy – *Oral communication* Title: “Morphological evidence of telocytes in skeletal muscle interstitium of exercised and sedentary rodents”

AWARD for Best Videoposter “Young Investigator Award” – 93rd National Congress of the Italian Society of Experimental Biology (SIBS) - 22-25 April 2021 – Palermo, Italy.

RINGRAZIAMENTI

Sento di destinare i miei più vivi ringraziamenti al Professore Giuseppe Musumeci che da subito mi ha accolto con sincero entusiasmo nel suo gruppo di ricerca e mi ha sempre guidata durante questo progetto, senza smettere mai di incoraggiarmi a crescere e ad apprendere. Lo ringrazio soprattutto per avermi insegnato, prima nei fatti che nelle parole, che non vi sono grandi o piccoli obiettivi che non possano essere perseguiti, se si sceglie per compagna una forte determinazione.

Esprimo il mio sincero ringraziamento al Professore Vito De Pinto per l'opportunità datami, per l'essenziale e costante lavoro svolto a pieno supporto di questo corso di studi e l'onesto affetto ed entusiasmo rivolto a noi studenti in ogni momento di questo percorso.

Un'altra menzione è dedicata a Michelino Di Rosa. Per quanto sia difficile dare forma verbale ad ogni singolo momento passato insieme a parlare di scienza e di vita, per sempre gli sarò grata per avermi insegnato ad avere il coraggio di pormi le più scomode domande e a non aver paura di ascoltare le risposte.

Apprezzo la fortuna di aver trascorso ogni giorno di questi tre anni in un ambiente che mi ha sempre dato affetto e rispetto, grazie alle Professoresse D'Agata, Castrogiovanni, Imbesi e Loreto, ai Professori Castorina e Giunta e alla presenza vera e sincera di colleghi che voglio chiamare amici, Marta, Graziana, Grazia, Rita, Giovanni, Federico, Benedetta, Bruno, Elisabetta.

Ai miei genitori, a ciascuno dei miei affetti della mia famiglia, in modo speciale a Walter e ai suoi genitori, a Greta, Fabrizio, Sabrina, Naomi e Vincenzo, per essere stati miei complici, ognuno a modo suo, nella sfera più intima di questo intenso percorso. Le mie emozioni accompagnano il mio amore e la gratitudine che ho per voi.